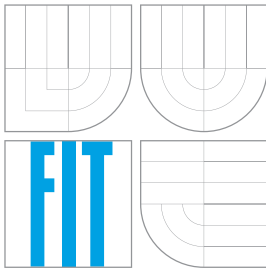


**VYSOKÉ UČENÍ TECHNICKÉ V BRNĚ**  
BRNO UNIVERSITY OF TECHNOLOGY



**FAKULTA INFORMAČNÍCH TECHNOLOGIÍ**  
**ÚSTAV POČÍTAČOVÉ GRAFIKY A MULTIMÉDIÍ**

FACULTY OF INFORMATION TECHNOLOGY  
DEPARTMENT OF COMPUTER GRAPHICS AND MULTIMEDIA

# **ODHAD LETOVÝCH PARAMETRŮ MALÉHO LETOUNU**

LIGHT AIRPLANE FLIGHT PARAMETERS ESTIMATION

**DISERTAČNÍ PRÁCE**

PHD THESIS

**AUTOR PRÁCE**

AUTHOR

Ing. PETR DITTRICH

**VEDOUCÍ PRÁCE**

SUPERVISOR

Ing. PETER CHUDÝ, Ph.D. MBA

BRNO 2016

## Abstract

This thesis is focused on a light airplane flight parameter estimation, specially aimed at the Eveztor SportStar RTC. For the purposes of flight parameter estimation the Equation Error Method, Output Error Method and Recursive Least-Squares methods were used. This thesis is focused on the investigation of the characteristics of the flight parameters of longitudinal motion and the verification, that this estimated parameters corresponds to the measured data and thus create a prerequisite for a sufficiently accurate airplane model. The estimated flight parameters are compared to the a-priori values obtained using the Tornado, AVL and Datcom softwares. The differences between the a-priori values and estimated flight parameters are also compared to the correction factors published for the subsonic flight regime of an F-18 Hornet model.

## Keywords

Airplane, System Identification, Parameter Estimation, Flight Parameters, Flight Envelope, Equations of Motion, Linearization, State-Space Model, Longitudinal Motion, Equation Error Method, Output Error Method, Recursive Least-Squares, Sensors, Flight Path Reconstruction, Kalman Filter, Model Validation.

## Citation

Petr Dittrich: Light airplane flight parameters estimation, PhD thesis, Brno, BUT FIT, 2016

# Abstrakt

Tato práce je zaměřena na odhad letových parametrů malého letounu, konkrétně letounu Evektor SportStar RTC. Pro odhad letových parametrů jsou použity metody “Equation Error Method”, “Output Error Method” a metody rekurzivních nejmenších čtverců. Práce je zaměřena na zkoumání charakteristik aerodynamických parametrů podélného pohybu a ověření, zda takto odhadnuté letové parametry odpovídají naměřeným datům a tudíž vytvářejí předpoklad pro realizaci dostatečně přesného modelu letadla. Odhadnuté letové parametry jsou dále porovnávány s a-priorními hodnotami získanými s využitím programů Tornado, AVL a softwarové verze sbírky Datcom. Rozdíly mezi a-priorními hodnotami a odhadnutými letovými parametry jsou porovnány s korekcemi publikovanými pro subsonické letové podmínky modelu letounu F-18 Hornet.

## Klíčová slova

Letoun, identifikace systému, odhad parametrů, letové parametry, letová obálka, pohybové rovnice, linearizace, stavový model, podélný pohyb, “Equation Error Method”, “Output Error Method”, rekurzivní nejmenší čtverce, senzory, rekonstrukce letové trajektorie, Kálmánův filtr, validace modelu.

## Citace

Petr Dittrich: Odhad letových parametrů malého letounu, disertační práce, Brno, FIT VUT v Brně, 2016

# Light airplane flight parameters estimation

## Declaration

I hereby declare that this thesis is my genuine work, created under the guidance of my supervisor Assistant professor Peter Chudý. All information sources and publications used are properly cited.

.....  
Petr Dittrich  
August 29<sup>th</sup>, 2016

## Acknowledgment

I would like to thank my supervisor Assistant professor Peter Chudý for his guidance and valuable comments on my research work. I also would like to thank my family, my friends and my colleagues at Faculty of Information Technology, Brno University of Technology for their support.

© Petr Dittrich, 2016.

*Tato práce vznikla jako školní dílo na Vysokém učení technickém v Brně, Fakultě informačních technologií. Práce je chráněna autorským zákonem a její užití bez udělení oprávnění autorem je nezákonné, s výjimkou zákonem definovaných případů.*

# Contents

<b>1</b>	<b>Introduction</b>	<b>15</b>
1.1	Objectives of the thesis . . . . .	16
1.2	Outline of the thesis . . . . .	16
<b>2</b>	<b>System identification</b>	<b>18</b>
2.1	Model structure identification . . . . .	18
2.2	Parameter estimation . . . . .	19
<b>3</b>	<b>Modeling</b>	<b>20</b>
3.1	Modeling frames . . . . .	20
3.1.1	Earth-related reference frames . . . . .	21
3.1.2	Aircraft-related reference frames . . . . .	22
3.2	Kinematic model . . . . .	24
3.2.1	Kinematics of translational motion . . . . .	24
3.2.2	Kinematics of rotational motion . . . . .	26
3.3	Dynamic model . . . . .	29
3.3.1	Dynamics of translational motion . . . . .	29
3.3.2	Dynamics of rotational motion . . . . .	30
3.4	Aircraft model . . . . .	32
3.4.1	Mass and inertia model . . . . .	32
3.4.2	Aerodynamic model . . . . .	33
3.4.3	Propulsion model . . . . .	34
3.5	Nonlinear Equations of Motion . . . . .	35
3.5.1	General nonlinear dynamic system . . . . .	36
3.5.2	Nonlinear kinematic Equations of Motion . . . . .	36
3.5.3	Nonlinear dynamic Equations of Motion . . . . .	37
3.5.4	Separation of dynamic Equations of Motion . . . . .	39
3.6	Linear Equations of Motion . . . . .	40
3.6.1	System linearization . . . . .	40
3.6.2	Linear Equations of Motion . . . . .	42
<b>4</b>	<b>Flight parameter estimation</b>	<b>45</b>
4.1	Control inputs for system identification . . . . .	45
4.1.1	Time domain based inputs for identification . . . . .	45
4.1.2	Frequency domain based inputs for identification . . . . .	46
4.1.3	Typical maneuvers in longitudinal and lateral/directional motion . . . . .	47
4.2	Data acquisition . . . . .	47
4.2.1	Pilot input and control surface deflection sensors . . . . .	47
4.2.2	Position, orientation and motion sensors . . . . .	49

4.2.3	Airdata sensors . . . . .	50
4.2.4	Engine data sensors . . . . .	51
4.3	Flight Path Reconstruction . . . . .	52
4.3.1	Bias and gain error . . . . .	52
4.3.2	Position error . . . . .	53
4.3.3	Measurement and process noise . . . . .	53
4.3.4	Kalman Filter . . . . .	53
4.4	A-priori values acquisition . . . . .	57
4.4.1	Tornado . . . . .	57
4.4.2	AVL . . . . .	58
4.4.3	Datcom . . . . .	58
4.5	Estimation methods . . . . .	58
4.5.1	Equation Error Method . . . . .	59
4.5.2	Output Error Method . . . . .	62
4.5.3	Recursive Least-Squares . . . . .	66
4.5.4	Other approaches . . . . .	67
<b>5</b>	<b>Experimental results</b> . . . . .	<b>68</b>
5.1	Research airplane . . . . .	68
5.1.1	Description of the airplane . . . . .	68
5.1.2	Flight envelope . . . . .	70
5.1.3	Airplane's center of mass . . . . .	71
5.2	Instrumentation . . . . .	72
5.2.1	Data Acquisition System . . . . .	72
5.2.2	Utilized sensors . . . . .	73
5.2.3	Primary Flight Display . . . . .	76
5.3	Flight data acquisition and preprocessing . . . . .	78
5.3.1	Dynamic longitudinal stability . . . . .	78
5.3.2	Flight campaign . . . . .	79
5.3.3	Flight Path Reconstruction . . . . .	79
5.4	A-priori data . . . . .	81
5.4.1	Tornado software estimates . . . . .	81
5.4.2	AVL software estimates . . . . .	82
5.4.3	Datcom software estimates . . . . .	82
5.5	Parameter estimation . . . . .	82
5.5.1	Force parameters . . . . .	83
5.5.2	Moment parameters . . . . .	85
5.5.3	Model validation . . . . .	87
5.6	Summary . . . . .	89
5.6.1	Linear dependency of parameters . . . . .	89
5.6.2	Simulation and model validation . . . . .	89
5.6.3	Correction of a-priori values . . . . .	89
5.6.4	Comparison with other airplane category . . . . .	90
<b>6</b>	<b>Conclusion and future work</b> . . . . .	<b>92</b>
<b>A</b>	<b>Coordinate systems</b> . . . . .	<b>99</b>
<b>B</b>	<b>WGS84 model</b> . . . . .	<b>102</b>

<b>C</b>	<b>ICAO Standard atmosphere</b>	<b>103</b>
<b>D</b>	<b>Aircraft regulatory authorities</b>	<b>104</b>
<b>E</b>	<b>EASA classification of aircraft</b>	<b>105</b>
<b>F</b>	<b>Airplane structure description</b>	<b>107</b>
<b>G</b>	<b>Additional results of model validation</b>	<b>109</b>
<b>H</b>	<b>Model of an F-18 Hornet</b>	<b>116</b>

# List of Figures

2.1	Airplane as a system . . . . .	18
3.1	Earth-related reference frames . . . . .	21
3.2	Aircraft-related reference frames . . . . .	22
3.3	Dataflow diagram of a nonlinear system . . . . .	36
3.4	Dataflow diagram of a linear State-Space model . . . . .	41
4.1	Identification process flow . . . . .	45
4.2	Input maneuver examples . . . . .	46
4.3	Dataflow diagram of a discrete state-space model . . . . .	55
4.4	Estimation methods categorization . . . . .	59
4.5	Block diagram of the EEM . . . . .	61
4.6	Block diagram of the OEM . . . . .	64
5.1	Photography of the experimental airplane . . . . .	68
5.2	Operational flight envelope . . . . .	70
5.3	Data Acquisition System with sensors and PFD . . . . .	72
5.4	The NI CompactRIO modules . . . . .	74
5.5	Xsens MTi-G Attitude and Heading Reference System . . . . .	74
5.6	Potentiometer SRS280 . . . . .	75
5.7	Installation of strain gauges used in the airplane . . . . .	75
5.8	Visualization of the SpaceAge 100400 Mini Air Data Boom . . . . .	75
5.9	Scheme of the Primary Flight Display . . . . .	76
5.10	Photography of the Primary Flight Display . . . . .	77
5.11	Comparison of the data before and after FPR process . . . . .	80
5.12	Airplane's model in Tornado software . . . . .	81
5.13	Airplane model in AVL software . . . . .	82
5.14	Graph of force parameters . . . . .	83
5.15	Graph of drag curve . . . . .	84
5.16	Graph of lift curve . . . . .	84
5.17	Graph of parameter $C_{m0}$ . . . . .	85
5.18	Graph of parameter $C_{m\alpha}$ . . . . .	86
5.19	Graph of parameter $C_{mq}$ . . . . .	86
5.20	Graph of parameter $C_{m\delta_e}$ . . . . .	87
5.21	Recorded data for maneuver N <sup>o</sup> 124 . . . . .	88
F.1	Airplane control surfaces . . . . .	107
G.1	Recorded data for maneuver N <sup>o</sup> 24 . . . . .	110
G.2	Recorded data for maneuver N <sup>o</sup> 127 . . . . .	111

G.3	Recorded data for maneuver N° 129	112
G.4	Recorded data for maneuver N° 132	113
G.5	Recorded data for maneuver N° 133	114
G.6	Recorded data for maneuver N° 182	115

# List of Tables

5.1	Control surface deflections of Evezkor SportStar RTC . . . . .	69
5.2	Propulsion parameters . . . . .	69
5.3	Tactical data of Evezkor SportStar RTC . . . . .	70
5.4	Tactical data of Primary Flight Display . . . . .	77
5.5	Location of LKKU aerodrome . . . . .	79
5.6	Comparison of a-priori force parameters and force parameters obtained by estimation methods based on experimental flight data . . . . .	89
5.7	Comparison of a-priori moment parameters and moment parameters obtained by estimation methods based on experimental flight data at center of mass position 30%MAC . . . . .	90
5.8	Comparison of a-priori moment parameters and moment parameters obtained by estimation methods based experimental flight data at center of mass position 32%MAC . . . . .	90
5.9	Comparison of relative values of low subsonic flight parameters between Sport-Star RTC and F-18 Hornet . . . . .	91
B.1	WGS84 Defining Parameters . . . . .	102
C.1	Selected parameters of ICAO Standard Atmosphere . . . . .	103
H.1	Corrections of flight parameter estimations for a F-18 Hornet model at Mach 0.2 . . . . .	116

# Glossary

## Abbreviations

<b>Symbol</b>	<b>Description</b>
ADC	Analog to Digital Converter
AFB	Air Force Base
AGARD	Advisory Group for Aerospace Research and Development
AHRS	Attitude and Heading Reference System
AIAA	American Institute of Aeronautics and Astronautics
AIM	Analog Input Module
AMRL	Aerospace Medical Research Laboratories
ANSI	American National Standards Institute
ARINC	Aeronautical Radio, Incorporated
AVL	Athena Vortex Lattice
BRP	Bombardier Recreational Products
CAA	Civil Aviation Authority
CAD	Computer Aided Design
CAN	Controller Area Network
CHT	Cylinder Head Temperature
CRC	Chemical Rubber Company
CS	Certification Specifications
DAQ	Data Acquisition System
DRAM	Dynamic Random Access Memory
DUT	Delft University of Technology
EASA	European Aviation Safety Agency
ECEF	Earth-Centered Earth-Fixed
ECI	Earth-Centered Inertial
EEM	Equation Error Method
EGT	Exhaust Gas Temperature
EKF	Extended Kalman Filter
EoM	Equations of Motion
FAA	Federal Aviation Administration
FOG	Fiber Optics Gyroscopes
FPGA	Field-Programmable Gate Array

FPR	Flight Path Reconstruction
GLONASS	ГЛОбальная НАвигационная Спутниковая Система
GNSS	Global Navigation Satellite System
GPS	Global Positioning System
HB	Hot Air Ballons
ICAO	International Civil Aviation Organization
ICRS	International Celestial Reference System
IEEE	Institute of Electrical and Electronics Engineers
IFNS	Integrated Flight State and Navigation Sensor
IMU	Inertial Measurement Unit
ISAIM	Isolated Simultaneous Analog Input Module
ISO	International Organization for Standardization
KF	Kalman Filter
LAA	Light Aircraft Association of the Czech Republic
LCD	Liquid Crystal Display
LED	Light-Emitting Diode
LSA	Light Sport Airplane
MAC	Mean Aerodynamic Chord
MADB	Mini Air Data Boom
MEMS	Microelectromechanical Systems
MIT	Massachusetts Institute of Technology
MNR	Modified Newton-Raphson
MTOW	Maximum Take-off Weight
NED	North-East-Down
NI	National Instruments
NIMA	National Imagery and Mapping Agency
OAT	Outside Air Temperature
OEM	Output Error Method
OLS	Ordinary Least-Squares
OM	Operator's Manual
PFD	Primary Flight Display
PZL	Polskie Zakłady Lotnicze
RAM	Random Access Memory
RIO	Reconfigurable Input/Output
RLG	Ring Laser Gyroscopes
RLS	Recursive Least-Squares

RON	Research Octane Number
RTC	Restricted Type Certificate
SRS	Sealed Rotary Sensor
SSD	Solid-State Drive
TGB	Tethered Gas Ballons
TPS	Test Pilot School
UAIM	Universal Analog Input Module
ULA	Ultralight Airplanes
ULG	Ultralight Gliders
ULH	Ultralight Helicopters
USAF	United States Air Force
UTC	Universal Time Coordinated
VLA	Very Light Airplane
VLM	Vortex Lattice Method
VLR	Very Light Rotorcraft
WGS	World Geodetic System
WLS	Weighted Least-Squares
WSCG	Winter School of Computer Graphics

## Greek Symbols

Symbol	Description
$\alpha$	Angle-of-attack
$\vec{\alpha}$	Angular acceleration vector
$\beta$	Angle-of-sideslip
$\beta_f$	Flank angle
$\mathbf{\Gamma}$	Discrete input matrix
$\delta_a$	Antisymmetric aileron deflection
$\delta_e$	Elevator deflection
$\delta_r$	Rudder deflection
$\vec{\eta}$	Step vector
$\theta$	Pitch/elevation angle
$\vec{\theta}$	Vector of parameters
$\vec{\Theta}$	Euler angles vector
$\dot{\Theta}$	Angular rates vector
$\kappa$	Ratio of specific heat at constant pressure to specific heat at constant volume

$\mathbf{\Lambda}$	Discrete noise input matrix
$\vec{\mu}$	Mean of normal distribution vector
$\vec{v}$	Measurement noise vector
$\rho$	Air mass density
$\rho_0$	Standard dry air mass density at sea level
$\mathbf{\Sigma}$	Covariance matrix of normal distribution
$\vec{\tau}$	Moment of force vector
$\phi$	Roll/bank angle
$\mathbf{\Phi}$	Discrete state matrix
$\varphi$	Geodetic latitude
$\vec{\chi}$	General vector
$\psi$	Heading/azimuth/yaw angle
$\omega$	Magnitude of angular velocity
$\vec{\omega}$	Angular velocity vector
$\omega_{ei}$	Angular velocity of the Earth

## Latin Symbols

Symbol	Description
$a$	Semi-major axis of the WGS84 ellipsoid
$\vec{a}$	Translational acceleration vector
$\mathbf{A}$	State/system matrix
$b$	Bias
$b_w$	Reference wingspan
$\mathbf{B}$	Input matrix
$\bar{c}$	Length of Mean Aerodynamic Chord
$C_D$	Drag coefficient
$C_{D0}$	Coefficient of drag force without contribution of angle-of-attack, pitch rate and elevator
$C_{D\alpha}$	Coefficient of drag force derivative with respect to angle-of-attack
$C_{D\delta_e}$	Coefficient of drag force derivative with respect to elevator deflection
$C_{Dq}$	Coefficient of drag force derivative with respect to pitch rate
$C_L$	Lift coefficient
$C_{L0}$	Coefficient of lift force without contribution of angle-of-attack, pitch rate and elevator
$C_{L\alpha}$	Coefficient of lift force derivative with respect to angle-of-attack
$C_{L\delta_e}$	Coefficient of lift force derivative with respect to elevator deflection

$C_{Lq}$	Coefficient of lift force derivative with respect to pitch rate
$C_{m0}$	Coefficient of pitching moment without contribution of angle-of-attack, pitch rate and elevator
$C_{m\alpha}$	Coefficient of pitching moment derivative with respect to angle-of-attack
$C_{m\delta_e}$	Coefficient of pitching moment derivative with respect to elevator deflection
$C_{mq}$	Coefficient of pitching moment derivative with respect to pitch rate
$C_T$	Dimensionless output thrust coefficient
$\mathbf{C}$	Output matrix
$\mathbf{C}_{ob}$	Rotation matrix
$D_P$	Propeller's diameter
$\mathbf{D}$	Feed-through/feed forward matrix
$e$	First eccentricity of the WGS84 ellipsoid
$f$	Flattening of the WGS84 ellipsoid
$\vec{f}$	Specific force vector
$f()$	State function
$f'()$	Discrete state function
$F$	Magnitude of force
$\vec{F}$	Force vector
$\vec{g}_0$	Gravitational acceleration
$\vec{G}$	Gravitational force vector
$G_0$	Magnitude of the standard acceleration of the free fall
$GM$	Gravitational constant of Earth
$\mathbf{G}$	Gradient matrix
$h$	Height above the WGS84 ellipsoid
$\vec{h}$	Angular momentum vector
$h()$	Output function
$h'()$	Discrete output function
$H$	Geopotential pressure altitude
$J$	Moment of inertia / Element of inertia tensor
$J()$	Cost function
$\mathbf{J}$	Inertia tensor
$K$	Scale factor
$\mathbf{K}$	Kalman gain matrix
$L$	Moment of force acting around axis $x_b$
$L_1$	Temperature gradient in the first layer of atmosphere
$m$	Mass of the object
$M$	Moment of force acting around axis $y_b$

$M_0$	Meridian radius of the curvature of the WGS84 ellipsoid
$\mathbf{M}$	System model
$\mathbf{M}_q$	Information matrix
$N$	Moment of force acting around axis $z_b$
$N_0$	Prime vertical radius of the curvature of the WGS84 ellipsoid
$n_P$	Propeller's rotational speed
$p$	Angular velocity around axis $x_b$
$p()$	Probability density function
$\vec{p}$	Translational momentum vector
$p^*$	Dimensionless angular velocity around axis $x_b$
$p_0$	Standard airpressure at the sea level
$p_s$	Instant static pressure of free stream
$\mathbf{P}$	Probability matrix
$\mathbf{P}_r$	State covariance matrix
$q$	Angular velocity around axis $y_b$
$\bar{q}$	Instant dynamic pressure
$q^*$	Dimensionless angular velocity around axis $y_b$
$\mathbf{Q}$	Process noise covariance matrix
$r$	Angular velocity around axis $z_b$
$r$	Radius
$\vec{r}$	Position vector
$r^*$	Dimensionless angular velocity around axis $z_b$
$R$	Specific gas constant for dry air
$\mathbf{R}$	Measurement noise covariance matrix
$S$	Reference wing area
$\mathbf{S}$	Sensitivity Jacobian matrix
$t$	Time
$T$	Instant thermodynamic temperature of the air
$T_0$	Standard thermodynamic temperature of air at sea level
$u$	Translational velocity along axis $x_b$
$\vec{u}$	Input/control vector
$v$	Translational velocity along axis $y_b$
$\vec{v}$	Translational velocity vector
$V$	Magnitude of the true airspeed
$V_{FE}$	Maximum flap extended speed
$V_H$	Maximum level speed

$V_{NE}$	Never exceed speed
$V_{S1}$	Stall speed
$\mathbf{V}$	Estimation of variance
$w$	Translational velocity along axis $z_b$
$\vec{w}$	Process noise vector
$x$	Position along x-axis
$\vec{x}$	State vector
$\vec{x}_0$	Initial state vector
$X$	Force acting along x-axis
$\mathbf{X}$	Matrix of regressors
$y$	Position along y-axis
$\vec{y}$	Output vector
$Y$	Force acting along y-axis
$z$	Position along z-axis
$Z$	Force acting along z-axis
$\vec{z}$	Measured output vector

## Other Symbols

Symbol	Description
0	Earth's center of mass
$\ell$	Geodetic longitude

## Superscripts

Symbol	Description
$C$	Cylindrical coordinate system
$G$	Geodetic coordinate system
$S$	Spherical coordinate system

## Subscripts

Symbol	Description
$a$	Aerodynamic reference frame
$A$	Aerodynamic
$b$	Body-fixed reference frame
$C$	Accelerometer

$d$	Design reference frame
$e$	Geocentric/ECEF reference frame
$f$	General reference frame
$F$	Front wheel
$G$	Aircraft's center of mass
$i$	Inertial/ECI reference frame
$L$	Left main wheel
$m$	Measured
$o$	Geodetic reference frame
$p$	Mean of normal distribution
$P$	Propulsion/Propeller
$R$	Right main wheel
$s$	Stability reference frame
$t$	Trim/equilibrium point
$x$	X-axis component
$X$	Arbitrary point
$y$	Y-axis component
$z$	Z-axis component

# 1. Introduction

In 2009, Federal Aviation Administration (FAA) conducted a study regarding the safety of Light Sport Airplanes (LSA) [39] in the USA. They have discovered that the LSA has over 2.5 times higher fatal accidents rate than the CS<sup>1</sup>-23 airplanes. During the investigated period, 39 fatal LSA accidents were observed, 54% were due to the loss of control, 10% were due to the structural failure. To decrease the high fatal accident rate of LSA, it seems to be necessary to increase the pilot awareness and to reduce pilots' workload during all phases of flight.

The estimation of the flight parameters and building a high fidelity model of the airplane enables manufacturing of build a flight simulators, which will be able to match the behavior of the real airplane more precisely and therefore improve pilot training. The estimated flight parameters are also the prerequisites in design of an advanced 4-axis autopilot, which can lower pilots' workload during the flight.

Moreover, knowledge of the flight parameters can be useful during the development of new airplane to verify the validity of the design within the flight envelope and to enable to focus the tests on specific points of the flight envelope.

Another major application of the identified aircraft model is the aircraft certification process, as the identified model can be used to investigate the stability point. The dynamic stability is one of the requirements of the EASA (European Aviation Safety Agency) Certification Standards, e.g., CS-23 paragraph 181, CS-25 paragraph 181 and CS-VLA<sup>2</sup> paragraph 181.

Due to the existence of a large amount of flight parameters, the author has decided to focus on the estimation of the static stability parameters, damping and control derivatives of the longitudinal motion. The input data were recorded during the test flights on an experimental airplane. For the purposes of the flight tests, the flight envelope was limited to the conditions of altitudes, airspeed and position of center of mass, as consulted with the airplane manufacturer. The limits reflect the safety constraints to prevent extreme attitudes.

---

<sup>1</sup>CS – Certification Specifications

<sup>2</sup>VLA – Very Light Airplane

## 1.1 Objectives of the thesis

According to the above mentioned facts, the objectives of this Ph.D. thesis were set as follows:

1. Research on the theory of flight data acquisition, flight parameters estimation, including the sensors used in avionics and Equations of Motion, respectively.
2. Selection of algorithms suitable for the flight parameters estimation of a light airplane.
3. Implementation of selected algorithms and evaluation of the results including proposals for future work.

In the evaluation of the results, following main research questions are addressed:

1. Do the flight parameters of the longitudinal motion fall within the range of values expected for this category of airplanes?
2. Do the force coefficients contained in the above mentioned flight parameters of longitudinal motion exhibit linear behavior for the investigated part of the flight envelope?
3. Do the estimated flight parameters describe sufficiently the airplane aerodynamics? Do, therefore, the simulated flight data based on the estimated flight parameters sufficiently correspond to the measured flight data?
4. What are the correction factors between the a-priori data and their refined values obtained using the parameter estimation methods on the basis of the measured flight data?
5. Are the above mentioned corrections similar to other categories of airplanes?

## 1.2 Outline of the thesis

This thesis is organized as follows. The Chapter 2 describes the basic terms and principles of the identification and the parameter estimation.

Chapter 3 contains description of the modeling of the airplane. This chapter starts with a description of the reference frames. Then kinematic and dynamic models of a physical object are given. This chapter also contains necessary description of the airplane models and introduces their flight parameters. Later in this chapter, detailed description of the non-linear kinematic and dynamic Equations of Motion is presented. Non-linear Equations of Motion are separated to the longitudinal motion equations and the lateral and direction motion equations. At the end of this chapter, a linearization process and resultant linearized Equations of Motion are presented. Due to the large amount of theory in these topics, only the parts needed as a theoretical background for the following chapters are introduced.

Chapter 4 starts with a brief overview of the whole process to estimate the flight parameters, followed by the control inputs for the estimation, as with an emphasis on light airplanes. The

chapter contains an overview of the Data Acquisition System and the commonly used aircraft sensors, e.g., position, orientation and motion sensors, and airdata sensors. It continues with the Flight Path Reconstruction (FPR) based on the non-linear kinematic Equations of Motion. The sources of a-priori flight parameters are described. The various methods for the estimation of the flight parameters along with their advantages and disadvantages are also discussed. This chapter includes the industry standard practices and also the recommended approaches, i.e., Equation Error Method (EEM), Output Error Method (OEM) and Recursive Least-Squares (RLS). At the end of this chapter, an alternative approach, e.g., Artificial neural networks and Genetic algorithms, are briefly discussed.

Chapter 5 contains description of the preparation of the flight experiments. This chapter starts with a detailed description of the experimental airplane, followed by the description of the used instrumentation. Later in this chapter, the flight data gathered during the flight campaign, flight campaign itself, and Flight Path Reconstruction results are presented. This is followed by the a-priori data from different estimation sources. Considering the large number of existing flight parameters, the output of EEM, OEM, RLS is compared and discussed for a selected group of the flight parameters. At the end of this chapter, the summary of experimental results is given.

The last chapter is dedicated to the Conclusion. It contains a brief summary of the whole thesis and a description of possible future work.

Moreover, this thesis contains several appendices, which provide supplementary information. The first appendix contains description of four coordinate system used in this thesis. The second and third appendices describe the WGS<sup>3</sup>84 model of the Earth and ICAO<sup>4</sup> Standard atmosphere, respectively, along with tables of constants. The fourth appendix deals with the aircraft regulatory authorities in the Czech Republic. The fifth appendix presents EASA classification of the aircrafts. The sixth appendix contains structural description of typical representative of light airplane category. The seventh appendix presents additional result of model validation. The last appendix contains correction factors for a F-18 Hornet model flight parameters estimations.

A list of publications, research and teaching activities during my Ph.D. study is also attached.

---

<sup>3</sup>WGS – World Geodetic System

<sup>4</sup>ICAO – International Civil Aviation Organization

## 2. System identification

It can be said, that identification is one of the control theory general problems. Control theory deals with three sources of information and three general problems. The control theory informations are: Input, System model and Output (see Figure 2.1). The control theory problems are: Simulation, Control and System Identification.

**Input**  $\vec{u}$  is vector of control variables, e.g., position of control surfaces, state of surrounding environment.

**Output**  $\vec{y}$  is vector of measurable variables on airplane, e.g., position, altitude, attitude and velocity.

**System model**  $M$  consists of a mass and inertia model, propulsion model, aerodynamic model, landing gear reaction model and structural model. Aerodynamic model contains the flight parameters, which are the characteristic of a particular airplane.

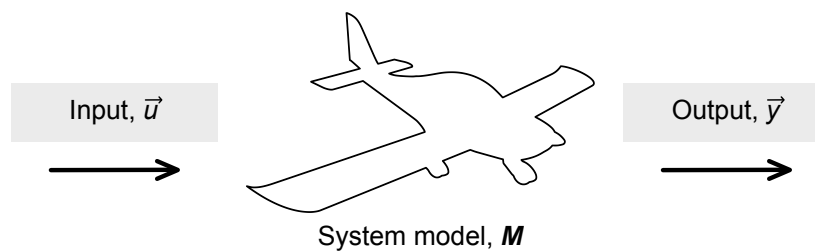


Figure 2.1: Airplane as a system.

**Simulation** solves the question: How will the aircraft, modeled by a system model  $M$ , react to input  $\vec{u}$ ? The reaction will be the output  $\vec{y}$ .

**Control** solves the question: Which input  $\vec{u}$  applied to the system model  $M$  leads to the state specified by the output  $\vec{y}$ ?

**Identification** solves the question: Which system model  $M$  describes the aircraft, which reacts to an input  $\vec{u}$  by an output  $\vec{y}$ ?

System identification consists of two main parts: model structure identification and parameter estimation.

### 2.1 Model structure identification

The model structure identification is a process of determining the system model. The system model is an abstract container and uses parameters for the particular model, i.e., aerodynamic model. There are three main types of system models: White-box, Gray-box and Black-box.

Systems known to its details are called the White-box systems as all their internal physical dependencies are known. Models of simple physical systems can be usually modeled as White-box systems.

Gray-box systems are empirically known, some of its internal is known, but some parts has purely stochastic form. The aircraft in general are usually modeled as Gray-box system, because the kinematic part of the description is known but dynamics of the aircraft is modeled stochastically.

The internal structure of the Black-box system is unknown and it is a part of the system identification to identify the model structure of the system.

For the purposes of this thesis, a Gray-box mathematical model is used. The model contains physical model of a rigid body and is described in details in the following chapter.

## 2.2 Parameter estimation

The parameter estimation is a process of matching parameters of a system model. The parameter estimation uses the model structure to estimate its parameters.

The specifics of the parameter estimation in aerospace are presented in Chapter 4. The parameter estimation includes the system model with parameters, the inputs injected into the system and the estimation methods.

The inputs used for the identification are used to excite the system response. This response is then used for parameter estimation. More details related to the used inputs are presented in Section 4.1.

The parameter estimation employs different methods of numerical optimization. Each system model restricts the usage of some methods. Some methods are more appropriate than others. The description of the estimation methods usable for flight parameter estimation is given in Section 4.5.

The system model originated from the model structure identification, uses the knowledge of the system behavior. Further details related to the model are introduced in the following chapter.

# 3. Modeling

In this chapter, it is necessary to describe the modeling behind the identification process, i.e., mostly kinematics and dynamics of motion, and present the used notation. Because of a large amount of theory, only parts needed as a theoretical background for this thesis are presented. Notation introduced in this thesis is based on standards ISO<sup>1</sup> 80000-1:2009 [51] and ISO 80000-2:2009 [52].

Firstly, the reference frame used for modeling of an airplane is presented. Secondly, kinematics of translational and rotational motion, e.g., positions, velocity and acceleration, is described. Thirdly, rigid body dynamics, e.g., force and moment of force, is given. Fourthly, the airplane subsystems modeling is presented. Fifthly, the nonlinear Equations of Motion are composed and split into symmetric and antisymmetric equations. Finally, the linearization process and the resultant linear Equations of Motion are described.

## 3.1 Modeling frames

A reference frame is the prerequisite in the description and modeling of motion. The reference frame is an axis system with a defined point at the origin [76]. This thesis considers three-dimensional orthogonal spaces only. Reference frames used in aerospace are right-hand orthogonal systems, which means that the relation between unit vectors  $\vec{x}$ ,  $\vec{y}$  and  $\vec{z}$  is [87]:

$$\vec{z} = \vec{x} \times \vec{y} \tag{3.1}$$

There are many reference frames used to describe the motion of an aircraft. For the purposes of this thesis, seven reference frames are used:

- $F_i$  – Inertial reference frame / Earth-Centered Inertial (ECI) reference frame;
- $F_e$  – Geocentric reference frame / Earth-Centered Earth-Fixed (ECEF) reference frame;
- $F_o$  – Geodetic reference frame / North-East-Down (NED) reference frame;
- $F_b$  – Body-fixed reference frame;
- $F_s$  – Stability reference frame;
- $F_a$  – Aerodynamic reference frame;
- $F_d$  – Design reference frame.

Reference frames can be divided into two categories according to the object defining axis system: Earth-related reference frames and Aircraft-related reference frames. However, in general, each rigid body is considered to have its own reference frame [64].

---

<sup>1</sup>ISO – International Organization for Standardization

### 3.1.1 Earth-related reference frames

There are three Earth-related reference frames used in this thesis for modeling (see Figure 3.1): Inertial reference frame, Geocentric reference frame and Geodetic reference frame.

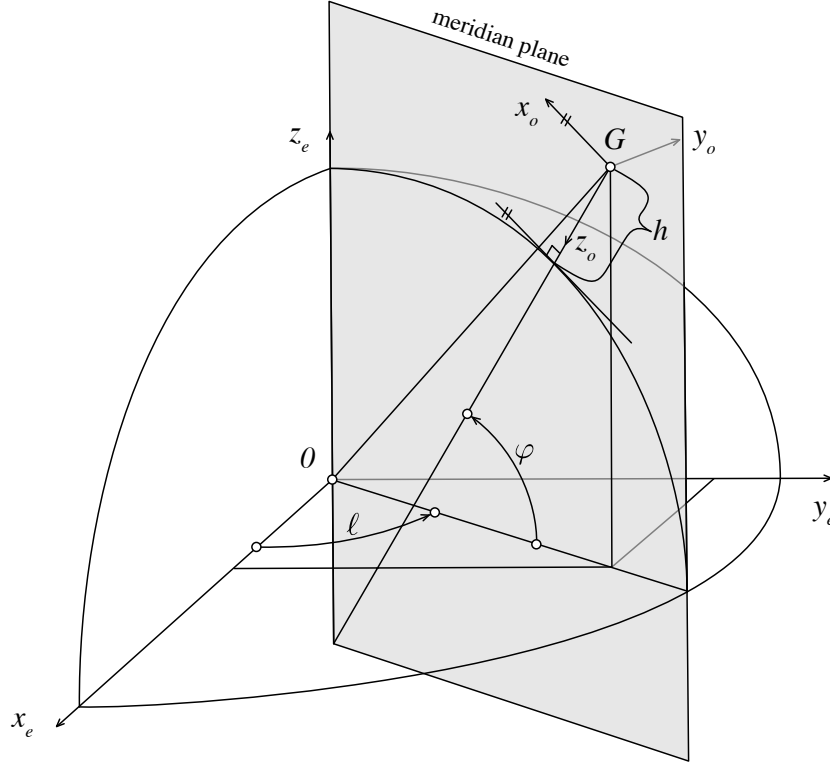


Figure 3.1: Earth-related reference frames.

**Inertial reference frame**, also known as the Earth-Centered Inertial (ECI) reference frame, is fixed to the distant stars [13, 49, 83]. Inertial reference frame is denoted by the subscript  $i$  and it is used to define the Earth's rotation. An origin of the Inertial reference frame is the Earth's center of mass  $0$ , axis  $x_i$  points toward the Alpha Arietis [1], axis  $z_i$  is the Earth rotation axis and axis  $y_i$  completes the right-hand system.

**Geocentric reference frame** is fixed to the Earth. This reference frame is sometimes called the ECEF (Earth-Centered Earth-Fixed) reference frame because its origin is the Earth's center of mass  $0$  and axes are fixed to the Earth [3, 13, 83]. ECEF reference frame is denoted by a subscript  $e$  and is used to determine the position with respect to the Earth. Axis  $x_e$  points through the prime meridian, axis  $z_e$  is the Earth's rotation axis and axis  $y_e$  completes the right-hand system. The rotation speed between the Inertial reference frame and the ECEF reference frame, i.e., Angular velocity of the Earth, is the  $\omega_{ei}$ .

A conversion between the reference frames  $F_i$  and  $F_e$  is defined by the rotation matrix  $\mathbf{C}_{ei}$  as follows [13, 87]:

$$\mathbf{C}_{ei} = \begin{bmatrix} \cos \omega_{ei} t & \sin \omega_{ei} t & 0 \\ -\sin \omega_{ei} t & \cos \omega_{ei} t & 0 \\ 0 & 0 & 1 \end{bmatrix} \quad (3.2)$$

where  $t$  is the time in seconds since the standard epoch. Currently used epoch is J2000.0 which started on 1<sup>st</sup> January 2000 11:58:55.816 UTC<sup>2</sup> [44].

**Geodetic reference frame**, also known as the North–East–Down (NED) reference frame, is fixed to the Earth’s surface and is used as a reference for the specification of the attitude of the aircraft [13, 80, 83]. Geodetic reference frame is denoted by a subscript  $o$ . Origin of this reference frame is in the aircraft’s center of mass  $G$ , the axis  $x_o$  is parallel to the local geoid surface, pointing to the geographic north, axis  $z_o$  is pointing downwards, perpendicular to the local geoid surface (surface normal does not cross point 0), axis  $y_o$  is parallel to the local geoid surface, pointing to the east to form a right–hand system.

A conversion between the reference frames  $F_e$  and  $F_o$  is defined by a rotation matrix  $\mathbf{C}_{oe}$  as follows [13, 87]:

$$\mathbf{C}_{oe} = \begin{bmatrix} -\cos \ell \sin \varphi & -\sin \ell & -\cos \ell \cos \varphi \\ -\sin \ell \sin \varphi & \cos \ell & -\sin \ell \cos \varphi \\ \cos \varphi & 0 & -\sin \varphi \end{bmatrix}_{oe} \quad (3.3)$$

where  $\ell$  is the geodetic longitude and  $\varphi$  is the geodetic latitude.

### 3.1.2 Aircraft–related reference frames

In this thesis, four Aircraft–related reference frames are used (see Figure 3.2): Body–fixed reference frame, Stability reference frame, Aerodynamic reference frame and a Design reference frame.

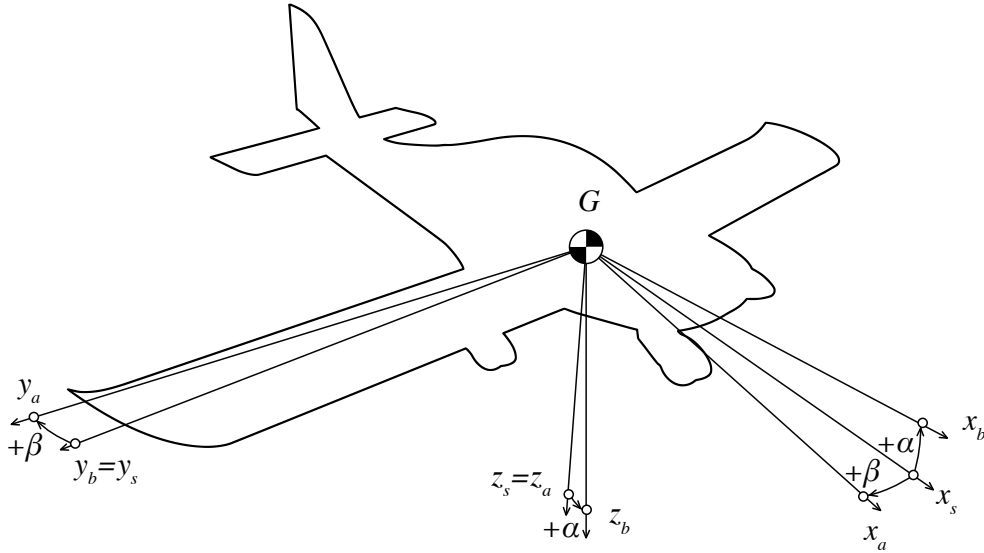


Figure 3.2: Aircraft–related reference frames.

**Body–fixed reference frame** is fixed to the aircraft body [34, 50, 80]. This reference frame is denoted by subscript  $b$ . Its origin is in the aircraft’s center of mass  $G$ , axis  $x_b$  is pointing forward along the fuselage of the aircraft in symmetric plane, axis  $z_b$  is pointing

<sup>2</sup>UTC – Universal Time Coordinated

downward in the aircraft symmetric plane and axis  $y_b$  is pointing to right (starboard) wing to form a right-hand system. Number of variables associated with the aircraft motion are referenced in this reference frame.

**Stability reference frame**, also known as the Intermediate reference frame, is used for the description of the aerodynamic properties [5, 50, 80]. Stability reference frame is denoted by a subscript  $s$ . The origin of the Stability reference frame is in the aircraft's center of mass  $G$ , axis  $x_s$  is a projection of the free stream air velocity to the  $x_b z_b$  plane of the aircraft's symmetry. The  $y_s$  axis is equal to the axis  $y_b$  of the Body-fixed reference frame. The  $z_s$  axis points downwards in the symmetry plane to form a right-hand system. The rotation angle between the Body-fixed reference frame and the Stability reference frame, i.e., the angle between axis  $x_s$  and axis  $x_b$ , is known as the angle-of-attack  $\alpha$  [34, 87].

A conversion between the  $F_b$  and the  $F_s$  is defined by the rotation matrix  $C_{sb}$  as follows [80, 87]:

$$C_{sb} = \begin{bmatrix} \cos \alpha & 0 & \sin \alpha \\ 0 & 1 & 0 \\ -\sin \alpha & 0 & \cos \alpha \end{bmatrix}_{sb} \quad (3.4)$$

**Aerodynamic reference frame**, sometimes called the Air-path reference frame, is used for the description of the airflow around an aircraft [34, 50, 80]. The aerodynamic reference frame is denoted by a subscript  $a$ . Origin of the Aerodynamic reference frame is in the aircraft's center of mass  $G$ , axis  $x_a$  is aligned with the free stream velocity, axis  $z_a$  pointing downwards in the symmetry plane of the aircraft and axis  $y_a$  is pointing right perpendicular to the  $x_a$  and  $z_a$  axes. Rotation angle between the Aerodynamic reference frame and the Stability reference frame, i.e., angle between axis  $x_s$  and axis  $x_a$ , is the angle-of-sideslip  $\beta$  [34, 87].

A conversion between the  $F_s$  and the  $F_a$  is defined by the rotation matrix  $C_{as}$  as follows [80, 87]:

$$C_{as} = \begin{bmatrix} \cos \beta & \sin \beta & 0 \\ -\sin \beta & \cos \beta & 0 \\ 0 & 0 & 1 \end{bmatrix}_{as} \quad (3.5)$$

**Design reference frame** is used for the description of the main aircraft parts and position of the center of mass of the aircraft [16]. This reference frame is denoted by a subscript  $c$ . Origin of the Design reference frame can be positioned differently depending on the type of aircraft (or manufacturer). For the purposes of this thesis, the origin of the Design reference frame is placed to the intersection of the fuselage base plane and the line passing through the nose cone point perpendicular to the base plane of the fuselage. The  $x_d$  axis is the intersection of the fuselage base plane and the symmetry plane of the aircraft and pointing towards the tail. The  $z_d$  axis is the line perpendicular to the fuselage base plane, passing through the nose cone and pointing upwards. The  $y_d$  axis is pointing to right (starboard) wing to form right-hand system. Axes  $x_d$  and  $x_b$  are parallel lines pointing in opposite directions, the same applies to the  $z_d$  and  $z_b$  axes. Axes  $y_d$  and  $y_b$  are parallel lines having the same spatial orientation.

## 3.2 Kinematic model

The kinematics describes the motion of an object without the consideration of its mass and forces acting on it. The kinematic model can be divided into two parts: kinematics of the translational motion and the kinematics of the rotational motion.

### 3.2.1 Kinematics of translational motion

First of all, it is necessary to describe the position of an object and then proceed its velocity and acceleration.

**Positions** in aerospace applications are often specified in a Cartesian coordinate system<sup>3</sup> using metric length units. [31, 62].

$$\vec{r}_{Xf} = \begin{bmatrix} x \\ y \\ z \end{bmatrix}_{Xf} \quad (3.6)$$

where  $x, y, z$  are the positions along particular axes and  $X$  is the arbitrary point.

**Translational velocity** describes the change of position in time and is given in meters per second [31, 87]. Translational velocity  $\vec{v}_{Gf}$  of the aircraft's center of mass  $G$  relative to the general reference frame  $F_f$  is defined in the following term:

$$\frac{d\vec{r}_{Gf}}{dt} = \begin{bmatrix} \dot{x} \\ \dot{y} \\ \dot{z} \end{bmatrix}_{Gf} \equiv \vec{v}_{Gf} = \begin{bmatrix} u \\ v \\ w \end{bmatrix}_{Gf} \quad (3.7)$$

where  $u, v, w$  are the translational velocities along particular axes.

The translational velocity can also be expressed using the transformation from the Geodetic coordinate system to the Geodetic reference frame in a Cartesian coordinate system as specified in the following term [3, 87]:

$$\vec{v}_{Xo} = \begin{bmatrix} \dot{\varphi}(M_0 + h) \\ \dot{\ell}(N_0 + h) \cos \varphi \\ -\dot{h} \end{bmatrix}_{Xo} \quad (3.8)$$

where  $h$  is the height above the ellipsoid,  $M_0$  is the meridian radius of curvature of the ellipsoid<sup>4</sup>, and  $N_0$  is the prime vertical radius of curvature of the ellipsoid. These quantities are given by following equations:

$$M_0 = \frac{a(1 - e^2)}{(1 - e^2 \sin^2 \varphi)^{3/2}} \quad (3.9a)$$

$$N_0 = \frac{a}{\sqrt{1 - e^2 \sin^2 \varphi}} \quad (3.9b)$$

<sup>3</sup>Detailed description of the coordinate systems used in aerospace together with the equations describing the conversion between the selected coordinate systems is given in Appendix A.

<sup>4</sup> For the purposes of this thesis, the WGS84 ellipsoid is used. For more details please see Appendix B.

where  $a$  is the semi-major axis of the ellipsoid and  $e$  is the first eccentricity of the ellipsoid equal to:

$$e^2 = 2f - f^2 \quad (3.10)$$

where  $f$  is the flattening of the ellipsoid.

**Aircraft airspeed** (the translational velocity of the aircraft's center of mass  $G$ , relative to the surrounding air) is usually measured in a Spherical coordinate system. A transformation of the translational velocities at point  $G$  in a Spherical coordinate system  $F_b$  to Cartesian coordinate system  $F_b$  are [58, 87]:

$$u_{Gb} = V \cos \beta \cos \alpha \quad (3.11a)$$

$$v_{Gb} = V \sin \beta \quad (3.11b)$$

$$w_{Gb} = V \cos \beta \sin \alpha \quad (3.11c)$$

where  $V$  is the magnitude of the true airspeed.

On the contrary, an inverse transformation, i.e., translational velocity at point  $G$  from a Cartesian coordinate system  $F_b$  to a Spherical coordinate system  $F_b$ , is determined using following expressions [58, 62]:

$$V = \sqrt{u_{Gb}^2 + v_{Gb}^2 + w_{Gb}^2} \quad (3.12a)$$

$$\alpha = \arctan \frac{w_{Gb}}{u_{Gb}} \quad (3.12b)$$

$$\beta = \arcsin \frac{v_{Gb}}{V} \quad (3.12c)$$

**Translational acceleration** describes a change of the translational velocity in time and is given in meters per second squared [3, 13]. The translational acceleration  $\vec{a}_{Gf}$  at point  $G$  relative to the general reference frame  $F_f$  is defined as:

$$\frac{d\vec{v}_{Gf}}{dt} = \begin{bmatrix} \dot{u} \\ \dot{v} \\ \dot{w} \end{bmatrix}_{Gf} \equiv \vec{a}_{Gf} = \begin{bmatrix} a_x \\ a_y \\ a_z \end{bmatrix}_{Gf} \quad (3.13)$$

where  $a_x, a_y, a_z$  are the translational accelerations along particular axes.

**The derivative of the airspeed** describes the translational acceleration of the aircraft's center of mass relative to the surrounding air. Based on Equations 3.12, the derivative of the aircraft airspeed is defined as follows [58, 87]:

$$\dot{V} = \frac{1}{V} (u_{Gb} \dot{u}_{Gb} + v_{Gb} \dot{v}_{Gb} + w_{Gb} \dot{w}_{Gb}) \quad (3.14a)$$

$$\dot{\alpha} = \frac{u_{Gb} \dot{w}_{Gb} - w_{Gb} \dot{u}_{Gb}}{u_{Gb}^2 + w_{Gb}^2} \quad (3.14b)$$

$$\dot{\beta} = \frac{V \dot{v}_{Gb} - v_{Gb} \dot{V}}{V \sqrt{u_{Gb}^2 + w_{Gb}^2}} \quad (3.14c)$$

### 3.2.2 Kinematics of rotational motion

After the kinematics of the translational motion was described, it is important to introduce physical quantities of the rotational motion, i.e., Euler angles, rotation matrix, angular rates, angular velocity and angular acceleration.

The coordinate rotation of a rigid body in a three-dimensional space is defined using a transformation between the reference frame of a rigid body and the reference frame in which we want to describe rotation [87, 91]. The coordinate rotation can be specified using the Rotation matrix or the Euler angles.

**The Euler angles**  $\vec{\Theta}$  are a sequence of three angles which represents the transformation from one reference frame to another [5, 87]. Each angle represents rotation in particular axis. Rotation order used in the aerospace domain is z-y-x. The transformation from the reference frame  $F_o$  to the reference frame  $F_b$  using Euler angles vector  $\vec{\Theta}_{ob}$  is given [5]:

$$\vec{\Theta}_{ob} = \begin{bmatrix} \phi \\ \theta \\ \psi \end{bmatrix}_{ob} \quad (3.15)$$

where  $\phi$  is the angle of rotation around  $x$ -axis (i.e., roll angle or bank angle),  $\theta$  is the angle of rotation around  $y$ -axis (i.e., pitch angle or elevation angle), and  $\psi$  is the angle of rotation around  $z$ -axis (i.e., yaw angle, heading angle or azimuth angle).

Considering the convention for the aerospace applications [5], the yaw angle  $\psi$  can range from  $-\pi$  to  $\pi$ , pitch angle  $\theta$  can range from  $-\pi/2$  to  $\pi/2$  and roll angle  $\phi$  can range from  $-\pi$  to  $\pi$ .

**Rotation matrix  $C$**  (sometimes called the Direction Cosine Matrix) describes the transformation from one reference frame to another frame in the Cartesian coordinate system [83, 87]. Rotation matrix is always orthogonal and its determinant is unity. For example, transformation from the reference frame  $F_o$  to the reference frame  $F_b$  is given by:

$$\vec{\chi}_b = C_{bo} \cdot \vec{\chi}_o \quad (3.16)$$

where  $\vec{\chi}_o$  is the general vector in the reference frame  $F_o$ ,  $\vec{\chi}_b$  is the general vector in the reference frame  $F_b$ , and  $C_{ob}$  is the rotation matrix from the reference frame  $F_o$  to the reference frame  $F_b$ .

Rotation matrix  $C_{ob}$  for an inverse coordinate rotation (i.e., from reference frame  $F_b$  to reference frame  $F_o$ ) is described using following term [13, 87]:

$$C_{ob} = C_{bo}^{-1} = C_{bo}^T \quad (3.17)$$

Rotation matrix  $C_{ab}$  used for the computation of two subsequent transformations (i.e., from reference frame  $F_b$  to reference frame  $F_s$  and then from reference frame  $F_s$  to reference frame  $F_a$ ) can be computed as follows [58, 87].

$$C_{ab} = C_{as} \cdot C_{sb} \quad (3.18)$$

The coordinate transformation in Euler angles can be converted to a rotation matrix, given that coordinate transformation can be divided into three subsequent transformations. The

resultant rotation matrix can be created by combining these three rotation matrices [83, 91]:

$$\mathbf{C}_{ob} = \mathbf{C}_x(\phi) \mathbf{C}_y(\theta) \mathbf{C}_z(\psi) \quad (3.19)$$

where  $\mathbf{C}_x(\phi)$  is the rotation matrix around  $x$  axis,  $\mathbf{C}_y(\theta)$  is the rotation matrix around  $y$  axis, and  $\mathbf{C}_z(\psi)$  is the rotation matrix around  $z$  axis, which are equal to:

$$\mathbf{C}_x(\phi) = \begin{bmatrix} 1 & 0 & 0 \\ 0 & \cos \phi & \sin \phi \\ 0 & -\sin \phi & \cos \phi \end{bmatrix} \quad (3.20a)$$

$$\mathbf{C}_y(\theta) = \begin{bmatrix} \cos \theta & 0 & -\sin \theta \\ 0 & 1 & 0 \\ \sin \theta & 0 & \cos \theta \end{bmatrix} \quad (3.20b)$$

$$\mathbf{C}_z(\psi) = \begin{bmatrix} \cos \psi & \sin \psi & 0 \\ -\sin \psi & \cos \psi & 0 \\ 0 & 0 & 1 \end{bmatrix} \quad (3.20c)$$

The resultant rotation matrix  $\mathbf{C}_{bo}$  is:

$$\mathbf{C}_{bo} = \begin{bmatrix} \cos \theta \cos \psi & \cos \theta \sin \psi & -\sin \theta \\ \sin \phi \sin \theta \cos \psi - \cos \phi \sin \psi & \sin \phi \sin \theta \sin \psi + \cos \phi \cos \psi & \sin \phi \cos \theta \\ \cos \phi \sin \theta \cos \psi + \sin \phi \sin \psi & \cos \phi \sin \theta \sin \psi - \sin \phi \cos \psi & \cos \phi \cos \theta \end{bmatrix}_{bo} \quad (3.21)$$

**The angular velocity** describes the rotation speed from one reference frame to another and is always given in radians per second [31, 87]. The angular velocity  $\vec{\omega}_{ob}$  of the reference frame  $F_o$  relative to the reference frame  $F_b$  is defined in following expression:

$$\vec{\omega}_{ob} = \begin{bmatrix} p \\ q \\ r \end{bmatrix}_{ob} \quad (3.22)$$

where  $p$ ,  $q$ ,  $r$  are the angular velocities around particular axes, whereby all rotations are simultaneous.

**Angular rates**, sometimes called the Euler angle rates, describe the change of the Euler angles in time and are given in radians per second [3, 49]. Angular rates  $\vec{\Theta}_{ob}$  are the time derivatives of the Euler angles of the reference frame  $F_o$  relative to the reference frame  $F_b$  and are defined as follows:

$$\vec{\Theta}_{ob} = \begin{bmatrix} \dot{\phi} \\ \dot{\theta} \\ \dot{\psi} \end{bmatrix}_{ob} \quad (3.23)$$

The transformation of the angular rates to the angular velocities with respect to the Euler angles ranges is defined using following equations [58, 103]:

$$p = \dot{\phi} - \dot{\psi} \sin \theta \quad (3.24a)$$

$$q = \dot{\psi} \cos \theta \sin \phi + \dot{\theta} \cos \phi \quad (3.24b)$$

$$r = \dot{\psi} \cos \theta \cos \phi - \dot{\theta} \sin \phi \quad (3.24c)$$

On the contrary, the transformation from the angular velocities to the angular rates is based on the Equations 3.24, and is given by [58, 62]:

$$\dot{\phi} = p + (q \sin \phi + r \cos \phi) \tan \theta \quad (3.25a)$$

$$\dot{\theta} = q \cos \phi - r \sin \phi \quad (3.25b)$$

$$\dot{\psi} = \frac{q \sin \phi + r \cos \phi}{\cos \theta} \quad (3.25c)$$

Equations 3.25 leads to singularity (similar to Gimbal-lock problem<sup>5</sup>) [46, 57], as there is no solution of Equation 3.25c for  $\theta = \pm\pi/2$ . Gimbal-lock problem can be avoided by using different computation theories (e.g., quaternions [91]).

**The angular acceleration** describes the change of the angular velocity in time and is given in radians per second squared [49, 87]. The angular acceleration  $\vec{\alpha}_{ob}$  of the reference frame  $F_o$  relative to the reference frame  $F_b$  is defined in following terms:

$$\vec{\alpha}_{ob} = \begin{bmatrix} \dot{p} \\ \dot{q} \\ \dot{r} \end{bmatrix}_{ob} \quad (3.26)$$

Given that some reference frames are rotating relative to others, e.g., reference frame  $F_b$  relative to reference frame  $F_o$ , it is necessary to adapt some of the above presented equation to this rotation.

The transformation between the general vectors  $\vec{\chi}$  in rotating reference frames  $F_o$  and  $F_b$  is defined as [58, 80]:

$$\frac{d\vec{\chi}_o}{dt} = \frac{d\vec{\chi}_b}{dt} + \omega_{ob} \times \vec{\chi}_b \quad (3.27)$$

**The translational acceleration**  $\vec{a}_o$ , can be calculated in rotating reference frames using two different approaches. The first approach is based on the use of the translational velocity vector. Given that the translational acceleration is the first derivative of the translational velocity, the  $\vec{a}_o$  can be expressed using Equation 3.27 as:

$$\vec{a}_o = \vec{a}_b + \vec{\omega}_{ob} \times \vec{v}_b \quad (3.28)$$

The second approach is based on the utilization of the position vector. Given that the translational acceleration is the second derivative of the position, the  $\vec{a}_o$  can be expressed using Equation 3.27 as:

$$\vec{a}_o = \vec{a}_b + 2\vec{\omega}_{ob} \times \vec{v}_b + \vec{\omega}_{ob} \times (\vec{\omega}_{ob} \times \vec{r}_b) + \vec{\alpha}_{ob} \times \vec{r}_b \quad (3.29)$$

---

<sup>5</sup>Gimbal-lock is a phenomenon related to mechanical gimbal, when gimbal system loses a degree of freedom due to parallel configuration of several axes.

### 3.3 Dynamic model

The dynamic model of the rigid body describes the causes of the motion, i.e., forces and moments of forces acting on the object. The dynamic model can be divided to two parts: dynamic model of the translational motion and dynamic model of the rotational motion.

#### 3.3.1 Dynamics of translational motion

At the beginning, it is necessary to introduce the translational momentum and then proceed with the description of the force and the specific force.

**Translational momentum**  $\vec{p}$  is given in kilogram meters per second. Translational momentum  $\vec{p}_{Xf}$  of an object in arbitrary point  $X$  relative to the general reference frame  $F_f$  is defined as follows [31, 58]:

$$\vec{p}_{Xf} = m \cdot \vec{v}_{Xf} \quad (3.30)$$

where  $m$  is the mass of the object.

**Force** is given in Newtons. Force  $\vec{F}_{Xi}$  acting on an object in point  $X$  relative to Inertial reference frame  $F_i$  is given by [3, 87]:

$$\vec{F}_{Xi} = \frac{d\vec{p}_{Xi}}{dt} \Rightarrow \vec{F}_{Xi} = \begin{bmatrix} X \\ Y \\ Z \end{bmatrix}_{Xi} \quad (3.31)$$

where  $X, Y, Z$  are the forces acting along particular axes.

According to the Second Newton's laws of motion, sum of external forces on the object in center of mass  $G$  is defined as follows [3, 31]:

$$\sum \vec{F}_{Gi} = m \cdot \vec{a}_{Gi} \quad (3.32)$$

Force  $\vec{F}_o$  was defined as a first derivative of the translational momentum  $\vec{p}_o$ , therefore it can be expressed in rotating reference frames using Equation 3.27 as:

$$\vec{F}_o = \frac{d\vec{p}_b}{dt} + \vec{\omega}_{ob} \times \vec{p}_b \quad (3.33)$$

Furthermore, the derivative of  $\vec{p}_b$  can be substituted with 3.31 followed by 3.32 and  $\vec{p}_b$  can be replaced with 3.30. The resultant equation can be written as

$$\vec{F}_o = m \vec{a}_b + m \vec{\omega}_{ob} \times \vec{v}_b \quad (3.34)$$

**The specific force** describes non-gravitational force per unit mass and is given in meter per second squared [49]. The specific force  $\vec{f}_{Xf}$  acting on an object in point  $X$  relative to the general reference frame  $F_f$  is defined as follows:

$$\vec{f}_{Xf} = \frac{\vec{F}_{Xf} - \vec{G}_{Xf}}{m} \Rightarrow \vec{f}_{Xf} = \begin{bmatrix} f_x \\ f_y \\ f_z \end{bmatrix}_{Xf} \quad (3.35)$$

where  $\vec{G}$  is the gravitational force and  $f_x, f_y, f_z$  are the specific forces acting along particular axes.

Based on the definition of the Geodetic reference frame  $F_o$ , see Section 3.1.1, gravitational force  $\vec{G}_b$  acting on an arbitrary object can be expressed as [58]:

$$\vec{G}_b = m \mathbf{C}_{bo} \vec{g}_0 = m \mathbf{C}_{bo} \begin{bmatrix} 0 \\ 0 \\ G_0 \end{bmatrix}_o \quad (3.36)$$

where  $\vec{g}_0$  is the gravitational acceleration and  $G_0$  is the magnitude of the standard acceleration of the free fall. For the purposes of this thesis the magnitude of the standard acceleration of the free fall is equal to  $9.80665 \text{ ms}^{-2}$ .

### 3.3.2 Dynamics of rotational motion

After the dynamics of the translational motion was described, it is necessary to present physical quantities for the rotational motion, i.e., the angular momentum and the moment of force.

**Angular momentum**  $\vec{h}$  is given in kilogram meters squared per second. Angular momentum  $\vec{h}_b$  of an object in Body-fixed reference frame  $F_b$  is defined in following term [31, 58]:

$$\vec{h}_b = \mathbf{J}_b \vec{\omega}_{ib} \quad (3.37)$$

where  $\mathbf{J}_b$  is the inertia tensor, i.e., tensor of moments of inertia:

$$\mathbf{J}_b = \begin{bmatrix} J_x & -J_{xy} & -J_{xz} \\ -J_{xy} & J_y & -J_{yz} \\ -J_{xz} & -J_{yz} & J_z \end{bmatrix}_b \quad (3.38)$$

where  $J_x, J_y, J_z, J_{xy}, J_{xz}$  and  $J_{yz}$  are the elements of the inertia tensor:

$$J_x = \int (y_b^2 + z_b^2) dm \quad (3.39a)$$

$$J_y = \int (x_b^2 + z_b^2) dm \quad (3.39b)$$

$$J_z = \int (x_b^2 + y_b^2) dm \quad (3.39c)$$

$$J_{xy} = \int x_b y_b dm \quad (3.39d)$$

$$J_{xz} = \int x_b z_b dm \quad (3.39e)$$

$$J_{yz} = \int y_b z_b dm \quad (3.39f)$$

Given that aircraft's plane of symmetry is  $x_b z_b$  and center of mass of aircraft is lying on this plane, inertia elements  $J_{xy}$  and  $J_{yz}$  are equal to zero. Therefore inertia tensor of symmetric aircraft is equal to [31]:

$$\mathbf{J}_b = \begin{bmatrix} J_x & 0 & -J_{xz} \\ 0 & J_y & 0 \\ -J_{xz} & 0 & J_z \end{bmatrix}_b \quad (3.40)$$

**Moment** or moment of force describes a tendency of a force to rotate an object about particular axes. Moment  $\vec{\tau}_f$  is given in Newton meters and is defined by [3, 58]:

$$\vec{\tau}_f = \frac{d\vec{h}_f}{dt} \Rightarrow \vec{\tau}_f = \begin{bmatrix} L \\ M \\ N \end{bmatrix}_f \quad (3.41)$$

or

$$\vec{\tau}_f = \vec{r}_{Xf} \times \vec{F}_{Xf} \quad (3.42)$$

where  $L$ ,  $M$ ,  $N$  are the moments of force acting around particular axes,  $\vec{r}_{Xf}$  is the vector from the origin of the general reference frame  $F_f$  to the point  $X$  where the force is applied.

Moment  $\vec{\tau}_o$ , defined as first derivative of angular momentum  $\vec{h}_b$ , can be expressed in rotating reference frames using Equation 3.27 as:

$$\vec{\tau}_o = \frac{d\vec{h}_b}{dt} + \vec{\omega}_{ob} \times \vec{h}_b \quad (3.43)$$

Moreover, the vector  $\vec{h}_b$  can be replaced by Equation 3.37. Given that  $\vec{\omega}_{ob} \approx \vec{\omega}_{ib}$ , and that the resulting derivative of  $\vec{\omega}_{ob}$  can be replaced by Equation 3.26, therefore Equation 3.43 can be rewritten as

$$\vec{\tau}_o = \mathbf{J}_b \vec{\alpha}_{ob} + \vec{\omega}_{ob} \times \mathbf{J}_b \vec{\omega}_{ob} \quad (3.44)$$

Applying the Second Newton's laws of motion to the rotational motion, sum of external moments is equal to [3]:

$$\sum \vec{\tau}_f = \mathbf{J}_f \vec{\alpha}_{if} \quad (3.45)$$

## 3.4 Aircraft model

Detailed aircraft models introduce the forces and moments caused by different elements of an aircraft. The model of a light airplane<sup>6</sup>, used in this thesis, consists of five main parts:

- Mass and inertia model (see Section 3.4.1);
- Aerodynamic model (see Section 3.4.2);
- Propulsion model (see Section 3.4.3);
- Landing gear reaction model; and
- Structural model.

The landing gear model is describing behavior of airplane during taxiing, take-off and landing. Because taxiing, take-off and landing part of the flight are out of the scope of this thesis, the landing gear model is omitted.

The structural model describes elastic properties of airplane structure. This thesis uses point mass approximation of airplane, so the structural model, is out of the scope of this thesis.

### 3.4.1 Mass and inertia model

The main purpose of a mass and inertia model is to compute the total mass of an aircraft, position of the center of mass and moment of inertia tensor. The change of inertia and mass during flight is so important, that it is necessary to compute this change continuously during the whole flight [97].

In this thesis, we consider only rigid body aircraft. Elastic body aircraft have to have more complex models of mass, inertia and aerodynamics. The model of an elastic aircraft has to account for structural responses changing of all during the flight.

**Mass and position of the center of mass** of an aircraft are conventionally measurable on the ground. The total mass  $m$  of the aircraft is a sum of all elements: empty aircraft, fuel in fuel tanks, pilot, crew and passengers, cargo and other load [59].

Position of the aircraft center of mass  $\vec{r}_G$  can be computed as a weighted mean using following formula:

$$\vec{r}_{Gd} = \frac{\sum_i m_i \cdot \vec{r}_{G_id}}{m} \quad (3.46)$$

where  $m_i$  is the mass of the aircraft element  $i$  and  $\vec{r}_{G_id}$  is the position of the center of mass of the  $i^{th}$  aircraft element.

**The inertia tensor  $\mathbf{J}$**  of an aircraft can be obtained in three different ways. The first option considers an experimental measurement using a special oscillation test rig. However this process is highly demanding in terms of infrastructure, equipment and resources [54].

---

<sup>6</sup>The scope of this thesis is focused a light airplanes, so only LSA and VLA (Very Light Airplane) categories are taken into account. A detailed description of the aircraft classification can be found in Appendix E.

The second option is the possibility to acquire an inertia tensor of any model by Computer Aided Design (CAD) software [98]. Nevertheless it is impractical to create model of every pilot, every cargo and fuel configuration; however, this approach can be easily used for computation of inertia tensor of empty aircraft.

The third option of how to acquire inertia tensor of the whole aircraft, is thus to be computed based on the inertia tensors of individual parts using parallel axis theorem [31, 40]:

$$J_x = \sum_i \left[ J_{x_i} + m_i \left( y_{G_i}^2 + z_{G_i}^2 \right) \right]_b \quad (3.47a)$$

$$J_y = \sum_i \left[ J_{y_i} + m_i \left( x_{G_i}^2 + z_{G_i}^2 \right) \right]_b \quad (3.47b)$$

$$J_z = \sum_i \left[ J_{z_i} + m_i \left( x_{G_i}^2 + y_{G_i}^2 \right) \right]_b \quad (3.47c)$$

$$J_{xy} = \sum_i \left[ J_{xy_i} + m_i x_{G_i} y_{G_i} \right]_b \quad (3.47d)$$

$$J_{yz} = \sum_i \left[ J_{yz_i} + m_i y_{G_i} z_{G_i} \right]_b \quad (3.47e)$$

$$J_{xz} = \sum_i \left[ J_{xz_i} + m_i x_{G_i} z_{G_i} \right]_b \quad (3.47f)$$

where the inertia tensor of an empty aircraft can be acquired from the manufacturer documentation, inertia tensor of the fuel in the fuel tank can be obtain using simulation result based on the shape of the fuel tank, and the inertia tensor of person on-board can be estimated based on procedures and data in specialised document [42].

### 3.4.2 Aerodynamic model

For the purposes of this thesis, the most important elements of the aerodynamic model are the aerodynamic force and moment of aerodynamic force along with their respective coefficients, i.e., aerodynamic parameters, because these coefficients can be used to approximate the individual flight parameters.

**The aerodynamic force**  $\vec{F}_A$  is often expressed in different coordinate systems. Mutual dependence of these expressions is given in the following equation [31]:

$$\vec{F}_A = \bar{q} S \begin{bmatrix} C_X \\ C_Y \\ C_Z \end{bmatrix}_b = \bar{q} S \cdot \mathbf{C}_{bs} \begin{bmatrix} -C_D \\ C_Y \\ -C_L \end{bmatrix}_s = \bar{q} S \cdot \mathbf{C}_{ba} \begin{bmatrix} -C_W \\ C_Q \\ -C_L \end{bmatrix}_a \quad (3.48)$$

where  $\bar{q}$  is the instant dynamic pressure;  $S$  is the reference wing area;  $C_X, C_Y, C_Z$  are the coefficients of the aerodynamic force in  $F_b$ ;  $C_D, C_L$  are the coefficients of the aerodynamic force in  $F_s$ ; and  $C_W, C_Q$  are the coefficients of aerodynamic force in  $F_a$ . The instant dynamic pressure can be computed using following equation [61, 87]

$$\bar{q} = \frac{1}{2} \rho V^2 \quad (3.49)$$

where  $\rho$  is the air mass density.

**Moment of aerodynamic force**  $\vec{\tau}_A$  calculated in Body-fixed reference frame is [31]:

$$\vec{\tau}_A = \bar{q} S \begin{bmatrix} b_w \cdot C_l \\ \bar{c} \cdot C_m \\ b_w \cdot C_n \end{bmatrix}_b \quad (3.50)$$

where  $b_w$  is the reference wingspan,  $\bar{c}$  is the length of Mean Aerodynamic Chord (MAC), and  $C_l$ ,  $C_m$ ,  $C_n$  are the moment coefficients of the aerodynamic force in the reference frame  $F_b$ .

**The aerodynamic parameters** can be obtained using force coefficients given in Equation 3.48 and moment coefficients given in Equation 3.50. These coefficients can be approximated with arbitrary accuracy in the vicinity of the trim point using Taylor's theorem [43]. The resultant equations are [58, 87]:

$$C_X = C_{X0} + \alpha \cdot C_{X\alpha} + q^* \cdot C_{Xq} + \delta_e \cdot C_{X\delta_e} \quad (3.51a)$$

$$C_Y = C_{Y0} + \beta \cdot C_{Y\beta} + p^* \cdot C_{Yp} + r^* \cdot C_{Yr} + \delta_a \cdot C_{Y\delta_a} + \delta_r \cdot C_{Y\delta_r} \quad (3.51b)$$

$$C_Z = C_{Z0} + \alpha \cdot C_{Z\alpha} + q^* \cdot C_{Zq} + \delta_e \cdot C_{Z\delta_e} \quad (3.51c)$$

$$C_D = C_{D0} + \alpha \cdot C_{D\alpha} + q^* \cdot C_{Dq} + \delta_e \cdot C_{D\delta_e} \quad (3.51d)$$

$$C_L = C_{L0} + \alpha \cdot C_{L\alpha} + q^* \cdot C_{Lq} + \delta_e \cdot C_{L\delta_e} \quad (3.51e)$$

$$C_W = C_{W0} + \alpha \cdot C_{W\alpha} + q^* \cdot C_{Wq} + \delta_e \cdot C_{W\delta_e} \quad (3.51f)$$

$$C_Q = C_{Q0} + \beta \cdot C_{Q\beta} + p^* \cdot C_{Qp} + r^* \cdot C_{Qr} + \delta_a \cdot C_{Q\delta_a} + \delta_r \cdot C_{Q\delta_r} \quad (3.51g)$$

$$C_l = C_{L0} + \beta \cdot C_{l\beta} + p^* \cdot C_{lp} + r^* \cdot C_{lr} + \delta_a \cdot C_{l\delta_a} + \delta_r \cdot C_{l\delta_r} \quad (3.51h)$$

$$C_m = C_{m0} + \alpha \cdot C_{m\alpha} + q^* \cdot C_{mq} + \delta_e \cdot C_{m\delta_e} \quad (3.51i)$$

$$C_n = C_{nb} + \beta \cdot C_{n\beta} + p^* \cdot C_{np} + r^* \cdot C_{nr} + \delta_a \cdot C_{n\delta_a} + \delta_r \cdot C_{n\delta_r} \quad (3.51j)$$

where  $C_{Ij}$  is the flight parameter (defined as a derivative of coefficient  $C_I$  with respect to  $j$  in general),  $\delta_e$  is the deflection of elevator,  $\delta_a$  is the antisymmetric aileron deflection,  $\delta_r$  is the deflection of rudder, and  $p^*$ ,  $q^*$ ,  $r^*$  are the dimensionless angular velocities defined as:

$$p^* = \frac{p b_w}{2V} \quad (3.52a)$$

$$q^* = \frac{q \bar{c}}{2V} \quad (3.52b)$$

$$r^* = \frac{r b_w}{2V} \quad (3.52c)$$

The aerodynamic force and aerodynamic moment, hence its coefficients and aerodynamic parameters, are included in the Equations of Motion. Values of the aerodynamic parameters are obtained by a parameter estimation process, which is based on utilization of Equations of Motion.

### 3.4.3 Propulsion model

Given that this thesis deals with a light airplane, the propulsion of an airplane is considered to be based on a single reciprocating 4 stroke combustion engine with a propeller. For the

purposes of this thesis, it is not necessary to describe the whole propulsion system in detail, therefore only the fuel inputs, propulsion force and moment due to propulsion force are considered.

**Fuel inputs** (fuel level and fuel flow) are necessary to compute the center of mass and the tensor of inertia of fuel in fuel tanks, as described in Section 3.4.1.

**Propulsion force** magnitude  $F_P$  can be computed using equation [3]:

$$F_P = C_T \rho n_P^2 D_P^4 \quad (3.53)$$

where  $C_T$  is the dimensionless output thrust coefficient (specified by the propeller manufacturer),  $n_P$  is the propeller's rotational speed in revolutions per second, and  $D_P$  is the diameter of the propeller.

The propulsion on most of the airplane acts along the  $x_b$  axis, so the propulsion force vector  $\vec{F}_{Pb}$  can be constructed as:

$$\vec{F}_P = \begin{bmatrix} F_P \\ 0 \\ 0 \end{bmatrix}_b \quad (3.54)$$

**Moment due to the propulsion force** can be evaluated considering three assumptions. Firstly, the  $x_b$  axis does not pass through the center of the propeller. Secondly, the propeller itself is a rotating mass and therefore it generates moment. Finally, the revolutions of the propeller cannot be considered constant, because the airplane used for the purposes of this thesis has fixed pitch propeller. The resultant moment of the propulsion force can be expressed as [31]:

$$\vec{\tau}_P = \vec{r}_{Pb} \times \vec{F}_P + \vec{\omega}_{ob} \times J_P \vec{\omega}_P - J_P \vec{\alpha}_P \quad (3.55)$$

and simplified to

$$\vec{\tau}_P = \begin{bmatrix} -J_P \dot{\omega}_P \\ F_P z_{Pb} + J_P r \omega_P \\ -F_P y_{Pb} - J_P q \omega_P \end{bmatrix} \quad (3.56)$$

where  $J_P$  is the moment of inertia of the propeller. The  $\vec{\alpha}_P$  and  $\vec{\omega}_P$  are acting only around the  $x_b$  axis, therefore their vectors contain only the first component, i.e.,  $\dot{\omega}_P$  and  $\omega_P$  respectively, and  $\omega_P$  is the magnitude of angular velocity of the propeller which can be computed as:

$$\omega_P = 2\pi n_P \quad (3.57)$$

## 3.5 Nonlinear Equations of Motion

The Equations of Motion (EoM) describe the behavior of an aircraft (or physical system in general) as a set of mathematical functions. The nonlinear Equations of Motion can be divided into two types: kinematic equations and dynamic equations. At first, the general nonlinear models are introduced. At second, the nonlinear kinematic Equations of Motion are presented. Then, the description of the merge of the Equations of Motion with the rest of aircraft models and the resultant nonlinear dynamic Equations of Motion are given. At the end of this section, dynamic Equations of Motion are divided into the longitudinal equations, and lateral-directional equations.

### 3.5.1 General nonlinear dynamic system

A general dynamic system is defined as a system, where the outputs in time  $t$  depends on inputs in time  $t$  and inputs in some of the previous time moment(s) [6, 9]. In general, dynamic system is defined by Equation 3.58 and its diagram is shown in Figure 3.3.

$$\dot{\vec{x}} = f(\vec{x}, \vec{u}) \quad (3.58a)$$

$$\vec{y} = h(\vec{x}, \vec{u}) \quad (3.58b)$$

$$\vec{x}(0) = \vec{x}_0 \quad (3.58c)$$

where  $\vec{x}$  is the state vector;  $f()$  is the state function;  $\vec{u}$  is the input/control vector;  $\vec{y}$  is the output vector;  $h()$  is the output function; and  $\vec{x}_0$  is the initial state vector.

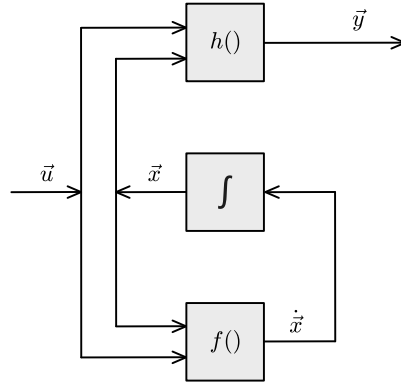


Figure 3.3: Dataflow diagram of a nonlinear system.

### 3.5.2 Nonlinear kinematic Equations of Motion

Nonlinear kinematic equations of the motion describe motion of an object without describing the reason of motion. There are three main nonlinear kinematic EoM: Attitude equations, Navigation equations and Velocity equations.

**Attitude equations** represent the rate of change of angular position given by transformation from angular velocities to angular rates. These equations were already introduced in Equations 3.25a – 3.25c, but for the sake of completeness are repeated below:

$$\dot{\phi} = p + (q \sin \phi + r \cos \phi) \tan \theta \quad (3.59a)$$

$$\dot{\theta} = q \cos \phi - r \sin \phi \quad (3.59b)$$

$$\dot{\psi} = \frac{q \sin \phi + r \cos \phi}{\cos \theta} \quad (3.59c)$$

**Navigation equations**, also known as the Position equations, represent the rate of change of the translational position. These equations are based on the transformation of the translational velocity from the reference frame  $F_b$  to the reference frame  $F_o$  using following equation:

$$\dot{\vec{r}}_{Go} = \mathbf{C}_{ob} \vec{v}_{Gb} \quad (3.60)$$

The scalar form is shown below [31, 87]:

$$\begin{aligned}\dot{x}_{Go} &= u_{Gb} \cos \theta \cos \psi + v_{Gb} (\sin \phi \sin \theta \cos \psi - \cos \phi \sin \psi) \\ &\quad + w_{Gb} (\cos \phi \sin \theta \cos \psi + \sin \phi \sin \psi)\end{aligned}\quad (3.61a)$$

$$\begin{aligned}\dot{y}_{Go} &= u_{Gb} \cos \theta \sin \psi + v_{Gb} (\sin \phi \sin \theta \sin \psi + \cos \phi \cos \psi) \\ &\quad + w_{Gb} (\cos \phi \sin \theta \sin \psi - \sin \phi \cos \psi)\end{aligned}\quad (3.61b)$$

$$\dot{z}_{Go} = -u_{Gb} \sin \theta + v_{Gb} \sin \phi \cos \theta + w_{Gb} \cos \phi \cos \theta \quad (3.61c)$$

The rate of change of the translational position, based on Equation 3.8, can also be expressed in the Geodetic coordinate system as:

$$\dot{\ell} = \frac{\dot{y}_{Go}}{(N_0 + h) \cos \varphi} \quad (3.62a)$$

$$\dot{\varphi} = \frac{\dot{x}_{Go}}{M_0 + h} \quad (3.62b)$$

$$\dot{h} = -\dot{z}_{Go} \quad (3.62c)$$

The **Velocity equations** describe the rate of change of the translational velocity. The Velocity equation is based on Equation 3.28 for the Translational acceleration in rotating reference frames. Given that the total acceleration can be decomposed into specific force and gravitational acceleration (see Equation 3.35), and that the acceleration is the first derivative of the velocity, the resulting equation can be written as

$$\dot{\vec{v}}_{Gb} = \vec{f}_G + \vec{g}_0 - \vec{\omega}_{ob} \times \vec{v}_{Gb} \quad (3.63)$$

Based on the Equations 3.36, Equation 3.63 can be given in the scalar form:

$$\dot{u}_{Gb} = f_x - G_0 \sin \theta + r v_{Gb} - q w_{Gb} \quad (3.64a)$$

$$\dot{v}_{Gb} = f_y + G_0 \cos \theta \sin \phi + p w_{Gb} - r u_{Gb} \quad (3.64b)$$

$$\dot{w}_{Gb} = f_z + G_0 \cos \theta \cos \phi + q u_{Gb} - p v_{Gb} \quad (3.64c)$$

### 3.5.3 Nonlinear dynamic Equations of Motion

Nonlinear dynamic EoM describe the forces and moments acting on the airplane. As it was mentioned before, there are three sources of forces and moments acting on an airplane in flight: the aerodynamic forces and moments, the propulsion forces and moments and finally the gravitational force. Gravitation does not generate moment, as the gravitational force is acting in the center of mass. Particular models of these forces and moments were introduced in Section 3.4.

**Force equations** describes the rate of change of the translational velocity. The Force equations are based on the Velocity equation given in 3.63, which is extended using substitution of the specific force with Equation 3.35 to include the forces affecting the motion of the airplane. The resultant Force equation is:

$$\dot{\vec{v}}_{Gb} = \frac{\vec{F}_A + \vec{F}_P + \vec{G}_G}{m} - \vec{\omega}_{ob} \times \vec{v}_{Gb} \quad (3.65)$$

Based on the Equations 3.36, 3.54 and 3.48, the Force equation can be expressed in the scalar form:

$$\dot{u}_{Gb} = \frac{\bar{q}S}{m} C_X + \frac{F_P}{m} - G_0 \sin \theta + r v_{Gb} - q w_{Gb} \quad (3.66a)$$

$$\dot{v}_{Gb} = \frac{\bar{q}S}{m} C_Y + G_0 \cos \theta \sin \phi + p w_{Gb} - r u_{Gb} \quad (3.66b)$$

$$\dot{w}_{Gb} = \frac{\bar{q}S}{m} C_Z + G_0 \cos \theta \cos \phi + q u_{Gb} - p v_{Gb} \quad (3.66c)$$

The Force equations can be also expressed in the Spherical coordinate system utilizing Equations 3.12, 3.14, 3.36, 3.54 and 3.48. The resultant equations are:

$$\begin{aligned} \dot{V} = & -\frac{\bar{q}S}{m} C_W + \frac{F_P}{m} \cos \beta \cos \alpha \\ & + G_0 (\sin \beta \cos \theta \sin \phi + \cos \beta \sin \alpha \cos \theta \cos \phi - \cos \beta \cos \alpha \sin \theta) \end{aligned} \quad (3.67a)$$

$$\begin{aligned} \dot{\alpha} = & -\frac{\bar{q}S}{m V \cos \beta} C_L - \frac{F_P \sin \alpha}{m V \cos \beta} - p \cos \alpha \tan \beta + q - r \sin \alpha \tan \beta \\ & + \frac{G_0}{V \cos \beta} (\cos \alpha \cos \theta \cos \phi + \sin \alpha \sin \theta) \end{aligned} \quad (3.67b)$$

$$\begin{aligned} \dot{\beta} = & \frac{\bar{q}S}{m V} C_Q - \frac{F_P}{m V} \sin \beta \cos \alpha + p \sin \alpha - r \cos \alpha \\ & + \frac{G_0}{V} [\cos \beta \cos \theta \sin \phi + \sin \beta (\cos \alpha \sin \theta - \sin \alpha \cos \theta \cos \phi)] \end{aligned} \quad (3.67c)$$

**Moment equations** represents the rate of change of the angular velocity. Moment equations are based on Equation 3.44 for the Moment of forces in rotating reference frames. Given that the moment of force acting on an airplane can be decomposed into a moment of aerodynamic force and a moment of propulsion force, the resultant equation is

$$\mathbf{J}_b \vec{\alpha}_{ob} = \vec{\tau}_A + \vec{\tau}_P - \vec{\omega}_{ob} \times \mathbf{J}_b \vec{\omega}_{ob} \quad (3.68)$$

This equation can be written in scalar form using Equations 3.38, 3.56 and 3.50 as follows [58]:

$$\begin{aligned} \dot{p} J_x - \dot{q} J_{xy} - \dot{r} J_{xz} = & \bar{q} S b_w C_l - J_P \dot{\omega}_P + \\ & q r (J_y - J_z) + J_{yz} (q^2 - r^2) + p q J_{xz} - p r J_{xy} \end{aligned} \quad (3.69a)$$

$$\begin{aligned} -\dot{p} J_{xy} + \dot{q} J_y - \dot{r} J_{yz} = & \bar{q} S \bar{c} C_m + J_P r \omega_P + F_P z_P + \\ & p r (J_z - J_x) + J_{xz} (r^2 - p^2) + q r J_{xy} - p q J_{yz} \end{aligned} \quad (3.69b)$$

$$\begin{aligned} -\dot{p} J_{xz} - \dot{q} J_{yz} + \dot{r} J_z = & \bar{q} S b_w C_n - J_P q \omega_P - F_P y_P + \\ & p q (J_x - J_y) + J_{xy} (p^2 - q^2) + p r J_{yz} - q r J_{xz} \end{aligned} \quad (3.69c)$$

Given that airplane's plane of symmetry is  $x_b z_b$  and center of mass of aircraft is lying on this plane, inertia elements  $J_{xy}$  and  $J_{yz}$  are equal to zero (see Equation 3.40). Therefore Equation 3.69 can be simplified to

$$\dot{p} J_x - \dot{r} J_{xz} = \bar{q} S b_w C_l - J_P \dot{\omega}_P + q r (J_y - J_z) + p q J_{xz} \quad (3.70a)$$

$$\dot{q} J_y = \bar{q} S \bar{c} C_m + J_P r \omega_P + F_P z_P + p r (J_z - J_x) + J_{xz} (r^2 - p^2) \quad (3.70b)$$

$$-\dot{p} J_{xz} + \dot{r} J_z = \bar{q} S b_w C_n - J_P q \omega_P - F_P y_P + p q (J_x - J_y) - q r J_{xz} \quad (3.70c)$$

and solved for  $\dot{p}$ ,  $\dot{q}$ , and  $\dot{r}$  as follows

$$\dot{p} = \frac{\bar{q} S b_w (J_z C_l + J_{xz} C_n) - J_{xz} (J_P q \omega_P + F_P P b) - J_z J_P \dot{\omega}_P + p q J_{xz} (J_x - J_y + J_z) + q r (J_y J_z - J_z^2 - J_{xz}^2)}{J_x J_z - J_{xz}^2} \quad (3.71a)$$

$$\dot{q} = \frac{\bar{q} S \bar{c} C_m - J_P r \omega_P + F_{Pb} z_{Pb} + p r (J_z - J_x) + J_{xz} (r^2 - p^2)}{J_y} \quad (3.71b)$$

$$\dot{r} = \frac{\bar{q} S b_w (J_{xz} C_l + J_x C_n) - J_x (J_P q \omega_P + F_P y_{Pb}) - J_{xz} J_P \dot{\omega}_P + p q (J_x^2 - J_x J_y + J_{xz}^2) + q r J_{xz} (J_y - J_x - J_z)}{J_x J_z - J_{xz}^2} \quad (3.71c)$$

### 3.5.4 Separation of dynamic Equations of Motion

There were four sets of the Equations of Motion presented before: Attitude equations, Navigation equation, Force equations (created from Velocity equations), and Moment equations. The Navigation equations are used for the purposes of the Flight Path Reconstruction only; therefore, it is not necessary to linearize them.

The remaining three sets of the Equations of Motion contain nine equations, which can be separated according to the type of the motion to the Symmetric equations (motion in the vertical plane), i.e.,  $V$ ,  $\alpha$ ,  $q$ , and  $\theta$ ; and Antisymmetric equations (motion out of the vertical plane), i.e.,  $\beta$ ,  $p$ ,  $r$ , and  $\phi$ . In order to complete the division of the equations into these two categories, it is necessary to neglect dependencies of symmetric equations on antisymmetric variables and vice versa. The remaining, ninth, variable  $\psi$  could be theoretically included among Antisymmetric equations; however, it is often omitted, because  $\psi$  influences only the orientation of the airplane and does not influence the motion of the airplane (other antisymmetric variables are  $\psi$ -independent).

**Symmetric equation** for the longitudinal motion, i.e., equations of  $V$ ,  $\alpha$ ,  $q$ , and  $\theta$ , are created from Equations 3.67a, 3.67b, 3.71b, 3.59b, respectively. At first, the antisymmetric variables  $\beta$ ,  $\phi$ ,  $p$ , and  $r$  are neglected, i.e., set equal to zero, to complete the separation of Symmetric and Antisymmetric equations. Then it is possible to substitute  $\bar{q}$  with Equation 3.49. The resultant Symmetric equations are:

$$\dot{V} = -\frac{\rho V^2 S}{2m} C_W + \frac{F_P}{m} \cos \alpha - G_0 \sin(\theta - \alpha) \quad (3.72a)$$

$$\dot{\alpha} = -\frac{\rho V S}{2m} C_L - \frac{F_P}{m V} \sin \alpha + q + \frac{G_0}{V} \cos(\theta - \alpha) \quad (3.72b)$$

$$\dot{q} = \frac{\rho V^2 S \bar{c}}{2 J_y} C_m + \frac{F_P z_{Pb}}{J_y} \quad (3.72c)$$

$$\dot{\theta} = q \quad (3.72d)$$

**Antisymmetric equation** for the lateral-directional motion, i.e., equations of  $\beta$ ,  $p$ ,  $r$ , and  $\phi$ , are created from Equations 3.67c, 3.71a, 3.71c, 3.59a, respectively. The symmetric variables  $V$ ,  $\alpha$ ,  $q$ , and  $\theta$  are neglected, i.e., set equal to zero, to complete the separation of Symmetric and Antisymmetric equations. The resultant Symmetric equations are:

$$\dot{\beta} = \frac{\bar{q} S}{m V} C_Q + \frac{F_P}{m V} \sin \beta \cos \alpha + \frac{G_0 \cos \alpha}{V} (\cos \beta \sin \phi - \sin \alpha \sin \beta (\cos \phi - 1)) + \frac{p \sin \alpha - r \cos \alpha}{\sin \alpha} \quad (3.73a)$$

$$\dot{p} = \frac{\bar{q} S b_w (J_z C_l + J_{xz} C_n) - J_{xz} (J_P q \omega_P + F_P P b) - J_z J_P \dot{\omega}_P}{J_x J_z - J_{xz}^2} \quad (3.73b)$$

$$\dot{r} = \frac{\bar{q} S b_w (J_{xz} C_l + J_x C_n) - J_x (J_P q \omega_P + F_P y_{Pb}) - J_{xz} J_P \dot{\omega}_P}{J_x J_z - J_{xz}^2} \quad (3.73c)$$

$$\dot{\phi} = p + r \frac{\tan \alpha}{\cos \phi} \quad (3.73d)$$

## 3.6 Linear Equations of Motion

In this section, system linearization including definition of the linear state-space model and derivation of a linearized system is described. At the end, the linearized Equations of Motion are given.

### 3.6.1 System linearization

Dynamic systems can be divided into two separate categories: nonlinear systems and linear systems. The difference between them is, that linear systems have to satisfy the property of superposition, which is defined by the following equations [6, 14]:

$$f(u_1 + u_2) = f(u_1) + f(u_2) \quad \wedge \quad f(k u_1) = k f(u_1) \quad (3.74)$$

where  $k$  is an arbitrary scalar.

There are many approaches to describe linear systems. In aviation, state-space model is the most commonly used one. The state-space model of a linear system is given by the equations [9, 14]:

$$\dot{\vec{x}} = \mathbf{A}\vec{x} + \mathbf{B}\vec{u} \quad (3.75a)$$

$$\vec{y} = \mathbf{C}\vec{x} + \mathbf{D}\vec{u} \quad (3.75b)$$

$$\vec{x}(0) = \vec{x}_0 \quad (3.75c)$$

where  $\mathbf{A}$  is the state/system matrix,  $\mathbf{B}$  is the input matrix,  $\mathbf{C}$  is the output matrix,  $\mathbf{D}$  is the feed-through/feed-forward matrix.

The nonlinear system described by the dynamic equations can be transformed into a linear system described by a state-space model (see Figure 3.4) using the following linearization process. Lets assume, that the deflections  $\Delta \vec{x}$  and  $\Delta \vec{u}$  from a trim/equilibrium point  $(x_t, u_t)$  and are very small [86, 87] and can be computed as follows:

$$\Delta \vec{x} = \vec{x} - \vec{x}_t \quad (3.76a)$$

$$\Delta \vec{u} = \vec{u} - \vec{u}_t \quad (3.76b)$$

and the first derivative of  $\vec{x}_t$ , i.e., result of the state function in the trim/equilibrium point is:

$$\dot{\vec{x}}_t = f(\vec{x}_t, \vec{u}_t) = 0 \quad (3.77)$$

Then Equation 3.58a can be modified to:

$$\dot{\vec{x}}_t + \Delta \dot{\vec{x}} = f(\vec{x}_t + \Delta \vec{x}, \vec{u}_t + \Delta \vec{u}) \quad (3.78)$$

This equation can be further expanded using Taylor series and neglecting the high-order terms [86, 87]. The resultant equation is:

$$\dot{\vec{x}}_t + \Delta \dot{\vec{x}} = f(\vec{x}_t, \vec{u}_t) + \frac{\partial f}{\partial \vec{x}} \Delta \vec{x} + \frac{\partial f}{\partial \vec{u}} \Delta \vec{u} \quad (3.79)$$

where  $\frac{\partial f}{\partial \vec{x}}$  and  $\frac{\partial f}{\partial \vec{u}}$  are the Jacobian matrices constructed as:

$$\frac{\partial f}{\partial \vec{x}} = \begin{bmatrix} \frac{\partial f_1}{\partial x_1} & \frac{\partial f_1}{\partial x_2} & \cdots & \frac{\partial f_1}{\partial x_{n_x}} \\ \frac{\partial f_2}{\partial x_1} & \frac{\partial f_2}{\partial x_2} & \cdots & \frac{\partial f_2}{\partial x_{n_x}} \\ \vdots & \vdots & \ddots & \vdots \\ \frac{\partial f_{n_x}}{\partial x_1} & \frac{\partial f_{n_x}}{\partial x_2} & \cdots & \frac{\partial f_{n_x}}{\partial x_{n_x}} \end{bmatrix} \quad (3.80)$$

$$\frac{\partial f}{\partial \vec{u}} = \begin{bmatrix} \frac{\partial f_1}{\partial u_1} & \frac{\partial f_1}{\partial u_2} & \cdots & \frac{\partial f_1}{\partial u_{n_u}} \\ \frac{\partial f_2}{\partial u_1} & \frac{\partial f_2}{\partial u_2} & \cdots & \frac{\partial f_2}{\partial u_{n_u}} \\ \vdots & \vdots & \ddots & \vdots \\ \frac{\partial f_{n_x}}{\partial u_1} & \frac{\partial f_{n_x}}{\partial u_2} & \cdots & \frac{\partial f_{n_x}}{\partial u_{n_u}} \end{bmatrix} \quad (3.81)$$

The Jacobian matrices  $\frac{\partial f}{\partial \vec{x}}$  and  $\frac{\partial f}{\partial \vec{u}}$  are equal to the state/system matrix  $\mathbf{A}$  and the input matrix  $\mathbf{B}$  of the state-space model, respectively.

The Output equation of the dynamic model (Equation 3.58b) can be processed using the same, above-mentioned approach. The resultant matrices will have following form:

$$\mathbf{C} = \frac{\partial h}{\partial \vec{x}} \quad (3.82a)$$

$$\mathbf{D} = \frac{\partial h}{\partial \vec{u}} \quad (3.82b)$$

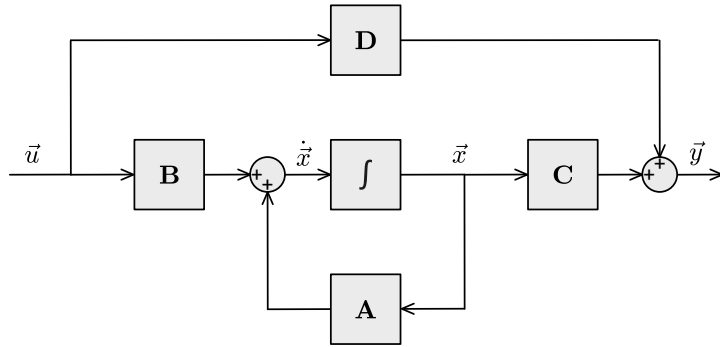


Figure 3.4: Dataflow diagram of a linear state-space model.

### 3.6.2 Linear Equations of Motion

The process described in Section 3.6.1 can be used to linearize nonlinear Equations of Motion introduced in Section 3.5. These resultant equations can be separated into sets of Symmetric and Antisymmetric equations.

**Symmetric equations** for the longitudinal motion, after the linearization procedure are described by the resultant state-space model shown below:

$$\begin{bmatrix} \dot{V} \\ \dot{\alpha} \\ \dot{q} \\ \dot{\theta} \end{bmatrix} = \begin{bmatrix} D_V & D_\alpha & D_q & D_\theta \\ L_V & L_\alpha & L_q & L_\theta \\ M_V & M_\alpha & M_q & 0 \\ 0 & 0 & 1 & 0 \end{bmatrix} \begin{bmatrix} V \\ \alpha \\ q \\ \theta \end{bmatrix} + \begin{bmatrix} D_{\delta_e} & D_{F_P} \\ L_{\delta_e} & L_{F_P} \\ M_{\delta_e} & M_{F_P} \\ 0 & 0 \end{bmatrix} \begin{bmatrix} \delta_e \\ F_P \end{bmatrix} \quad (3.83)$$

where particular elements of respective matrices can be expressed as:

$$D_V = -\frac{\rho V S}{m} \left( C_{W0} + \alpha C_{W\alpha} + \delta_e C_{W\delta_e} + \frac{\bar{c}q}{4V} C_{Wq} \right) \quad (3.84a)$$

$$D_\alpha = -\frac{\rho V^2 S}{2m} C_{W\alpha} - \frac{F_P}{m} \sin \alpha + G_0 \cos(\theta - \alpha) \quad (3.84b)$$

$$D_q = -\frac{\rho V S \bar{c}}{4m} C_{Wq} \quad (3.84c)$$

$$D_\theta = -G_0 \cos(\theta - \alpha) \quad (3.84d)$$

$$D_{\delta_e} = -\frac{\rho V^2 S}{2m} C_{W\delta_e} \quad (3.84e)$$

$$D_{F_P} = \frac{\cos \alpha}{m} \quad (3.84f)$$

$$L_V = \frac{F_P \sin \alpha}{V^2 m} - \frac{\rho S}{2m} \left( C_{L0} + \alpha C_{L\alpha} + \delta_e C_{L\delta_e} + \frac{\bar{c}q}{V} C_{Lq} \right) - \frac{G_0}{V^2} \cos(\theta - \alpha) \quad (3.84g)$$

$$L_\alpha = \frac{G_0}{V} \sin(\theta - \alpha) - \frac{\rho V S}{2m} C_{L\alpha} + \frac{F_P \cos \alpha}{V m} \quad (3.84h)$$

$$L_q = 1 - \frac{\rho S \bar{c}}{4m} C_{Lq} \quad (3.84i)$$

$$L_\theta = -\frac{G_0}{V} \sin(\theta - \alpha) \quad (3.84j)$$

$$L_{\delta_e} = -\frac{\rho V S}{2m} C_{L\delta_e} \quad (3.84k)$$

$$L_{F_P} = -\frac{\sin \alpha}{V m} \quad (3.84l)$$

$$M_V = \frac{\rho V S \bar{c}}{J_y} \left( C_{m0} + \alpha C_{m\alpha} + \delta_e C_{m\delta_e} + \frac{\bar{c}q}{4V} C_{mq} \right) \quad (3.84m)$$

$$M_\alpha = \frac{\rho V^2 S \bar{c}}{2 J_y} C_{m\alpha} \quad (3.84n)$$

$$M_q = \frac{\rho V S \bar{c}^2}{4 J_y} C_{mq} \quad (3.84o)$$

$$M_{\delta_e} = \frac{\rho V^2 S \bar{c}}{2 J_y} C_{m\delta_e} \quad (3.84p)$$

$$M_{F_P} = \frac{z_P}{J_y} \quad (3.84q)$$

**Antisymmetric equation** for the lateral-directional motion, after the linearization procedure are described by the resultant state-space model shown below:

$$\begin{bmatrix} \dot{\beta} \\ \dot{p} \\ \dot{r} \\ \dot{\phi} \end{bmatrix} = \begin{bmatrix} Y_\beta & Y_p & Y_r & Y_\phi \\ L_\beta & L_p & L_r & 0 \\ N_\beta & N_p & N_r & 0 \\ 0 & 1 & \phi_r & \phi_\phi \end{bmatrix} \begin{bmatrix} \beta \\ p \\ r \\ \phi \end{bmatrix} + \begin{bmatrix} Y_{\delta_a} & Y_{\delta_r} & 0 \\ L_{\delta_a} & L_{\delta_r} & L_{\omega_P} \\ N_{\delta_a} & N_{\delta_r} & N_{\omega_P} \\ 0 & 0 & 0 \end{bmatrix} \begin{bmatrix} \delta_a \\ \delta_r \\ \omega_P \end{bmatrix} \quad (3.85)$$

where particular elements of respective matrices can be expressed as:

$$Y_\beta = \frac{G_0}{V} (\sin \alpha - \sin \alpha \cos \phi - \sin \beta \sin \phi) \cos \alpha \cos \beta + \frac{F_P}{m V} \cos \alpha \cos \beta + \frac{\bar{q} S}{m V} C_{Q\beta} \quad (3.86a)$$

$$Y_p = \frac{\bar{q} S b_w}{2 V^2 m} C_{Qp} + \sin \alpha \quad (3.86b)$$

$$Y_r = \frac{\bar{q} S b_w}{2 V^2 m} C_{Qr} - \cos \alpha \quad (3.86c)$$

$$Y_\phi = \frac{G_0}{V} (\cos \beta \cos \phi + \sin \alpha \sin \beta \sin \phi) \cos \alpha \quad (3.86d)$$

$$Y_{\delta_a} = \frac{\bar{q} S}{m V} C_{Q\delta_a} \quad (3.86e)$$

$$Y_{\delta_r} = \frac{\bar{q} S}{m V} C_{Q\delta_r} \quad (3.86f)$$

$$L_\beta = -\frac{\bar{q} S b_w}{J_{xz}^2 - J_x J_z} (J_z C_{l\beta} + J_{xz} C_{n\beta}) \quad (3.86g)$$

$$L_p = -\frac{\bar{q} S b_w^2}{2 V (J_{xz}^2 - J_x J_z)} (J_z b_w C_{lp} + J_{xz} b_w C_{np}) \quad (3.86h)$$

$$L_r = -\frac{\bar{q} S b_w^2}{2 V (J_{xz}^2 - J_x J_z)} (J_z b_w C_{lr} + J_{xz} b_w C_{nr}) \quad (3.86i)$$

$$L_{\delta_a} = -\frac{\bar{q} S b_w}{J_{xz}^2 - J_x J_z} (J_z C_{l\delta_a} + J_{xz} C_{n\delta_a}) \quad (3.86j)$$

$$L_{\delta_r} = -\frac{\bar{q} S b_w}{J_{xz}^2 - J_x J_z} (J_z C_{l\delta_r} + J_{xz} C_{n\delta_r}) \quad (3.86k)$$

$$L_{\omega_P} = \frac{J_P J_z}{J_{xz}^2 - J_x J_z} \quad (3.86l)$$

$$N_\beta = -\frac{\bar{q} S b_w}{J_{xz} - J_x J_z} (J_{xz} C_{l\beta} + J_x C_{n\beta}) \quad (3.86m)$$

$$N_p = -\frac{\bar{q} S b_w^2}{2 (J_{xz}^2 - J_x J_z)} (J_{xz} b_w C_{lp} + J_x b_w C_{np}) \quad (3.86n)$$

$$N_r = -\frac{\bar{q} S b_w^2}{2 (J_{xz}^2 - J_x J_z)} (J_{xz} b_w C_{lr} + J_x b_w C_{nr}) \quad (3.86o)$$

$$N_{\delta_a} = -\frac{\bar{q} S b_w}{J_{xz}^2 - J_x J_z} (J_{xz} C_{l\delta_a} + J_x C_{n\delta_a}) \quad (3.86p)$$

$$N_{\delta_r} = -\frac{\bar{q} S b_w}{J_{xz}^2 - J_x J_z} (J_{xz} C_{l\delta_r} + J_x C_{n\delta_r}) \quad (3.86q)$$

$$N_{\omega_P} = \frac{J_P J_{xz}}{J_{xz}^2 - J_x J_z} \quad (3.86r)$$

$$\dot{\phi}_r = \frac{\tan \alpha}{\cos \phi} \quad (3.86s)$$

$$\dot{\phi}_\phi = r \frac{\tan \alpha \tan \phi}{\cos \phi} \quad (3.86t)$$

As it was mentioned earlier, this thesis is primarily focused on longitudinal motion of airplane, therefore the antisymmetric equations are listed only for the sake of completeness.

## 4. Flight parameter estimation

Parameter estimation consists of following elements: optimization algorithm, identification criteria, mathematical model, model structure and model requirements. The process of parameter estimation has following prerequisites: input maneuvers, data acquisition, Flight Path Reconstruction and a-priori values. The result of parameter estimation process is subjected to the model validation. For the description of the whole process flow, see Figure 4.1.

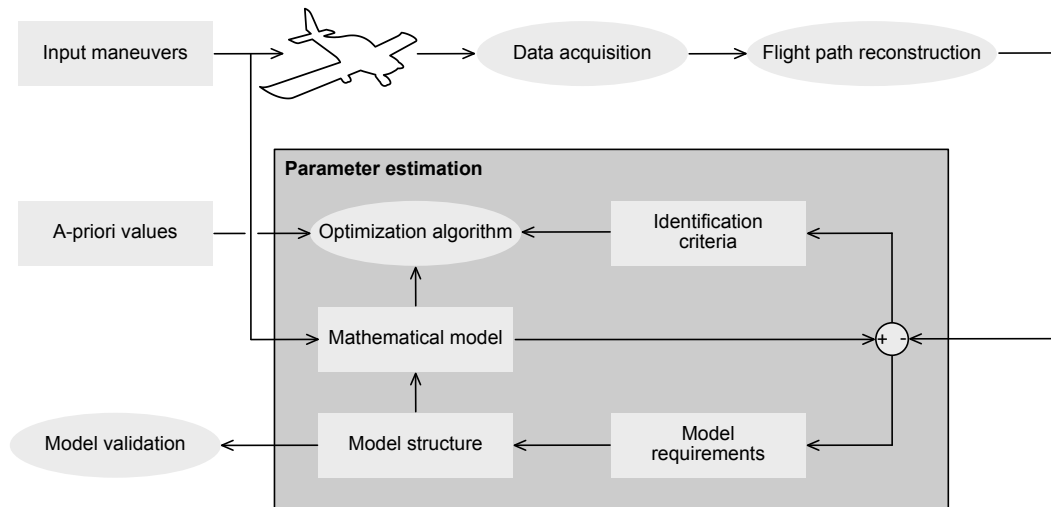


Figure 4.1: Identification process flow.

The description of the input maneuvers is given in Section 4.1. The Data Acquisition System and a general overview of the sensors used for aerospace applications is shown in the Section 4.2. The Section 4.3 discusses sensor errors and the Flight Path Reconstruction process. The description of the sources of a-priori values of respective aerodynamic parameters is given in Section 4.4. The estimation methods for the estimation of the flight parameters of a light airplane are discussed in Section 4.5.

### 4.1 Control inputs for system identification

For the purposes of the identification, it is necessary to properly excite the airplane's response. Optimal input design is a trade-off between sufficient frequency bandwidth and task complexity for the pilot to execute the control input.

#### 4.1.1 Time domain based inputs for identification

Time domain identification inputs use inputs with several steps. Time between steps is derived from input maneuver timing step  $\Delta t$ . For the demonstration of different inputs, timing step  $\Delta t = 0.5 s$  is used on graphs in this section.

**Pulse** is the simplest maneuver to excite oscillatory aircraft motion. It consists of injecting a deflection to control surface from a trimmed position and returning the control surface back to a trimmed position. The main advantage of this identification maneuver is its simplicity of execution for the pilot. On the contrary, the main disadvantage is the asymmetry about the trim point, which leads to a nonzero energy at zero frequency. The example of pulse input is shown in Figure 4.2a.

**Doublet** is a commonly used maneuver to excite oscillatory motion. Doublet is a double pulse which is skew symmetric with time [95]. Doublet consists of two immediately following pulses with opposite direction. The symmetric shape of a doublet is its main advantage. A minor disadvantage of doublet is its narrow bandwidth of energy content. With the a-priori knowledge of characteristic frequency, doublet is a convenient identification input maneuver. The example of a doublet input is displayed in Figure 4.2b.

A more sophisticated approach features multistep input. In aerospace, **multistep 3-2-1-1 input** is commonly used. The main advantage of this input is in its wide bandwidth of energy content. Disadvantage of this input is the necessity of a highly trained test pilot or an automatic task execution control system which is able to precisely execute the maneuver. The example of a multistep 3-2-1-1 input is presented in Figure 4.2c.

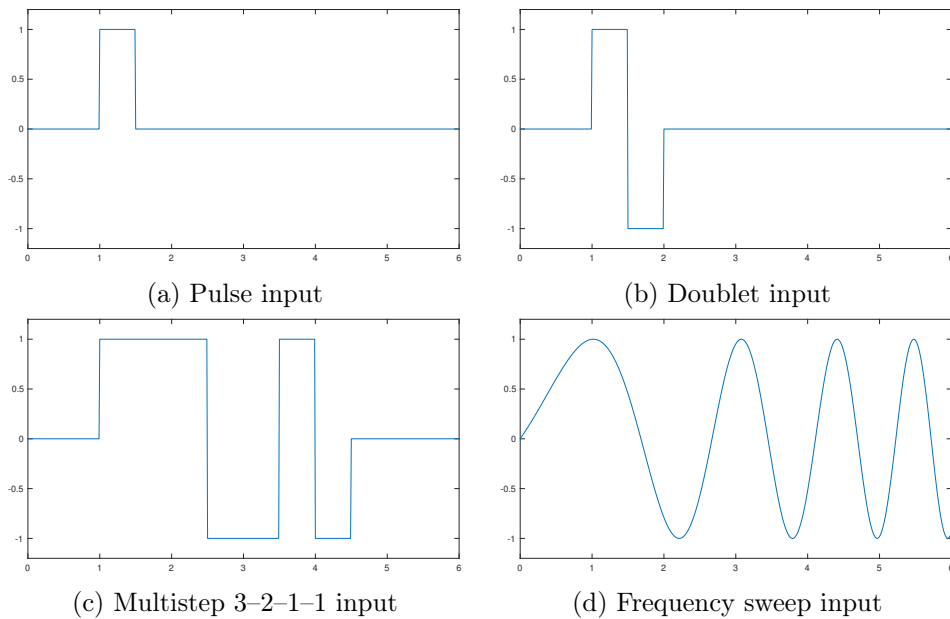


Figure 4.2: Input maneuver examples.

#### 4.1.2 Frequency domain based inputs for identification

The frequency domain identification inputs ask for a more wider bandwidth of energy content. These inputs are sometimes called harmonic inputs and they are very difficult to be executed manually.

**Frequency sweep** consists of a sinusoidal signal with a frequency changing during a time. Frequency sweep inputs are usually used in rotorcraft identification [54]. An example of a frequency sweep input is drawn in Figure 4.2d.

Other complex input signals were proposed by Jategaonkar in [54]. The examples of complex inputs signals are: the Mehra–input and the DUT–input<sup>1</sup>. These inputs consist of a combination of harmonic signals intended to excite the dynamics of the observed system.

### 4.1.3 Typical maneuvers in longitudinal and lateral/directional motion

Maneuvers for the identification of the longitudinal motion properties are designed to excite two principal longitudinal motion modes: short–period mode and phugoid mode. Each of longitudinal modes has different properties. For excite short–period mode elevator doublet or elevator 3–2–1–1 input with  $\Delta t \in (0.5, 1.0)$  s are recommended. Phugoid mode excitation uses long elevator pulse with  $\Delta t \approx 10$  s or throttle doublet with  $\Delta t \approx 10$  s.

For the purposes of this thesis, elevator doublets are used as a input maneuvers for longitudinal motion.

Maneuvers for the identification of the lateral–directional motion properties are designed to excite three principal lateral–directional motion modes: roll mode, Dutch roll mode and spiral mode. Excitation of roll mode uses several aileron pulses. Roll mode pulses is defined by maximum roll angle  $\phi \in \pm 30^\circ$ . For dutch roll mode excitation, rudder doublet with  $\Delta t \approx 1.0$  s is recommended.

## 4.2 Data acquisition

This section is dedicated to the data acquisition part of the identification process. The most important aspect of the data acquisition is the time synchronization of recorded channels. As the identification describes the relations between respective variables, i.e., the causes and the effects, it is very desirable not to introduce unwanted time delays into the measured data.

Hence, all measured data is gathered from sensors. Following section introduces a description of sensors and their measuring principles. Sensors, which are commonly used in aeronautical applications, can be divided into four categories: pilot’s input and control surface deflection sensors; position, orientation and motion sensors; airdata sensors; and engine data sensors.

In general, there are three optional types of signals coming from the sensors: analog, pulse and digital. Most of the sensors have analog output, so the signal needs to be digitalized by Analog to Digital Converters (ADC) [3]. Minority of sensors have a pulse output, e.g., sensing the rotation of the engine or propeller shaft (see Section 4.2.4). There are only few sensors with a direct digital output, e.g., Grey coded optical sensors (see Section 4.2.1).

### 4.2.1 Pilot input and control surface deflection sensors

As a pilot inputs are considered manipulation with pilot control stick or yoke, pedals, flaps, gear and control levers. Usually there are measured position and orientations of the above mentioned controls and applied force [54, 100]. For the purposes of this thesis, control surface deflection, i.e., position and orientation of elevator, ailerons, rudder, flaps and trim

---

<sup>1</sup>DUT – Delft University of Technology

surfaces, are measured in a same way and using the same sensors as above mentioned pilot inputs.

In the aviation, there are three main principles of measuring the position or orientation of an aircraft component: electrical, magnetic and optical. On the contrary, there is only one principle used for measuring the applied force, i.e., strain gauge [36, 101].

**Electrical principle** of measuring of the position and orientation is based on utilization of potentiometers [70, 100]. Potentiometers act as variable voltage dividers. They consist of a resistive element, sliding contact (called wiper) and an isolating housing. Wiper is connected to the measured object and the resistive element is placed nearby the measured object so that wiper divide resistive element into two segments. The resistive element can be either straight (to measure the position) or curved (to measure the orientation).

Generally, there are two approaches to construct a resistive element. The first approach is based on the utilization of a wire coil [36, 70]. The advantage of this solution is in its longer service life. On the contrary, the potentiometers based on the usage of a wire coil have a quantization error, because the wire acts as a minimum step in value. The second approach is based on the application of a resistive material onto an underlying isolation base [70]. Disadvantage of this solution is that wiper is scratching the resistive material which can lead to a short service life. On the other hand, the resistive material is homogenous and has no discrete steps.

**Magnetic principle** uses sensing of magnetic field of permanent magnet for measuring of orientation. Magnet is attached to the measured object and Hall effect sensor is placed nearby measured object so that the Hall effect sensor can sense a change of orientation of magnetic field [4, 100]. Advantage of Hall effect sensors is that these sensors enable contactless sensing. Unfortunately, this sensor can be influenced by the magnetic field generated by electric motors and high-current wires.

**Optical principle** sensors in aviation are represented mostly by the Gray coded sensors and direct distance sensors. Direct distance sensors use laser to measure the distance from the reflector [70]. Reflector is attached to the measured object and an optical distance sensor is placed nearby. Direct distance sensors are costly but also very accurate.

Gray coded optical sensors consist of a Gray coded disc or ruler attached to the measured object, multiple optical photosensitive elements and lighting elements [70]. There are two approaches for lighting the disc or ruler: backlighting (uses perforated disc or ruler) or reflection (disc or ruler from reflective material). Gray coded optical sensors have digital output and its size increase with the required precision of the sensor.

**Strain gauges** measure the applied force and usually consist of a thin foil with resistive path [36, 101]. Strain gauge sensors are sensitive only in one direction. Stretching/shortening the strain gauge in this direction causes thinning/thickening of the resistive path, therefore changing the resistance. Disadvantage of the strain gauges is its temperature sensitivity. Therefore usually a pair of strain gauges has to be used (second one is used for temperature compensation).

## 4.2.2 Position, orientation and motion sensors

The position, orientation and motion of the airplane is measured using, Global Navigation Satellite System sensors, Magnetometers and Gyroscopes/Accelerometers, respectively.

**Global Navigation Satellite System (GNSS) receiver** provides the timestamp, position (geodetic latitude, longitude and height above the WGS84 ellipsoid) and the velocity in a Geodetic reference frame [71, 83]. The antenna of a GNSS receiver has to be placed on the fuselage of an airplane so that it meets the requirement of an unobstructed sky visibility. Nowadays, there are only two fully operational GNSS: Global Positioning System (GPS) [71] and ГЛОБАЛЬНАЯ НАВИГАЦИОННАЯ СПУТНИКОВАЯ СИСТЕМА (GLONASS) [84]. The most commonly used system is the GPS; however, the newer sensors often utilize both systems [38].

**Magnetometer** [74] is a device able to measure orientation of an airplane, i.e., the vector of the Earth magnetic field. The magnetometer is usually placed in the tail part of the fuselage or in the wing of the airplane due to its sensitivity to the magnetic field generated by the electric motors and magnetic materials. The orientation of magnetometer should be aligned with the Body-fixed reference frame axes to simplify its calibration and subsequent calculation. In aviation, there are two main used types of magnetometers: Hall effect (see 4.2.1) magnetometers and magneto-resistive element (permalloy foil coils) magnetometers.

**Gyroscope** [13, 74] measures angular velocity relative to the Inertial reference frame. Gyroscope is not sensitive to its installation position in an airplane (usually it is a part of the inertial sensors assembly and is located near accelerometers). The orientation of gyroscopes should be aligned with the Body-fixed reference frame axes to simplify the calibration and subsequent calculation. Currently most used types of gyroscopes in aviation are: mechanical, Microelectromechanical Systems (MEMS) and optical.

Mechanical gyroscope (also known as the gyrostat) is based on a massive rotating flywheel [74]. Massive flywheel requires a substantial amount of power to maintain its rotation. It also has to be perfectly balanced, which makes the manufacturing and subsequent maintenance of the mechanical gyroscopes very expensive. Unfortunately, the mechanical gyroscopes are prone to the Gimbal-lock phenomena.

MEMS introduce the design of the gyroscopes based on the Foucault pendulum principle [74]. Foucault pendulum is a free to swing pendulum used to show the precession created by the Coriolis force. MEMS gyroscopes have a small size and are relatively low price sensors.

In aviation, there are two types of optical gyroscopes. Ring Laser Gyroscopes (RLG) based on a gas laser [13, 67] and Fiber Optics Gyroscopes (FOG) designed around the semiconductor laser [13, 74]. Optical gyroscopes are currently the most precise type of gyroscopes but at the same time also the most expensive.

**Accelerometer** [54, 74] is a device able to measure acceleration, i.e., specific force. Accelerometers should be installed in the center of mass of an airplane, as otherwise they will be influenced by the translational acceleration generated by aircraft angular rotation. In practice, it is not applicable to position the accelerometer precisely in the airplane's center of mass because the position of center of mass is slowly but continuously changing during the flight due to the fuel consumption (see Section 3.4.1). The orientation of accelerometers should be aligned with Body-fixed reference frame axes in order to simplify the calibration

and a subsequent calculation.

Nowadays, the most used types of accelerometers in aviation are the proof mass accelerometers [67, 74]. The principle of proof mass accelerometers is based on the attachment of a proof mass to a force measuring element (directly or using flexible connection) and a subsequent computation of the force based on the Second Newton's law of motion. Currently, there are three used types of the force measuring elements: piezoelectric element (voltage is generated by the deformation of a piezoelectric element), strain gauge (see Section 4.2.1) or a vibrating string (frequency of vibration is changed according to the tension on the string).

### 4.2.3 Airdata sensors

The airdata sensors are sensors measuring properties of the surrounding air, i.e., pressures, air temperature and the direction of the airflow.

**Pressure transducer** is a sensor used for measuring of applied pressure. In aerospace, there are three types of pressure to be considered [100]: static pressure (supplied through the static ports), total pressure (supplied through the pitot tube) and an impact pressure (computed as a difference between the total pressure and the static pressure).

To perform pressure measurement, we can consider one of the two main types of pressure transducers: piezoresistive and resonant [36, 100]. Piezoresistive pressure transducer consists of two chambers separated by membrane with an attached piezoresistive element. The difference of pressure between the chambers deforms the membrane, which is measured by a piezoresistive element. The resonant pressure transducer uses a vibrating chamber, where the difference in pressure inside and outside of the chamber changes the chamber's resonance frequency.

**Temperature sensors** used in aerospace measure the Outside Air Temperature (OAT) and are usually located at the bottom side of the fuselage or wing. For the purposes of this thesis, the mechanical temperature sensors, i.e., bimetalic and liquid, cannot be used due to the digitalization problems, therefore only electronic temperature sensors are considered.

Electronic temperature sensors can be divided into three major types: thermistors, thermocouples and diode based temperature sensors [101]. Thermistors are resistors with defined temperature dependence. According to the ARINC's<sup>2</sup> recommendation [7], platinum thermistors with nominal resistance  $500\ \Omega$  at  $0\ ^\circ\text{C}$  should be used due to its higher precision. Thermocouples are used in the high temperature application like measuring of Exhaust Gas Temperature (see Section 4.2.4). Diode based temperature sensors are based on measuring of voltage on PN-junction that is temperature dependent. Diode based temperature sensors are usually used for the measuring temperature on silicon chips because PN-junctions are already contained and there is no need to incorporate additional element.

**Direction of the airflow sensors** [54, 77] measure the direction of the aerodynamic velocity, i.e., angle-of-attack and flank angle (from which the angle-of-sideslip can be calculated). There are two main types of these sensors: flush airdata sensors and flow vanes sensors. Flush airdata sensors, sometimes called five-hole probe [54], utilize five or more tubes placed in different directions to measure the difference between the pressure in these tubes. The flow vane sensors consist of two vanes whose axes of rotation are perpendicular

---

<sup>2</sup>ARINC – Aeronautical Radio, Incorporated

to each other [74]. The vane with horizontal rotation axis measures the angle-of-attack and the vane with vertical rotation axis measures the flank angle.

The direction of the airflow sensors are influenced by the distortion of the airflow created by the pressure field around an aircraft in top—bottom direction (upwash phenomena) and left—right direction (sidewash phenomena) [63, 74]. This effect can be minimized by installing the flow vane sensors further from aircraft. The recommended position of this type of sensor is the leading edge on the tip of the wing.

#### 4.2.4 Engine data sensors

In aviation, a variety of engine types is used, e.g., piston engines with propeller, turboprop engines and a spectrum of jet engines. This thesis focused on airplanes with a single piston engine with propeller. Propulsion sensors used in this type of engines can be divided to three main categories: propeller sensors, engine sensors and fuel sensors.

**Propeller sensor**, i.e., tachometer, measures the rotation speed of the propeller. Most piston engines have an equal rotation speed of the engine shaft and the propeller. Nevertheless, engines in the Bombardier Rotax 912 family [12], which is the type of engine used for the purposes of this thesis, feature a mechanical gearbox for the reduction of the rotation speed of the propeller.

The rotation speed of the propeller is measured using a pulse signal [74]. Generally, the tachometers can utilize two different principles: measuring the time between the pulses and counting the revolutions per time interval. The values measured using the sensor based on the first principle are more accurate. Nevertheless, the sensor based on the second principle is easier to manufacture and is cheaper.

**Engine sensors** measure temperature, pressure and rotation speed of the engine shaft. For the purposes of this thesis, temperatures measured on the piston engine are the Exhaust Gas Temperature (EGT), Cylinder Head Temperature (CHT), and oil temperature [3, 101]. EGT has to be measured by a thermocouple because other approaches are not able to withstand long-term temperatures of about  $1000^{\circ}\text{C}$  [74, 101]. CHT and oil temperature are measured either by thermistors or by thermocouples. The working principle of both sensors is given in Section 4.2.3.

Pressures measured on the piston engine are the oil pressure and the manifold pressure [101], both are measured using piezoresistive pressure transducers (see Section 4.2.3). The oil pressure acts as a control mechanism for determining the engine health. Manifold pressure indicates the amount of air entering the engine thus the amount of engine power available for propelling the airplane.

The rotation speed of the piston engine shaft is measured using the tachometer [101]. For a more detailed description of the tachometers see the Propeller sensor paragraph above.

**Fuel sensors** measure the fuel level, fuel flow, fuel temperature and pressure. For the purposes of this thesis only the fuel flow and fuel level are measured. The fuel flow sensor measures the fuel consumption. The commonly used types of the fuel flow sensors use an inlet and a rotor with a tachometer [74, 100], because the angular velocity of the rotor is directly proportional to the fuel flow. State-of-the-art injection type engines can have the fuel flow detection embedded inside the engine control electronics.

The fuel level sensors measure the amount of the fuel inside the fuel tank [74, 100]. There are two main construction principles for the fuel level sensors: float based sensors or capacitive sensors. Float based sensors contain a float floating on surface of the fuel and measure its position. Capacitive sensors measure the electric capacity on a dielectrically isolated probe inside the fuel tank, as electric capacity is proportional to amount of the fuel in the fuel tank. It should be noted that the precision of the fuel level measurement depends on the tilt of the airplane. Therefore it is advised to combine the fuel level measurement with a fuel flow measurement to ensure a precision reading of fuel quantity in maneuvers.

### 4.3 Flight Path Reconstruction

As introduced in Section 4.2, all sensor outputs are affected by errors. The output of the sensors is effected by the deterministic and stochastic errors. Deterministic errors contain the sensor errors and the position errors. Stochastic errors are difficult to predict, e.g., noise. Hence, some of the variables are measured by more than one sensor, or estimated using the integration or derivation of specific variable. It is also possible to use a redundancy in sensor output as a way to minimize some of the errors.

Some sensors do not directly measure required quantity, but the required quantity can be estimated from these measurements. The angle-of-sideslip cannot be measured directly, but it is convenient to measure the flank angle. Measured flank angle  $\beta_f$  is further used for the computation of the angle-of-sideslip using Equation [58, 63]:

$$\beta = \arctan(\tan \beta_f \cdot \cos \alpha) \quad (4.1)$$

First part of this section introduces common sensor errors. In the following part, the position errors of the sensors are described. Further, the measurement and the process noises are analyzed. At the end of this section, Kalman Filter and its variants are discussed.

#### 4.3.1 Bias and gain error

Most of the sensor outputs contain sensor errors, and most sensors errors can be corrected by calibration.

The direction of the airflow sensors suffers from sensors errors which can be compensated using gains and bias values. The sensor error in the direction of the airflow sensor is caused by the pressure field created around the airplane. The effect on the flow vanes is also called upwash or sidewash and can be computed using the equation:

$$\alpha_m = K_\alpha \alpha + b_\alpha \quad (4.2a)$$

$$\beta_{fm} = K_\beta \beta_f + b_{\beta_f} \quad (4.2b)$$

where  $\alpha_m$  is the measured angle-of-attack,  $\beta_{fm}$  is the measured flank angle,  $b_\alpha$  and  $b_\beta$  are the biases, and  $K_\alpha$  and  $K_\beta$  are the scale factors caused by upwash or sidewash.

### 4.3.2 Position error

The position error affects the sensor output due to an inconvenient installation position of the sensor or an incorrect axis alignment.

An accelerometer output suffers from an incorrect installation position relative to the airplane centre of mass, as the center of mass is changing during the flight as a result of the fuel consumption as introduced in Section 3.4.1. Given that the specific force is a type of acceleration, the specific force of the whole airplane can be computed using an acceleration Equation 3.29. The resultant equation can be simplified by neglecting the velocity of change of accelerometers position to [54, 97]:

$$\vec{f}_G = \vec{f}_C + \begin{bmatrix} (q^2 + r^2) & -(pq - \dot{r}) & -(pr + \dot{q}) \\ -(pq + \dot{r}) & (p^2 + r^2) & -(qr - \dot{p}) \\ -(pr - \dot{q}) & -(qr + \dot{p}) & (p^2 + q^2) \end{bmatrix} \cdot \vec{r}_C \quad (4.3)$$

where  $\vec{f}_C$  is the specific force measured by the accelerometer, which is installed in position  $\vec{r}_C$  in the reference frame  $F_b$ .

In addition to that the position of the direction of the airflow sensors cause an apparent velocity due to airplane rotation. Equation 3.27 describes this effect in following form:

$$u_{Xb} = u_{Gb} + q_{ob} z_{Xb} - r_{ob} y_{Xb} \quad (4.4a)$$

$$v_{Xb} = v_{Gb} + r_{ob} x_{Xb} - p_{ob} z_{Xb} \quad (4.4b)$$

$$w_{Xb} = w_{Gb} + p_{ob} y_{Xb} - q_{ob} x_{Xb} \quad (4.4c)$$

### 4.3.3 Measurement and process noise

**The measurement noise** describes the stochastic error of a sensor. The measurement noise of most of the sensors exhibits Gaussian normal distribution.

The probability density function  $p(\vec{\chi})$  of a normal distribution  $\mathbb{N}$  of a general  $\vec{\chi} \sim \mathbb{N}(\vec{\mu}_\chi, \Sigma_\chi)$  is defined as:

$$p(\vec{\chi}) = \frac{1}{\sqrt{(2\pi)^{n_\chi} \det(\Sigma_\chi)}} \exp\left(-\frac{1}{2}(\vec{\chi} - \vec{\mu}_\chi)^T \Sigma_\chi^{-1} (\vec{\chi} - \vec{\mu}_\chi)\right) \quad (4.5)$$

where  $n_\chi$  is the count of elements of  $\vec{\chi}$ ,  $\Sigma$  is a covariance matrix of normal distribution and  $\vec{\mu}$  is a mean of normal distribution.

**The process noise** is the way to resolve uncertainties in inputs to a dynamic system.

Because input variables are measured similarly to output variables, process noise has also a normal distribution. For the purposes of this thesis, the turbulence is neglected.

### 4.3.4 Kalman Filter

Kalman Filter is based on the nonlinear kinematic Equations of motion described in Section 3.5.2.

**A bayesian model** for the uncertainties is based on the Bayesian estimation theory and assumed a-priori known probability densities of  $p(\vec{\theta})$  and  $p(\vec{z})$ . The conditional probability density  $p(\vec{\theta}|\vec{z})$  can be expressed using the Bayes' rule as:

$$p(\vec{\theta}|\vec{z}) = \frac{p(\vec{z}|\vec{\theta})p(\vec{\theta})}{p(\vec{z})} \quad (4.6)$$

where  $\vec{\theta}$  is the vector of parameters and  $\vec{z}$  is the measured output vector.

If  $\vec{\theta}$  has a normal distribution defined as:

$$\vec{\theta} \sim \mathbb{N}(\vec{\theta}_p, \Sigma_p) \quad (4.7)$$

then  $p(\vec{\theta})$  is:

$$p(\vec{\theta}) = \frac{1}{\sqrt{(2\pi)^n \det(\Sigma_p)}} \exp\left(-\frac{1}{2}(\vec{\theta} - \vec{\theta}_p)^T \Sigma_p^{-1} (\vec{\theta} - \vec{\theta}_p)\right) \quad (4.8)$$

where  $n$  is the number of parameters.

The probability density  $p(\vec{\theta}|\vec{z})$  can be expressed using Equation 4.6 as:

$$p(\vec{\theta}|\vec{z}) = \frac{1}{p(\vec{z})} \frac{1}{\sqrt{(2\pi)^{N+n} \det(\mathbf{R}) \det(\Sigma_p)}} \exp\left(-\frac{1}{2}(\vec{z} - \mathbf{X}\vec{\theta})^T \mathbf{R}^{-1} (\vec{z} - \mathbf{X}\vec{\theta}) - \frac{1}{2}(\vec{\theta} - \vec{\theta}_p)^T \Sigma_p^{-1} (\vec{\theta} - \vec{\theta}_p)\right) \quad (4.9)$$

where  $\mathbf{R}$  is the measurement noise covariance matrix,  $\mathbf{X}$  is the matrix of regressors and with the most probable estimate  $\hat{\vec{\theta}}$  being:

$$\hat{\vec{\theta}} = \max_{\vec{\theta}} p(\vec{\theta}|\vec{z}) \quad (4.10)$$

The cost function  $J()$  for minimization is derived to have following form:

$$J(\vec{\theta}) = \frac{1}{2}(\vec{z} - \mathbf{X}\vec{\theta})^T \mathbf{R}^{-1} (\vec{z} - \mathbf{X}\vec{\theta}) + \frac{1}{2}(\vec{\theta} - \vec{\theta}_p)^T \Sigma_p^{-1} (\vec{\theta} - \vec{\theta}_p) \quad (4.11)$$

**A discrete state-space model** can be described by following set of equations:

$$\vec{x}(k+1) = \Phi \vec{x}(k) + \Gamma \vec{u}(k) \quad (4.12a)$$

$$\vec{y}(k) = \mathbf{C} \vec{x}(k) + \mathbf{D} \vec{u}(k) \quad (4.12b)$$

$$\vec{x}(0) = \vec{x}_0 \quad (4.12c)$$

where  $k$  is the sample number,  $\Phi$  is the discrete state matrix and  $\Gamma$  is the discrete input matrix.

A diagram of a discrete state-space model is shown in Figure 4.3.

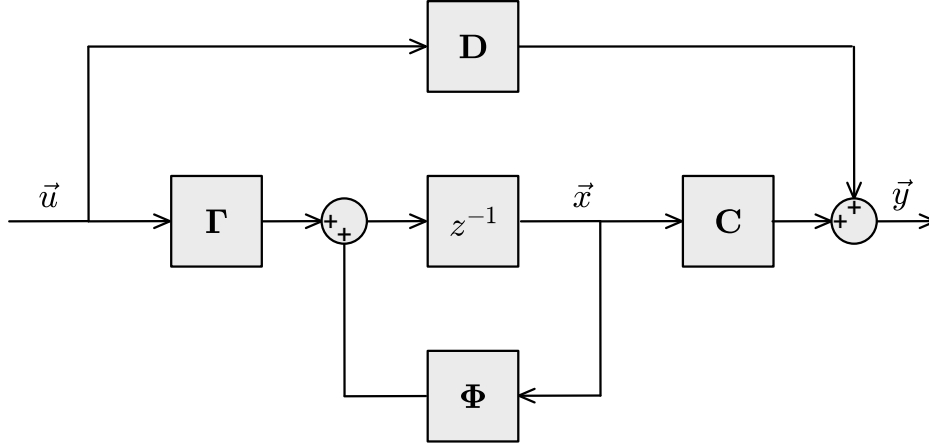


Figure 4.3: Dataflow diagram of a discrete state–space model.

The transformation of the continuous state–space matrices to the discrete state–space matrices becomes [9, 37]:

$$\Phi = e^{A\delta t} \Rightarrow \Phi = I + A\delta t + A^2 \frac{\delta t^2}{2!} + A^3 \frac{\delta t^3}{3!} + \dots \quad (4.13)$$

$$\Gamma = \int_0^{\delta t} e^{A\delta t} B \Rightarrow \Gamma = B\delta t + A \frac{\delta t^2}{2!} B + A^2 \frac{\delta t^3}{3!} B + \dots \quad (4.14)$$

where  $\delta t$  is a time step.

The most commonly used state estimation algorithm is the Kalman Filter (KF). The KF algorithm is divided into the prediction step and the correction step. The prediction step uses the system input to predict the probable state. Correction step uses a noisy measurement to improve the prediction of the state. The basic KF is a discrete version of the **Linear Kalman Filter**. The Linear Kalman Filter is an optimal estimator [60].

Assuming a discrete linear dynamic system with a process and measurement noises and a zero feed–through matrix as described by equation [60]:

$$\vec{x}(k+1) = \Phi \vec{x}(k) + \Gamma \vec{u}(k) + \Lambda \vec{w}(k) \quad (4.15a)$$

$$\vec{z}(k) = C \vec{x}(k) + \vec{v}(k) \quad (4.15b)$$

$$\vec{x}(0) = \vec{x}_0 \quad (4.15c)$$

where  $\Lambda$  is a discrete noise input matrix and  $\vec{w}$  is the process noise with a normal distribution defined as:

$$\vec{w} \sim \mathcal{N}(0, \mathbf{Q}) \quad (4.16)$$

where  $\mathbf{Q}$  is the process noise covariance matrix.

The prediction step of a Linear Kalman Filter is defined using following equation:

$$\vec{x}(k+1|k) = \Phi \vec{x}(k|k) + \Gamma \vec{u}(k) \quad (4.17)$$

where  $\vec{x}(k+1|k)$  is the state vector in step  $k+1$  based on information in step  $k$ .

The prediction of the probability of state  $\vec{x}$  is  $\mathbf{P}$  defined in equation:

$$\mathbf{P}(k+1|k) = \mathbf{\Phi} \mathbf{P}(k|k) \mathbf{\Phi}^T + \mathbf{\Lambda} \mathbf{Q} \mathbf{\Lambda}^T \quad (4.18)$$

The correction step of a Linear Kalman Filter is defined using following equation:

$$\vec{x}(k+1|k+1) = \vec{x}(k+1|k) + \mathbf{K}_{k+1} [\vec{z}(k+1) - \mathbf{C} \vec{x}(k+1|k)] \quad (4.19)$$

where  $\mathbf{K}_{k+1}$  is the Kalman gain matrix in step  $k+1$  defined in equation:

$$\mathbf{K}_{k+1} = \mathbf{P}(k+1|k) \mathbf{C}^T [\mathbf{C} \mathbf{P}(k+1|k) \mathbf{C}^T + \mathbf{R}]^{-1} \quad (4.20)$$

The correction of the probability of state  $\vec{x}$  is  $\mathbf{P}$  defined in following equation:

$$\mathbf{P}(k+1|k+1) = [\mathbf{I} - \mathbf{K}_{k+1} \mathbf{C}] \mathbf{P}(k+1|k) \quad (4.21)$$

The **Extended Kalman Filter** (EKF) is an approximate filter for nonlinear systems, based on local first-order linearization (see Section 3.6.1) and utilization of Linear Kalman Filter.

Assume discrete continuous dynamic system without feed-through inputs described by equation:

$$\vec{x}(k+1) = f'(\vec{x}(k), \vec{u}(k), \vec{w}(k)) \quad (4.22a)$$

$$\vec{y}(k) = h'(\vec{x}(k)) + \vec{v}(k) \quad (4.22b)$$

$$\vec{x}(0) = \vec{x}_0 \quad (4.22c)$$

where  $f'()$  is the discrete state function and  $h'()$  is the discrete output function.

The prediction step of the Extended Kalman Filter is defined using the equation:

$$\vec{x}(k+1|k) = f'(\vec{x}(k|k), \vec{u}(k), 0) \quad (4.23)$$

Prediction of the probability of the state  $\vec{x}$  is  $\mathbf{P}$  defined in Equation 4.18 in which  $\mathbf{\Phi}$  and  $\mathbf{\Lambda}$  are equal to:

$$\mathbf{\Phi} = \frac{\partial f'(\vec{x}(k|k), \vec{u}(k), 0)}{\partial \vec{x}} \quad (4.24a)$$

$$\mathbf{\Lambda} = \frac{\partial f'(\vec{x}(k|k), \vec{u}(k), 0)}{\partial \vec{w}} \quad (4.24b)$$

The correction step of a Extended Kalman Filter is defined using equation:

$$\vec{x}(k+1|k+1) = \vec{x}(k+1|k) + \mathbf{K}_{k+1} [\vec{z}(k+1) - h'(\vec{x}(k+1|k))] \quad (4.25)$$

where  $\mathbf{K}_{k+1}$  is the Kalman gain matrix, computed using Equation 4.20 and  $\mathbf{C}$  is the defined in equation:

$$\mathbf{C} = \frac{\partial h'(\vec{x}(k+1|k))}{\partial \vec{x}} \quad (4.26)$$

The correction of probability of state  $\vec{x}$  is  $\mathbf{P}$  defined in Equation 4.21.

Because the EKF use local linearization, it is no longer an optimal estimator. **Iterative EKF** uses internal iteration to compensate inaccuracies from linearization of output equation [62, 97].

The prediction step uses EKF Equations 4.18, 4.23 and 4.24.

The correction step is iterative and it starts with assigning  $\vec{\eta}_1$  to predicted state:

$$\vec{\eta}_1 = \vec{x}(k+1|k) \quad (4.27)$$

Next, output matrix  $\mathbf{C}$  and Kalman gain  $\mathbf{K}$  are computed using Equations 4.26 and 4.20. Then, new corrected state  $\vec{\eta}_2$  is computed using equation:

$$\vec{\eta}_2 = \vec{x}(k+1|k) + \mathbf{K}_{k+1} \left[ \vec{z}(k+1) - h'(\vec{\eta}_1) - \mathbf{C}(\vec{x}(k+1|k) - \vec{\eta}_1) \right] \quad (4.28)$$

Iteration stops if condition of inequality 4.29 is met:

$$\vec{\epsilon} \geq \frac{\|\vec{\eta}_2 - \vec{\eta}_1\|}{\|\vec{\eta}_1\|} \quad (4.29)$$

Next iteration starts with assigning  $\vec{\eta}_1$  to last estimate  $\vec{\eta}_2$ :

$$\vec{\eta}_1 = \vec{\eta}_2 \quad (4.30)$$

After the stop of iteration process, the corrected state is equal to:

$$\vec{x}(k+1|k+1) = \vec{\eta}_2 \quad (4.31)$$

The correction of the probability of the state  $\vec{x}$  is  $\mathbf{P}$  defined in Equation 4.21.

## 4.4 A-priori values acquisition

A-priori aerodynamic parameters are usually computed using predictive tools, based on statistical data or advanced numerical simulations. Prediction tools based on the Vortex Lattice Method (VLM) theory, mainly software packages Tornado and Athena Vortex Lattice (AVL) were used in this thesis. To augment the computed results with a set of differently estimated data, the United States Air Force (USAF) Datcom predictions have been utilized.

All above mentioned sources of the a-priori values are described in detail in following sections.

### 4.4.1 Tornado

The Tornado is a VLM software for the estimation of flight parameters on the basis of airplane geometry [66]. The shape of the airplane is transformed to its planar representation featuring respective airfoil data. The planar representation of the airplane serves as an input for the solver.

A missing support for fuselage parts modeling is the main disadvantage of the Tornado calculations. Although the fuselage can be substituted by its planar representation or can be completely omitted for the case of longitudinal motion analysis.

The Tornado software covers the effects of the linear aerodynamics [66], which can limit its usability. However, for the purposes of this thesis its prediction fall into the region of validity.

The Tornado software is programmed in Matlab and distributed as source code under a GNU General Public License.

#### 4.4.2 AVL

The AVL (Athena Vortex Lattice) is a VLM software for the analysis of a rigid aircraft flight mechanics [19]. For the output, the AVL offers linearization of the flight parameters in any flight state and mass properties settings. Linearization is based on small perturbations theory and is not completely valid when velocity perturbations from the free-stream become large.

The main advantage of AVL is the support of a slender-body models for fuselages and nacelles. All bodies has to have circular cross-section. According to manual, the non-round bodies must be approximated with an equivalent round body which has roughly the same cross-sectional areas.

The AVL software is programmed in Fortran and distributed in source code and binaries for major platforms. The AVL software is released under the GNU General Public License.

#### 4.4.3 Datcom

The USAF Datcom is systematic summary of methods for estimating stability and control characteristics in preliminary design phase [99]. The Datcom was developed by McDonnell Douglas Corporation [99] under contract of USAF in cooperation with Wright-Patterson Air Force Base.

Limitations of Datcom is lack of support of the tapered wing, the H-tail and canard control surface. Those limitations are not important for light airplane category which is focus of this thesis.

The USAF Datcom is written completely in American National Standards Institute (ANSI) Fortran.

### 4.5 Estimation methods

Parameter estimation uses system models and optimization methods to estimate the values of investigated parameters.

The two basic approaches in estimation are the offline estimation and the online estimation. The offline estimation uses all measured values in all iterations of the algorithm. The online

estimation uses currently measured values and previous estimate in current iteration of algorithm.

Two different estimators can be conveniently used for an offline parameter estimation: Least-Squares estimator and maximum likelihood estimator. Least-Squares is a simple estimator providing very good results. The maximum likelihood estimator requires complex knowledge of the investigated system, but its estimates provide high fidelity results.

There is a variety of estimation approaches for the estimation of the flight parameters. The most often used and also the most often recommended methods are: Equation Error Method (based on the Least-Squares estimator), Output Error Method (based on the maximum likelihood estimator) and Recursive Least-Squares (based on the Least-Squares estimator). These approaches are described in Sections 4.5.1 to 4.5.3. The alternative approaches, e.g., Artificial neural network estimation and Genetic algorithm estimation, are given in Section 4.5.4.

The overview of the estimation methods is given in Figure 4.4.

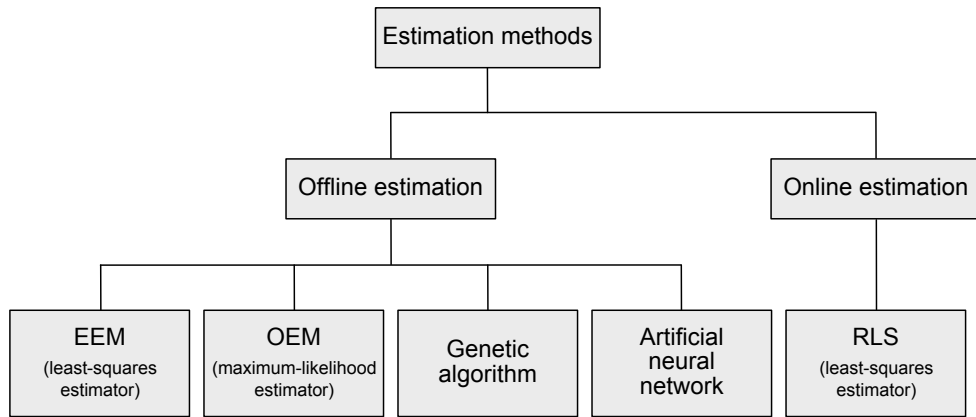


Figure 4.4: Estimation methods categorization.

### 4.5.1 Equation Error Method

The Equation Error Method (EEM) is based on the Least-Squares model, which was perhaps the first approach to the concept of optimality. The Least-Squares technique is mainly known in its application to the curve fitting or regression analysis. In these problems it is desired to represent the measured data by simple functional relationship or by a smooth curve. The solution minimizes the sum of the squares of deviations between data points and corresponding points obtained from the solution.

Measurement vector consists of the output vector and measurement noise  $\vec{v}$ :

$$\vec{z} = \vec{y} + \vec{v} \quad (4.32)$$

Simplification of the dynamic system equations to linear combination of regressors to:

$$\vec{y} = \mathbf{X} \vec{\theta} \quad (4.33)$$

where  $\mathbf{X}$  is the matrix of regressors.

Ordinary Least-Squares (OLS) model is well-known estimation model. Model is assumption free, so no a-priori known probability densities of  $p(\vec{\theta})$  and  $p(\vec{v})$  are required. OLS is sometimes called just a Least-Squares. Model uses cost function expressed as a sum of squares [58]:

$$J(\vec{\theta}) = \frac{1}{2} (\vec{z} - \mathbf{X}\vec{\theta})^T (\vec{z} - \mathbf{X}\vec{\theta}) \quad (4.34)$$

Generalization of the Ordinary Least-Squares to Weighted Least-Squares (WLS) uses inversion of weight matrix  $\mathbf{R}^{-1}$  and cost function became to:

$$J(\vec{\theta}) = \frac{1}{2} (\vec{z} - \mathbf{X}\vec{\theta})^T \mathbf{R}^{-1} (\vec{z} - \mathbf{X}\vec{\theta}) \quad (4.35)$$

The extension of the Least-Squares technique to the estimation of parameters of the dynamic system from measured time histories of the input and output is based on the assumption:

$$\vec{y} = \dot{\vec{x}} \quad (4.36)$$

Using this assumption measured output  $\vec{z}$  is equal to:

$$\vec{z} = \dot{\vec{x}} + \vec{v} \quad (4.37)$$

Given that:

- $\vec{x}$  and  $\vec{u}$  are known from the measurements without errors; and
- $\vec{z}$  are measured values, corrupted by measurement errors.

Using the measured data and above mentioned equations, the resultant aerodynamic forces and moments acting on the airplane are expressed by means of the aerodynamic model equations which may be written as

$$\dot{\vec{x}} = \theta_0 + \theta_1 \vec{x}_1 + \dots + \theta_n \vec{x}_n + \theta_{n+1} \vec{u} + \dots + \theta_{n+m} \vec{u}_m \quad (4.38)$$

In this equation  $\dot{\vec{x}}$  represents the resultant coefficient of the aerodynamic force or moment,  $\theta_1$  through  $\theta_{n+m}$  are the stability and control derivatives,  $\theta_0$  is the value of any particular coefficient corresponding to the initial steady-state flight conditions,  $\vec{x}_1$  to  $\vec{x}_n$  are the airplane states, and  $\vec{u}_1$  to  $\vec{u}_m$  are the control variables.

By substituting  $\vec{y}$  in Equation 4.38 the measured values of  $x$  and  $u$  could be taken into form of Equation 4.33. Then the equation error can be expresses as:

$$\vec{v} = \vec{z} - \mathbf{X}\vec{\theta} \quad (4.39)$$

where:

$$\mathbf{X} = [1, \vec{x}_1, \dots, \vec{x}_n, \vec{u}_1, \dots, \vec{u}_m] \quad (4.40a)$$

$$\vec{\theta} = [\theta_0, \theta_1, \dots, \theta_{n+m}]^T \quad (4.40b)$$

The minimization of the cost function 4.34:

$$J(\vec{\theta}) = \frac{1}{2} (\vec{z} - \mathbf{X}\vec{\theta})^T (\vec{z} - \mathbf{X}\vec{\theta}) \quad (4.41)$$

is obtained by setting

$$\frac{\partial J(\vec{\theta})}{\partial \theta} = 0 \quad (4.42)$$

Because of

$$\frac{\partial J(\hat{\vec{\theta}})}{\partial \vec{\theta}} = -\mathbf{X}^T (\vec{z} - \mathbf{X}\hat{\vec{\theta}}) = 0 \quad (4.43)$$

then  $\hat{\vec{\theta}}$  can be solved as

$$\hat{\vec{\theta}} = (\mathbf{X}^T \mathbf{X})^{-1} \mathbf{X}^T \vec{z} \quad (4.44)$$

This result is called the Least-Square estimate of  $\vec{\theta}$ .

The Figure 4.5 represents the dataflow diagram of Equation Error Method for the flight parameter estimation.

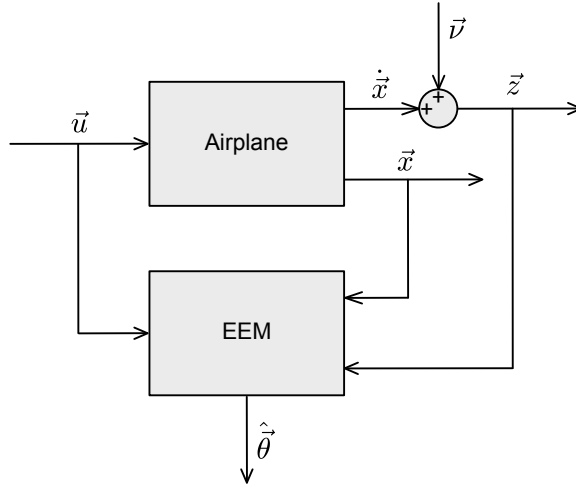


Figure 4.5: Block diagram of the EEM.

The estimation of longitudinal motion model parameters utilizes a linear model structure described in Equation 3.83. As an example for parameter estimation, the velocity can be used. In this case the vectors of parameters, regressors are defined as follows:

$$\mathbf{X} = [\vec{V}, \vec{\alpha}, \vec{q}, \vec{\theta}, \vec{\delta}_e, \vec{F}_P] \quad (4.45a)$$

$$\vec{\theta} = [D_V, D_\alpha, D_q, D_\theta, D_{\delta_e}, D_{F_P}]^T \quad (4.45b)$$

The derivative of velocity was numerically computed using the smoothed local numerical differentiation and it is considered as the left side of Equation 4.38. Both regressor and derivative are substituted into Equation 4.44.

The identified model in a state–space representation has certain advantages e.g. it is possible to use it for a stability analysis, express dynamic characteristic of the system. In some cases it can be useful to express the aerodynamic derivatives directly. This approach requires to compute the forces and moments acting on the aircraft according to Equation 3.66 and Equation 3.70:

$$X = m (\dot{u} + G_0 \sin \theta - r v + q w) \quad (4.46a)$$

$$Y = m (\dot{v} - G_0 \cos \theta \sin \phi - p w + r u) \quad (4.46b)$$

$$Z = m (\dot{w} - G_0 \cos \theta \cos \phi - q u + p v) \quad (4.46c)$$

$$L = J_x \dot{p} - J_{xz} \dot{r} + q r (J_z - J_y) - p q J_{xz} \quad (4.46d)$$

$$M = J_y \dot{q} + p r (J_x - J_z) + J_{xz} (p^2 - r^2) \quad (4.46e)$$

$$N = -J_{xz} \dot{p} + J_z \dot{r} + p q (J_y - J_x) + q r J_{xz} \quad (4.46f)$$

and express the forces and moments coefficients in body fixed frame as follows:

$$C_X = \frac{m (\dot{u} + G_0 \sin \theta - r v + q w)}{\bar{q} S} \quad (4.47a)$$

$$C_Y = \frac{m (\dot{v} - G_0 \cos \theta \sin \phi - p w + r u)}{\bar{q} S} \quad (4.47b)$$

$$C_Z = \frac{m (\dot{w} - G_0 \cos \theta \cos \phi - q u + p v)}{\bar{q} S} \quad (4.47c)$$

$$C_l = \frac{J_x \dot{p} - J_{xz} \dot{r} + q r (J_z - J_y) - p q J_{xz}}{\bar{q} S b_w} \quad (4.47d)$$

$$C_m = \frac{J_y \dot{q} + p r (J_x - J_z) + J_{xz} (p^2 - r^2)}{\bar{q} S \bar{c}} \quad (4.47e)$$

$$C_n = \frac{-J_{xz} \dot{p} + J_z \dot{r} + p q (J_y - J_x) + q r J_{xz}}{\bar{q} S b_w} \quad (4.47f)$$

In this case the model for parameter estimation is inspired by the aerodynamic model from Equations 3.51, the only difference is that it is necessary to add the effect of the aircraft propulsion. The regressor and parameter vectors are expressed as follows:

$$\mathbf{X} = [1, \vec{V}, \vec{\alpha}, \vec{q}^*, \vec{\delta}_e, \vec{F}_P] \quad (4.48a)$$

$$\vec{\theta} = [C_{Xb}, C_{X\alpha}, C_{Xq}, C_{X\delta_e}, C_{XF_P}]^T \quad (4.48b)$$

where the forces and moments coefficients are taken as the left side of the regression model described in Equation 4.38. Direct computation of aerodynamic coefficients can be beneficial for building the dynamic model of the examined aircraft or aerodynamic analysis.

## 4.5.2 Output Error Method

The Output Error Method (OEM) belongs to the category of the maximum likelihood parameter estimators and it is a widely used technique in the field of aircraft parameters estimation. The advantage of this approach is in its simple utilization for systems with nonlinear dynamics. The necessity of the initial parameters estimate can be taken as a

minor drawback, the OEM is thus assumed as the algorithm for initial model improvement according to real measurement.

The OEM parameter estimator was designed for the Fisher model structure, that can be considered in either linear or nonlinear form and is described in Equations (4.49). The uncertainties are based on a-priori knowledge of the measurement noise  $\vec{v}$ .

$$\vec{z} = \mathbf{H}\vec{\theta} + \vec{v} \quad (4.49a)$$

$$\vec{z} = h(\vec{\theta}) + \vec{v} \quad (4.49b)$$

The measurement noise  $\vec{v}$  has the normal distribution defined as:

$$\vec{v} \sim \mathbf{N}(0, \mathbf{R}) \quad (4.50)$$

In practical applications the noise covariance matrix is usually estimated from measurement noise  $\vec{v} = \vec{y} - h(\vec{\theta})$ . The estimation process is shown in the following equation.

$$\hat{\mathbf{R}} = \frac{1}{N} \sum_{i=1}^N \vec{v}(i) \vec{v}^T(i) \quad (4.51)$$

Using the property of normal distribution from Equation 4.5:  $p(\vec{z}|\vec{\theta})$  is defined as:

$$p(\vec{z}|\vec{\theta}) = \frac{1}{\sqrt{(2\pi)^{n_z} \det(\mathbf{R})}} \exp\left(-\frac{1}{2}(\vec{z} - \mathbf{X}\vec{\theta})^T \mathbf{R}^{-1}(\vec{z} - \mathbf{X}\vec{\theta})\right) \quad (4.52)$$

where  $n_z$  is the number of measured variables in  $\vec{z}$ .

The likelihood function is considered to have normal distribution, thus it is possible to express it as the conditioned probability function from foregoing equation. The Fisher model is based on the Fisher estimation theory using:

$$\mathbb{L}(\vec{z}; \vec{\theta}) = p(\vec{z}|\vec{\theta}) \quad (4.53)$$

The maximum likelihood estimator that is recommended for the linear form of the Fisher model searches a maximum of the following likelihood function.

$$\mathbb{L}(\vec{z}; \vec{\theta}) = \frac{1}{\sqrt{(2\pi)^{n_z} \det(\mathbf{R})}} \exp\left(-\frac{1}{2}(\vec{z} - \mathbf{X}\vec{\theta})^T \mathbf{R}^{-1}(\vec{z} - \mathbf{X}\vec{\theta})\right) \quad (4.54)$$

Therefore the parameter estimate  $\hat{\vec{\theta}}$  can be expressed as:

$$\hat{\vec{\theta}} = \max_{\vec{\theta}} \mathbb{L}(\vec{z}; \vec{\theta}) \quad (4.55)$$

The maximum of the likelihood function is found with the utilization of logarithm and the becoming a negative log-likelihood.

$$-\ln \left[ \mathbb{L}(\vec{z}; \vec{\theta}) \right] = \frac{1}{2}(\vec{z} - \mathbf{X}\vec{\theta})^T \mathbf{R}^{-1}(\vec{z} - \mathbf{X}\vec{\theta}) + \frac{1}{2} \ln [\det(\mathbf{R})] \quad (4.56)$$

Using known measurement noise covariance matrix cost function became:

$$J(\vec{\theta}) = \frac{1}{2} (\vec{z} - \mathbf{X}\vec{\theta})^T \mathbf{R}^{-1} (\vec{z} - \mathbf{X}\vec{\theta}) \quad (4.57)$$

The cost function for minimization is equal to Weighted Least-Squares.

Using the estimation of measurement noise covariance matrix from Equation 4.51, the cost function with omitted constant terms becomes:

$$J(\vec{\theta}) = \frac{1}{2} \ln [\det(\mathbf{R})] \quad (4.58)$$

The Output Error Method (OEM) minimizes the errors between the actual output and the model output by using the same input. It is assumed that only measured outputs are corrupted by noise and that there are no gust or other disturbances to the airplane. The optimization problem, involved is nonlinear and requires the use of an iterative solution. The Modified Newton-Raphson (MNR) technique is usually applied because of its good convergence rate even for large number of unknown parameters. The OEM is also called the maximum likelihood method because Fisher model is used for the parameter estimation in the output error cost function.

The Figure 4.6 represents the dataflow diagram of Output Error Method for the flight parameter estimation.

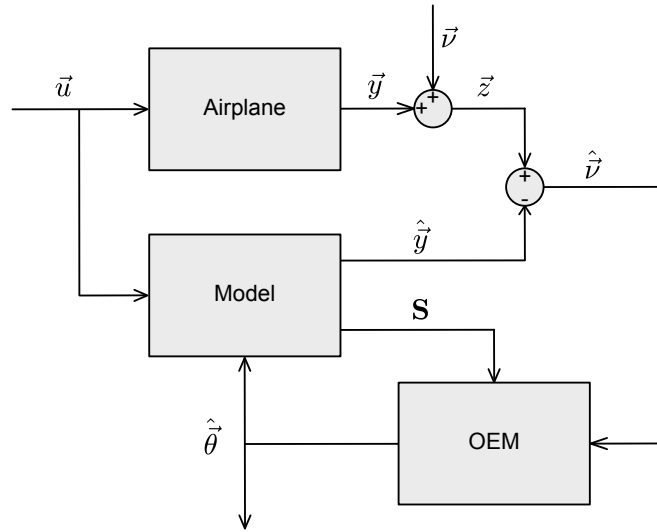


Figure 4.6: Block diagram of the OEM.

Linear OEM is based on the linear system described in Equations 3.75 and the measured output is corrupted by error. Using this assumption measured output  $\vec{z}$  is equal to:

$$\vec{z} = \vec{x} + \vec{v} \quad (4.59)$$

The vector of unknown parameters include, in general, the elements of all matrices in the model equations and the initial conditions. As indicated in the reference [54], the minimization of the cost function with respect to the unknown parameters can be solved by several gradient-based nonlinear programming methods.

The iteration in these methods in general is given as:

$$\vec{\theta}_{r+1} = \vec{\theta}_r - c_r \mathbf{M}_{qr}^{-1} \mathbf{G}_r \quad (4.60)$$

where  $c_r$  is the scalar step size parameter in  $r^{th}$  iteration chosen to improve the convergence,  $\mathbf{M}_{qr}$  is the information matrix in  $r^{th}$  iteration and  $\mathbf{G}_r$  is the gradient matrix of the cost function in  $r^{th}$  iteration.

The gradient matrix of the cost function of Fisher model (see Equation 4.57) has the form:

$$\mathbf{G}_r = \left. \frac{\partial J(\vec{\theta})}{\partial(\vec{\theta})} \right|_{\vec{\theta}=\vec{\theta}_r} = \sum_{i=1}^N \mathbf{S}_i^T(\theta_r) \mathbf{R}^{-1} [z(i) - \hat{y}(i, \theta_r)] \quad (4.61)$$

where  $\mathbf{S}$  is the sensitivity Jacobian matrix constructed as:

$$\mathbf{S} = \frac{\partial \vec{y}}{\partial \vec{\theta}} = \begin{bmatrix} \frac{\partial y_1}{\partial \theta_1} & \frac{\partial y_1}{\partial \theta_2} & \cdots & \frac{\partial y_1}{\partial \theta_{n_x}} \\ \frac{\partial y_2}{\partial \theta_1} & \frac{\partial y_2}{\partial \theta_2} & \cdots & \frac{\partial y_2}{\partial \theta_{n_x}} \\ \vdots & \vdots & \ddots & \vdots \\ \frac{\partial y_{n_x}}{\partial \theta_1} & \frac{\partial y_{n_x}}{\partial \theta_2} & \cdots & \frac{\partial y_{n_x}}{\partial \theta_{n_x}} \end{bmatrix} \quad (4.62)$$

The output sensitivities were numerically computed with utilization of central finite differences.

$$\frac{\partial \vec{y}}{\partial \theta_j} = \frac{\hat{y}(\vec{\theta} + \delta \vec{\theta}_j) - \hat{y}(\vec{\theta} - \delta \vec{\theta}_j)}{2 |\delta \vec{\theta}_j|} \quad (4.63)$$

where  $\delta \vec{\theta}_j$  is the vector of perturbation of parameter  $j = 1, \dots, n_\theta$  with other parameters equal to zero. For the purposes of this thesis, the magnitude of perturbation  $|\delta \vec{\theta}_j|$  is equal to  $10^{-3}$ .

The Fischer information matrix  $\mathbf{M}_{qr}$  for the Modified Newton–Raphson method is approximated as

$$\mathbf{M}_{qr} = \sum_{i=1}^N \mathbf{S}_i^T(\vec{\theta}_r) \mathbf{R}^{-1} \mathbf{S}_i(\vec{\theta}_r) \quad (4.64)$$

The OEM with the Modified Newton–Raphson algorithm was introduced in [58, 54] and it has been used extensively for the past several years. It usually takes the results from the EEM as the initial values for the parameter estimates. As long as the method is applied to linear flight regimes or where the form of equations is known, it works very well. The disadvantage of the OEM is in the degradation of the results in the presence of the process noise. This may result in the computer program not converging or in poor estimates with large variances and or high correlation coefficients.

Another approach of computing the information matrix that can improve the bad conditioning and which can give more reasonable inverse is the Levenberg–Marquardt method.

Information matrix computed using Equation 4.64 is improved using following equation:

$$\mathbf{M}_q^{-1} = (\mathbf{M}_{q0} + \lambda \mathbf{I})^{-1} \quad (4.65)$$

where  $\lambda$  is a positive nonzero scalar parameter. The initial value of  $\lambda$  is taken equal to  $10^{-3}$ . As  $\lambda$  increases, Levenberg–Marquardt method starts to follow the cost gradient vector.

### 4.5.3 Recursive Least–Squares

Previous mentioned methods (EEM and OEM) are one step identification methods, that process all measured data in one step and determine parameters of modeled dynamic system, this approach is usually called offline identification. Recursive Least–Squares (RLS) algorithm process the data recursively over time, the term online identification is used in this case. It means that parameter estimate  $\hat{\theta}(t)$  is computed partly from estimate in time  $t - 1$  and new information.

The recursive identification algorithms in general have following important features:

- They are the core part of adaptive algorithms employed in automatic control or signal processing.
- The memory requirements are much lower when compared to the one step methods.
- They are a suitable approach for online parameter identification.
- They are a part of algorithms for major fault or change detection at observed system.

Recursive Least–Squares method is based on reformulation of EEM to recursive form [58]. New parameter estimate  $\vec{\theta}_{r+1}$  is defined as:

$$\vec{\theta}_{r+1} = \vec{\theta}_r + \mathbf{K}_{r+1} \left( \vec{z}_{r+1} - \vec{x}_{r+1}^T \vec{\theta}_r \right) \quad (4.66)$$

where  $\mathbf{K}_{r+1}$  is the update gain matrix defined as:

$$\mathbf{K}_{r+1} = \mathbf{P}_r \vec{x}_{r+1} \left( \frac{1}{a} + \vec{x}_{r+1}^T \mathbf{P}_r \vec{x}_{r+1} \right)^{-1} \quad (4.67)$$

where  $a$  is the forgetting factor and  $\mathbf{P}_r$  is a state covariance matrix. The forgetting factor can range from 0 (which means remember nothing) to 1 (which means no forgetting).

Update of covariance  $\mathbf{P}_{r+1}$  is defined as:

$$\mathbf{P}_{r+1} = \mathbf{P}_r - \mathbf{K}_{r+1} \vec{x}_{r+1}^T \mathbf{P}_r \quad (4.68)$$

The forgetting factor enhance capability of the RLS to cope with time variant parameters. This approach will perform well when parameters are changing slowly, e.g., change of air density due to change of flight altitude. Quick changes of parameters due to structural changes cannot be followed. Therefore an adaptive Recursive Least–Squares parameter estimation is introduced.

Adaptive Recursive Least–Squares uses estimation of variance  $\mathbf{V}$  to work with sudden changes of system:

$$\mathbf{V}_{r+1} = \frac{1}{N} \sum_{i=1}^N \left( \vec{z}_{r-i+1} - \vec{x}_{r-i+1}^T \vec{\theta}_{r-i} \right)^2 \quad (4.69)$$

where  $N$  is size of window for variance estimation.

Update gain matrix is then reformulated as:

$$\mathbf{K}_{r+1} = \mathbf{P}_r \vec{x}_{r+1} \mathbf{V}_{r+1}^{-1} \quad (4.70)$$

#### 4.5.4 Other approaches

There are other approaches to identify flight parameters. The advantages and disadvantages of these approaches along with their short description are pointed in following paragraphs.

**Genetic algorithms** are inspired by evolution. First step of genetic algorithms is creating the population of first generation of candidate solutions (set of flight parameters) by random number generator. Each individual is evaluated by cost function and best individuals are used to prepare new population using genetic operators: crossover and mutation. Generation of new population and evaluation of individuals is repeated until some individuals reach or exceed predefined threshold value of cost function.

The main issue of the genetic algorithms is the high computational cost, high time consumption and lack of determinism, i.e., it is not assured that the genetic algorithm finds global optimum. Therefore the usage of a genetic algorithm is not suitable for the purposes of this thesis.

**Artificial neural network** consists of interconnected neurons. Each neuron has three parts: inputs weighing, summing junction and activation function. Input weighting assign different importance to each input. Summing junction combines all inputs into one signal. Activation function transforms summed signal to the output, e.g., using thresholding or sigmoid function.

Neurons are organized usually into several layers. The first layer is called input layer and is connected to artificial neural network inputs. The last layer is called output layer and is connected to output of artificial neural network. Other layers are called hidden, because they are not visible from outside of the artificial neural network.

Artificial neural networks can be trained to perform certain tasks. During the training, inputs are filled by sets of defined inputs and outputs are compared to defined outputs. Difference in outputs are propagated thru network and input weightings are corrected to mitigate errors in outputs.

In aerospace, artificial neural networks can be used to model aircraft. An artificial neural network is trained to predict aerodynamic coefficients or time derivatives of state variables. The first major issue of artificial neural network estimation is that it is not possible to obtain flight parameters from the trained artificial neural network. Second issue with artificial neural network is the requirement of large dataset of training data. These two issues prevent the usage of artificial neural network estimation for flight parameters estimation.

## 5. Experimental results

This chapter contains description of the conducted flight experiments. Firstly, the used airplane is described in detail. Secondly, it is necessary to describe the used sensors, Data Acquisition System and the Primary Flight Display, which were used during the flight experiments. Thirdly, the flight maneuvers, the flight campaign and results of the Flight Path Reconstruction process will be introduced. Fourthly, the a-priori values of the investigated flight parameters are presented. Fifthly, the estimated flight parameters are presented. Finally, the summary of a-priori values and estimated flight parameters is given.

### 5.1 Research airplane

For the purposes of flight tests, the Evektor SportStar RTC<sup>1</sup> [32] airplane was used. Evektor SportStar RTC is an experimental Light Sport Airplane (CS-LSA certified) manufactured by Evektor–Aerotechnik, a.s. The photography of this airplane can be seen in Figure 5.1.



Figure 5.1: Photography of the experimental airplane.

#### 5.1.1 Description of the airplane

The experimental airplane Evektor SportStar RTC is a two-seater airplane. Crew consists of a qualified test pilot from Evektor s.r.o. and flight engineer from Brno University of Technology.

Evektor SportStar RTC has a robust all metal airframe made of anodized duraluminum. The undercarriage consist of a three wheel fixed landing gear with steerable nose wheel and two main landing gear wheels equipped with hydraulic brakes. The airplane is configured as low-wing with conventional tail unit. To increase the safety of the flight crew in accordance to the modern trends is the aircraft equipped with a parachute rescue system [32].

---

<sup>1</sup>RTC – Restricted Type Certificate

The airplane is controlled via dual control stick and rudder pedal installation. There are three main control surfaces on this airplane: elevator with a trim surface, ailerons with trim surface on the left aileron, and rudder without an active trim surface. Flaps are electrically operated (lever on dashboard) and enable to be set to four positions: cruise position  $0^\circ$ , take-off position  $15^\circ$  and two landing positions  $30^\circ$  and  $50^\circ$ . This airplane does not have any air-brakes or spoilers. Deflections of all control surfaces of the Evektor SportStar RTC are given in Table 5.1.

Table 5.1: Control surface deflections of Evektor SportStar RTC [16].

Parameter	Notation	Value
Elevator	$\delta_e$	$[-25^\circ, +20^\circ]$
Ailerons	$\delta_a$	$[-17.5^\circ, 17.5^\circ]$
Rudder	$\delta_r$	$[-30^\circ, 30^\circ]$
Elevator trim	$\delta_{te}$	$[-5^\circ, +25^\circ]$
Aileron trim	$\delta_{ta}$	$[-15^\circ, +20^\circ]$
Flaps	$\delta_f$	$0^\circ, 15^\circ, 30^\circ, 50^\circ$

Evektor SportStar RTC uses the Bombardier Rotax 912ULS engine, which is an internal combustion piston engine with four stroke cycle, four horizontally opposed cylinders and reduction gearbox. Its fuel tanks have a volume of 60 liters in each wing. The engine is designed to use Unleaded fuel RON<sup>2</sup> 95. The airplane uses a 3-blade composite propeller of type WOODCOMP KLASSIC 170/3/R. This type of propeller is ground adjustable with a fixed pitch setting for the flight.

As it is not convenient directly measure the propeller rotational speed, it is proposed to be beneficial to measure the engine crankshaft speed and to divide the obtained value by reduction ratio. The propulsion parameters can be found in Table 5.2.

Table 5.2: Propulsion parameters [11, 55].

Parameter	Notation	Value
Engine reduction ratio	$n$	2.43
Propeller diameter	$D_P$	1.7 m
Engine maximum torque	—	128 Nm
Engine take-off power	—	73.5 kW

The tactical data of the airplane, based on [55], are given in Table 5.3.

<sup>2</sup>RON –Research Octane Number

Table 5.3: Tactical data of Evektor SportStar RTC [32, 55].

Parameter	Notation	Value
Length of airplane	—	5.98 m
Height of airplane	—	2.48 m
Reference wingspan	$b_w$	8.65 m
Reference wing area	$S$	10.6 m <sup>2</sup>
Length of MAC	$\bar{c}$	1.25 m
Never exceed speed	$V_{NE}$	75 m/s
Maximum flap extended speed	$V_{FE}$	36 m/s
Maximum level speed	$V_H$	59 m/s
Stall speed	$V_{S1}$	20.6 m/s
Service ceiling	$H_{max}$	4720 m

### 5.1.2 Flight envelope

The flight envelope describes the limits of flight. The limitations originate from different sources such as engine power, maximum speed, stall speed, service ceiling etc.

For the purposes of the flight tests, the flight envelope was limited to the conditions, as altitudes, airspeed and position of center of mass, as consulted with the airplane manufacturer. The limits reflect the safety constraints to prevent extreme attitudes.

The operational flight envelope and point of testing are presented in Figure 5.2.

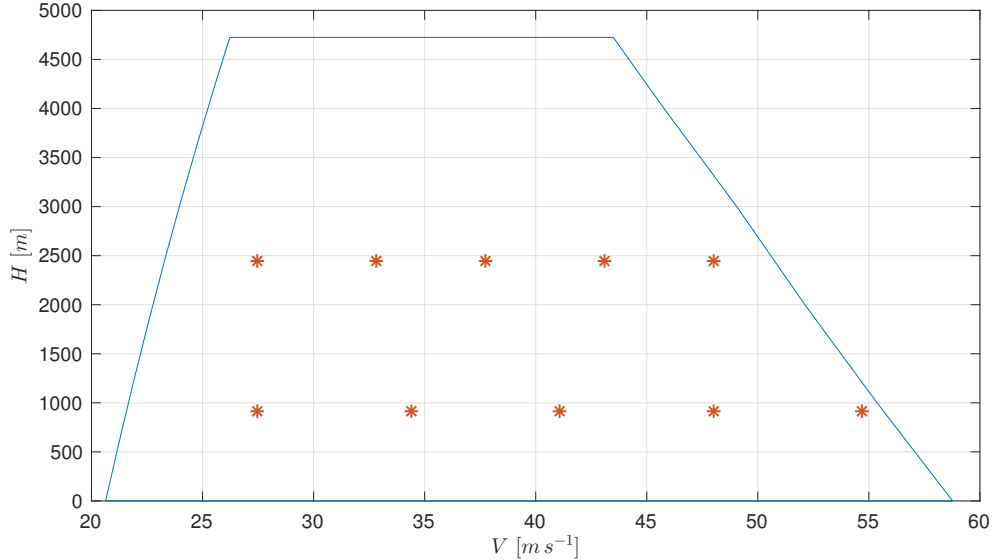


Figure 5.2: Operational flight envelope, the blue area denotes the envelope and red stars show the testing points.

### 5.1.3 Airplane's center of mass

The mass and the center of mass of the empty airplane was determined experimentally. First, it was necessary to empty the fuel tanks. Then, every wheel of the landing gear was put on a weighing scale. For this purpose, three weighing scales Soehnle Professional Digital Indicators 2755 were used. Next, it was necessary to put small blocks under the main wheels to ensure that the base plane of fuselage is horizontal, i.e., parallel to the floor.

After that, it was possible to start the measurement. To ensure the high accuracy of the results, five measurements was taken for each case. These measurements were used not only for determining the total mass of the empty airplane, but also to find the horizontal position of the center of mass of the empty airplane in the  $x_d y_d$  plane.

The mass of the empty airplane was calculated to be  $m_{empty} = 375 \text{ kg}$ . It is necessary to say, that the measured airplane had a unique configuration and built-in parachute system, several sensor systems, including wiring, therefore the above mentioned mass of the empty airplane is unique for this particular experimental airplane and it cannot be compared to another unit of the same type.

The position of the center of mass of the empty airplane in Design reference frame was calculated using following formulas:

$$x_{Gd} = \frac{m_F x_{Fd} + m_L x_{Ld} + m_R x_{Rd}}{m_{empty}} \quad (5.1)$$

$$y_{Gd} = \frac{m_F y_{Fd} + m_L y_{Ld} + m_R y_{Rd}}{m_{empty}} \quad (5.2)$$

where  $F$  is the point of contact of front wheel with weighing scale,  $L$  is the point of contact of left wheel with weighing scale and  $R$  is the point of contact of right wheel with weighing scale.

At last, it was necessary to find the position of the center of mass of the empty airplane in the  $z_d$  axis. For this purpose, two laser distance sensors Leica Geosystems DISTO lite5 were attached to the airplane. Using these sensors the distance from placement of the sensors to the nearby vertical wall was measured several times. Firstly, one block was inserted under the front wheel to change tilt of the aircraft. Secondly, the laser distance sensors were used to measure distance from the same wall again to compute the angle of tilt. Finally, the distribution of mass on all three wheels was repeatedly measured. The whole process of inserting blocks below the front wheel, measuring distance from nearby wall and weighing of all three wheels was repeated three times to obtain sufficient quantity of data to determine position of center of mass in  $z_d$  axis. For this purpose, the following equation was used:

$$z_{Gd} = \frac{x_{G'd} - x_{Ld} + (x_{Ld} - x_{Gd}) \cos \theta}{\sin \theta} - z_{Ld} \quad (5.3)$$

where  $\theta$  is tilt angle (pitch angle) and  $G'$  is projection of point  $G$  to the horizontal plane after tilting the airplane.

To obtain center of mass of the experimental airplane, it is necessary to take weight of the empty airplane and add the weight of other parts. Weights of the pilot and operator with their safety parachutes and the fuel weight are measured before every flight. Additional cargo was not present on-board during any of the experimental flights.

## 5.2 Instrumentation

During the test flights, the measured values of selected physical quantities were recorded. To collect and store measured data, a Data Acquisition System (DAQ) described in Section 5.2.1 was used. A list of on-board sensors is given in Section 5.2.2. To ensure that the conducted flight maneuver meet specified requirements, the Primary Flight Display (PFD) is used (see Section 5.2.3).

The overall Data Acquisition System with sensors and PFD is introduced in Figure 5.3.

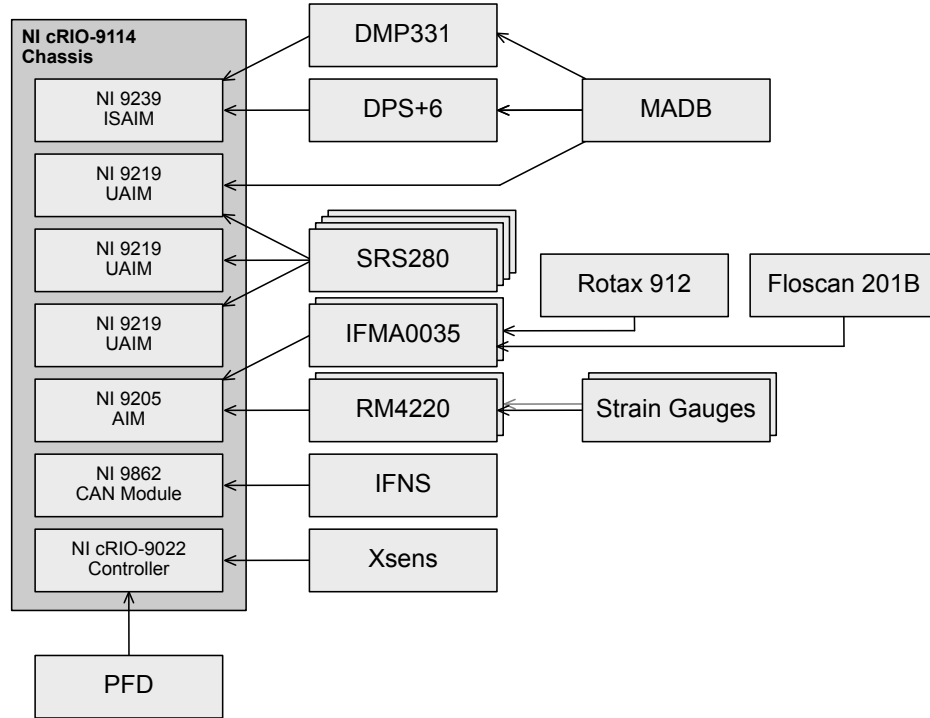


Figure 5.3: Data Acquisition System with sensors and PFD.

### 5.2.1 Data Acquisition System

The DAQ used to collect and store data from sensors was composed of selected modules of industrial CompactRIO<sup>3</sup> platform manufactured by National Instruments Corporation [73]. The flight ready DAQ was located in the cargo compartment of the experimental airplane and connected to a network of sensors (listed in following section). The DAQ was powered by a standalone battery power supply 24 – 28 V, as the experimental airplane was capable to provide only 12 – 14 V from its engine-driven alternator.

The DAQ used in the flight tests is composed of following modules:

<sup>3</sup>RIO – Reconfigurable Input/Output

- **Real-Time Controller** NI<sup>4</sup> cRIO-9022 is powered by a 533 MHz PowerPC processor and includes 256 MiB DRAM<sup>5</sup> and 2 GiB Solid-State Drive (SSD) for data storage. The Real-Time Controller controls other modules and can be programmed using the graphical programming system LabView.
- **CompactRIO Reconfigurable Chassis** NI cRIO-9114 can hold up to 8 modules. Only six slots were used for the purposes of flight tests. To sequence and synchronize these modules, Field-Programmable Gate Array (FPGA) Virtex-5 was used.
- **High-Speed CAN Module** NI 9862 provides an interface to the Controller Area Network (CAN) bus, which allows to connect devices with baud rate up to 1 Mbps on the bus with a maximum length of 40 m.
- **Isolated Simultaneous Analog Input Module (ISAIM)** NI 9239 has 4 channels to connect the sensors having a signal range of  $\pm 10 V$  and an update rate of 50 kS/s. This module has 24-bit resolution which is required for critical sensors. It also has isolated inputs which reduce the risk of interferences and ground loops.
- **Universal Analog Input Module (UAIM)** NI 9219 has 4 channels to connect sensors having signal range of  $\pm 10 V$  and an update rate of 100 S/s/ch. This module has 24-bit resolution which is required for critical sensors. It also provides excitation current for potentiometers. For the purposes of the flight tests, three Universal Analog Input Modules are used.
- **Analog Input Module (AIM)** NI 9205 has 32 channels to connect sensors having update rate 250 kS/s. Each channel has configurable signal range from  $\pm 200 mV$  to  $\pm 10 V$ . This module has 16-bit resolution which is sufficient for non-critical sensors.

Visualizations of the CompactRIO modules are shown in Figure 5.4.

### 5.2.2 Utilized sensors

There are eight types of sensors which were connected to the Data Acquisition System during test flights: Xsens MTi-G, Integrated Flight State and Navigation Sensor (IFNS), potentiometers, strain gauge, flowmeter, flow vanes, pressure transducers and rotational speed sensors.

**Xsens MTi-G** sensor, manufactured by Xsens Technologies B.V. [102], integrates accelerometers, gyroscopes, GPS and magnetometers in its sensor fusion algorithms. The output of Xsens are Euler angles, specific forces, angular velocities, translational velocities and geodetic position in the WGS84. This sensor is connected to the DAQ using a RS-232 serial port interface. The Xsens sensor (see Figure 5.5) was placed in the cargo compartment behind the pilot's and operator's seats as this location was closest to the center of mass of the airplane.

**Integrated Flight State and Navigation Sensor (IFNS)**, manufactured by Stock Flight Systems [89], integrates accelerometers, gyroscopes, GPS and magnetometers. Therefore the

---

<sup>4</sup>NI – National Instruments

<sup>5</sup>DRAM – Dynamic Random Access Memory

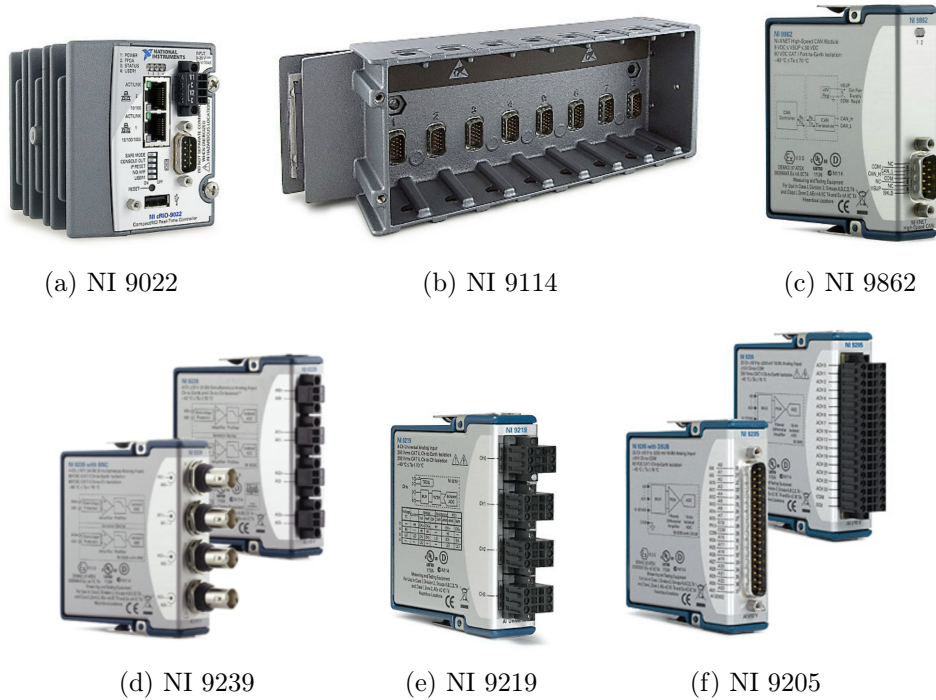


Figure 5.4: The NI CompactRIO modules [73].



Figure 5.5: Xsens MTi-G Attitude and Heading Reference System [102].

outputs of IFNS are Euler angles, specific forces, angular velocities, translational velocities and geodetic position in the WGS84 format. This sensor was connected using Controller Area Network (CAN) bus to the NI 9862 module. IFNS was placed in the cargo compartment behind the pilot's and operator's seats next to the Xsens sensor as this location is close to the center of mass of the airplane. IFNS was used as a secondary data source in case of the Xsens' malfunction.

**Potentiometers** SRS280<sup>6</sup>, manufactured by Penny & Giles Controls Limited [78], were connected to the NI 9219 module. Potentiometers in above mentioned experimental airplane measure the position and orientation of the elevator, rudder, right aileron, flaps, pilot's control stick, throttle lever, and rudder pedals. Picture of the potentiometer SRS280 can be seen in Figure 5.6.

<sup>6</sup>SRS – Sealed Rotary Sensor



Figure 5.6: Potentiometer SRS280 [18].

**Strain gauges** CEA-13-250UN-120, manufactured by Vishay Precision Group, Inc. [96], sense control forces. These strain gauges were mounted on the elevator and left aileron control rods, and on both rudder links. All strain gauges were wired as full Wheatstone bridges. They are connected thru a precision amplifier RM4220, manufactured by Hottinger Baldwin Messtechnik GmbH. [47], to the NI 9205 module. Example of one strain gauge is shown in Figure 5.7.

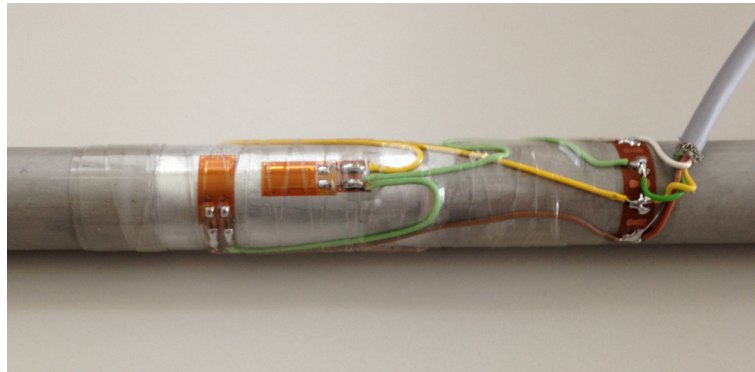


Figure 5.7: Installation of strain gauges used in the airplane.

**Flowmeter** Floscan 201B, manufactured by FloScan Instrument Co., Inc. [35], measured the fuel flow on the fuel line from fuel switch to the engine. This sensor was connected thru a pulse rate to analog converter IFMA 0035, manufactured by Red Lion Controls, Inc. [81], to the NI 9205 module. Flowmeter was attached near to the firewall.

**Flow vanes** were part of the SpaceAge 100400 Mini Air Data Boom (MADB), manufactured by the SpaceAge Control, Inc. [85], which was mounted on the right wing. Mini Air Data Boom was equipped with the angle-of-attack and flank angle flow vanes. Outputs from



Figure 5.8: Visualization of the SpaceAge 100400 Mini Air Data Boom [85].

these flow vanes were connected to the NI 9219 module. A 3D visualization of the SpaceAge 100400 Mini Air Data Boom is shown in Figure 5.8.

**Pressure transducers** DMP 331 and DPS+6, manufactured by the BD Sensors s.r.o. [8], were integrated for measurement of the static and impact pressure. They were connected to the pitot–static tube and to the NI 9239 module. The pitot–static tube is located at the front part of the SpaceAge 100400 Mini Air Data Boom (see Figure 5.8).

**Rotational speed** sensor was an integral part of the Bombardier Rotax engine [11]. It was connected to the NI 9205 module. The rotational speed sensor was the measuring rotational speed of the engine crankshaft.

### 5.2.3 Primary Flight Display

Primary Flight Display – PFD was used to show graphs of selected physical quantities to ensure that the conducted flight maneuvers meet specified requirements (see next section). It was also used as a secondary flight recording system.

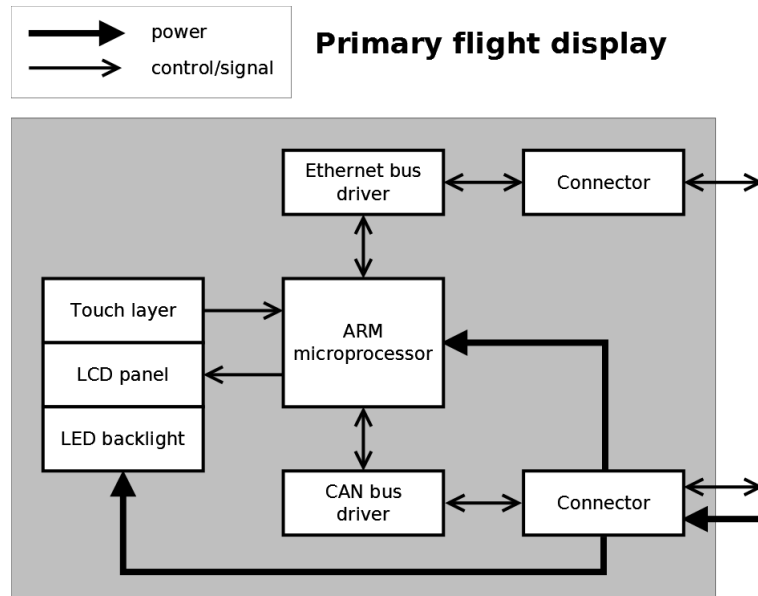


Figure 5.9: Scheme of the Primary Flight Display.

The PFD consists of a display, an ARM microprocessor with 512 *MiB* RAM<sup>7</sup> and 2 *GiB* Flash, and two buses – Ethernet bus and CAN bus (see Figure 5.9). The display contains a Liquid Crystal Display (LCD) panel with Light–Emitting Diode (LED) backlight and a capacitive touch layer. The size of the display is 10" to increase the user–friendliness/readability of the whole system (and provide optimal performance even during difficult maneuvers).

On the back side of the PFD, there are six connectors (see Figure 5.10):

- Power input connector has three pins: common negative pin, positive battery pin for connecting 12 *V* backup battery and positive main power input pin. The main power input of the PFD is connected to the 14 *V* avionics bus thru the circuit breaker.

<sup>7</sup>RAM – Random Access Memory

- Two CANbus connectors have integrated power output and support the CANaerospace protocol [88]. Having two connectors enables a simultaneous connection of the IFNS and a second display for a more complex avionics solution.
- Ethernet connector is used to provide connection to the DAQ. Data coming thru Ethernet are presented on the PFD to ensure that the conducted flight maneuver meets specified requirements.
- The RS-232 connector is used as a debug interface for the PFD. A computer connected to the RS-232 connector is able to open a software terminal for managing the PFD software. Managing of PFD enables reading log messages, checking of the errors and warnings, and verification of the internal components of the PFD. RS-232 also enables to download logged records and an upload of new software versions.
- The auxiliary connector is used to connect up to 4 external buttons and an audio panel. Audio panel connection enables to send the audio information to the pilot's and operator's headphones.



(a) Front view



(b) Rear view

Figure 5.10: Photography of the Primary Flight Display.

The PFD was designed and developed at the Faculty of Information Technology. For the purposes of mounting the PFD on-board of the airplane, the airplane manufacturer equipped the experimental airplane with a custom dashboard containing prepared installation space according to the PFD specification. Dimensions and other tactical data of the PFD are shown in Table 5.4.

Table 5.4: Tactical data of Primary Flight Display [15].

Parameter	Value
Height	212 mm
Width	242 mm
Depth	54 mm
Weight	1.30 kg
Power	14 V with battery backup
Databus	CANaerospace & Ethernet

The software for visualization of the flight maneuvers on the Primary Flight Display was programmed in LabView [72]. The LabView is a graphical system design software.

## 5.3 Flight data acquisition and preprocessing

The data were recorded during the flight experiments conducted on the experimental airplane Evektor SportStar RTC, owned by Evektor s.r.o., which operates an Authorized aircraft testing laboratory (authorization N<sup>o</sup> L-3-060 issued by Civil Aviation Authority of Czech Republic – CAA [93]). The experimental airplane was equipped with Data Acquisition System sensors and a Primary Flight Display, see Section 5.2.

Gathered data were post-processed using Flight Path Reconstruction.

### 5.3.1 Dynamic longitudinal stability

The reason behind the acquisition of the flight data is the estimation of dynamic longitudinal stability characteristics. This task is based on exciting the investigated airplane dynamic response in longitudinal motion.

For the excitation of the system's dynamic response, a doublet maneuver described in Section 4.1.1 was used. The doublet is a suitable testing maneuver as high complex maneuvers like 3-2-1-1 have to be executed using an automatic flight control system and simple pulses do not fully excite dynamic modes of the aircraft [54].

After exciting a dynamic mode of motion with an input and removing the pilot from the control loop, the system can record an aircraft open loop motion. A physical system's dynamic stability analysis is concerned with the resulting time history of motion of a system when displaced from an equilibrium condition [95].

A sophisticated solution to the aircraft Equations of Motion with valid aerodynamic inputs can result in good theoretically obtained time histories. However, the fact remains that the only way to discover the aircraft's actual dynamic motion is to flight test and record its motion for analysis [95].

Before the maneuver, the pilot has to meet these conditions [55]:

- Airplane must fly straight, steady and horizontal, so roll angle and flight path angle must be smaller than 5°.
- Airplane must maintain specified airspeed and at a specified altitude.
- All forces on control stick must be trimmed, no additional force should appear on the control stick.
- Airplane must have specified weight and position of center of mass.
- Airplane must have specified position of flaps.

The maneuver is started at specified airspeeds ranging from  $1.2 V_{S1}$  to  $V_H$ , or  $1.2 V_{S1}$  to  $V_{FE} - 15\%$  with extended flaps [55]. The maneuver is conducted by inducing a doublet

by pushing and pulling the control stick, when subsequent elevator deflection introduce the longitudinal motion.

### 5.3.2 Flight campaign

During the flight campaign, seven flights were conducted in the period of July and August 2012. The weather conditions while testing were without significant wind or mechanical or thermal turbulence. Flights were conducted in altitudes of  $915\text{ m}$  and  $2438\text{ m}$  ( $3000\text{ ft}$  and  $8000\text{ ft}$ ). Three flights were conducted with a front center of gravity position, two of them were conducted with “fixed control” after inducing the doublet maneuver and one of it was conducted with “free control”. Another four flights were conducted at the rear center of gravity position. Two of the flights were conducted with a “fixed control” after inducing the doublet and two were conducted under “free control” conditions.

All flight tests were performed at a certified aerodrome in Kunovice. ICAO code of aerodrome is LKKU and its location is specified in Table 5.5.

Table 5.5: Location of LKKU aerodrome [2].

Parameter	Notation	Value
Longitude of LKKU	$\ell_{LKKU}$	$17.439722^\circ$
Latitude of LKKU	$\varphi_{LKKU}$	$49.029444^\circ$
Altitude of LKKU	$h_{LKKU}$	$177.089\text{ m}$

### 5.3.3 Flight Path Reconstruction

The Flight Path Reconstruction (FPR) post-processes the raw measured data. Angle-of-attack is being corrected for upwash effect described in Section 4.3.1. Specific forces and angle-of-attack are corrected for the position error using equations in Section 4.3.2. On the corrected data, Kalman Filter described in Section 4.3.4 is used to minimize the effects of measurement noise.

For the purposes of this thesis, the author has implemented the algorithm with all the corrections necessary. The Flight Path Reconstruction algorithm is implemented in Matlab [65].

An example of few chosen physical quantities during a flight maneuver is presented in Figure 5.11. Blue lines represent raw measured data and red lines represent data after the corrections and Flight Path Reconstruction.

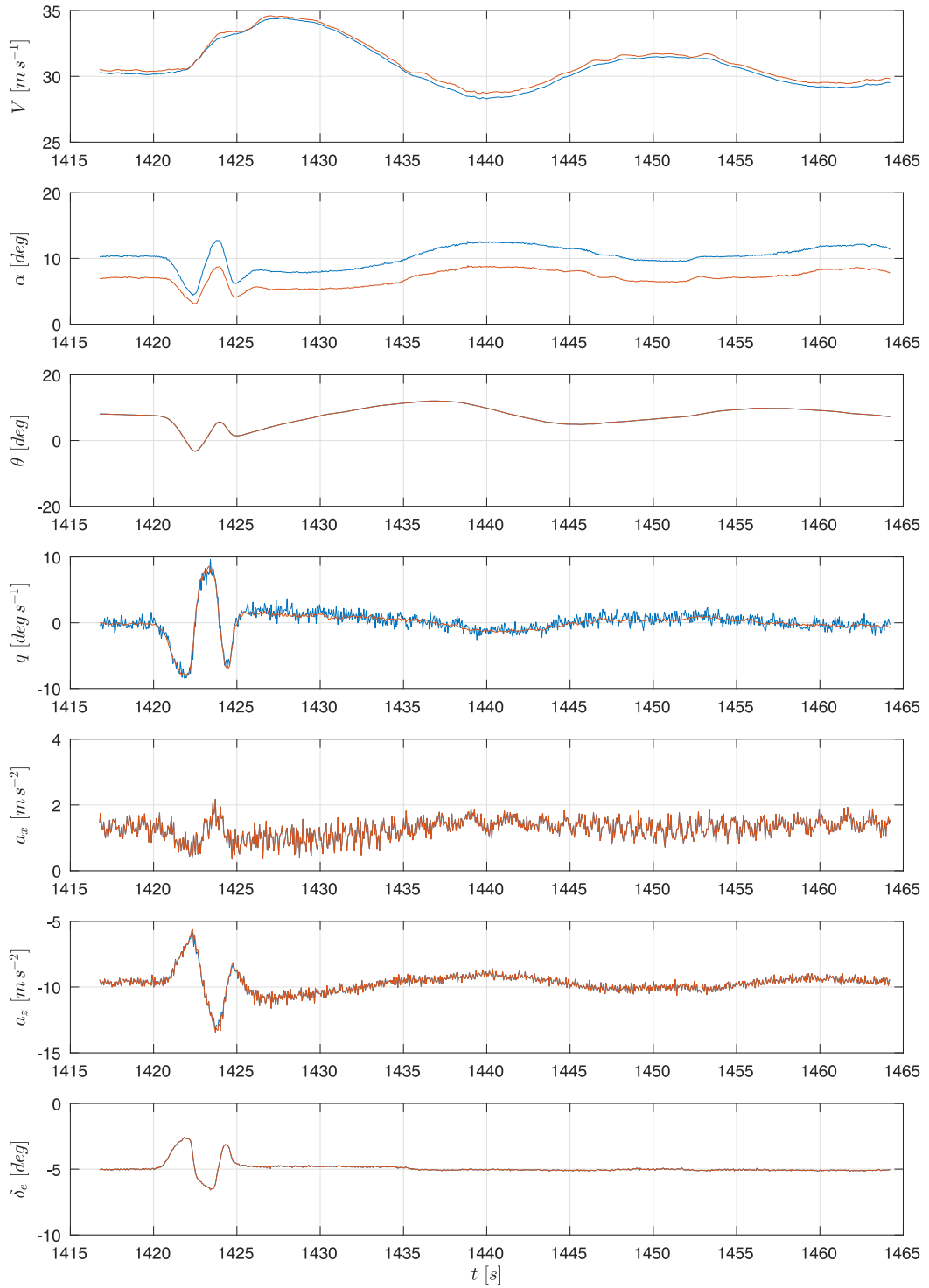


Figure 5.11: Comparison of the data before and after FPR process (Blue lines represents raw measured data and red lines represents data after FPR).

## 5.4 A-priori data

The a-priori data are the outputs from the softwares described in Section 4.4. All models used in this thesis are based on the information provided by the airplane manufacturer [55]. More information about the numerical models providing the flight parameters is introduced in following sections.

### 5.4.1 Tornado software estimates

For the purposes of obtaining the a-priori values from the Tornado software, the author has created a model of the investigated airplane based on the information provided by airplane manufacturer [55]. Picture of the airplane's model is presented in Figure 5.12.

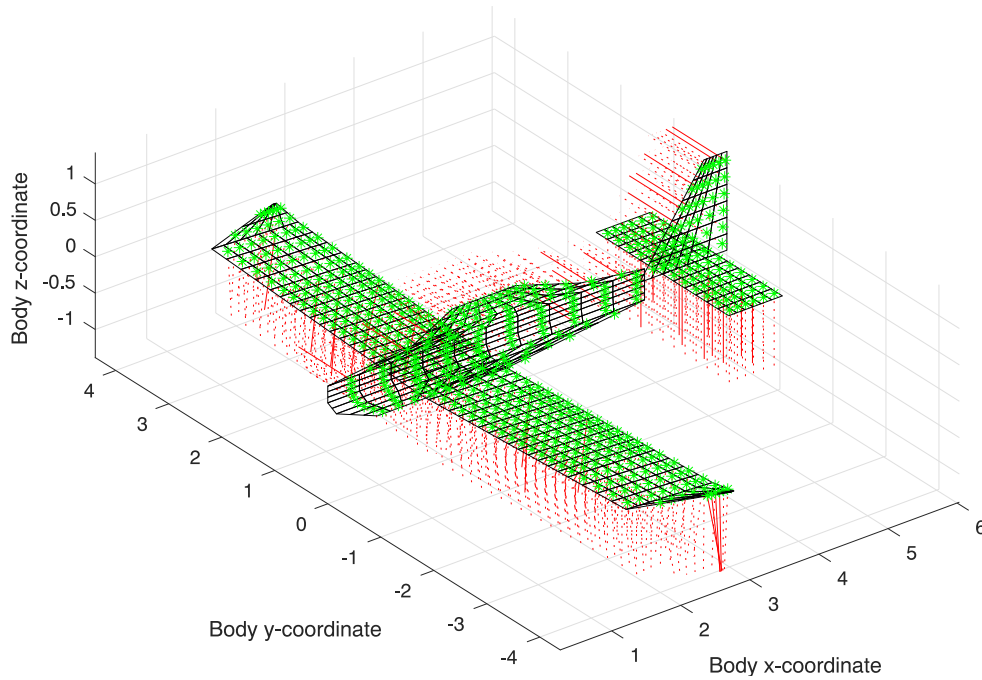


Figure 5.12: Airplane's model in Tornado software.

The model of the whole airplane has been split into panels of equal ratios. On the figure, the green stars show the position of the control points and the red dotted lines indicates the normals to each panel surface. The model coordinates are shown in the Design Reference Frame  $F_d$ .

The model consists of the wing, fuselage, vertical and horizontal tail units. The wing has been divided into 126 panels. The horizontal and vertical tail units are divided into 24 panels each. The fuselage is substituted by its planar projection, as Tornado does not support slender body modeling. The fuselage is divided into 130 panels.

### 5.4.2 AVL software estimates

For the purposes of obtaining a-priori values from the AVL software, the author has created a model of the investigated airplane based again on the information provided by the airplane manufacturer [55]. Picture of the AVL airplane model is shown in Figure 5.13.

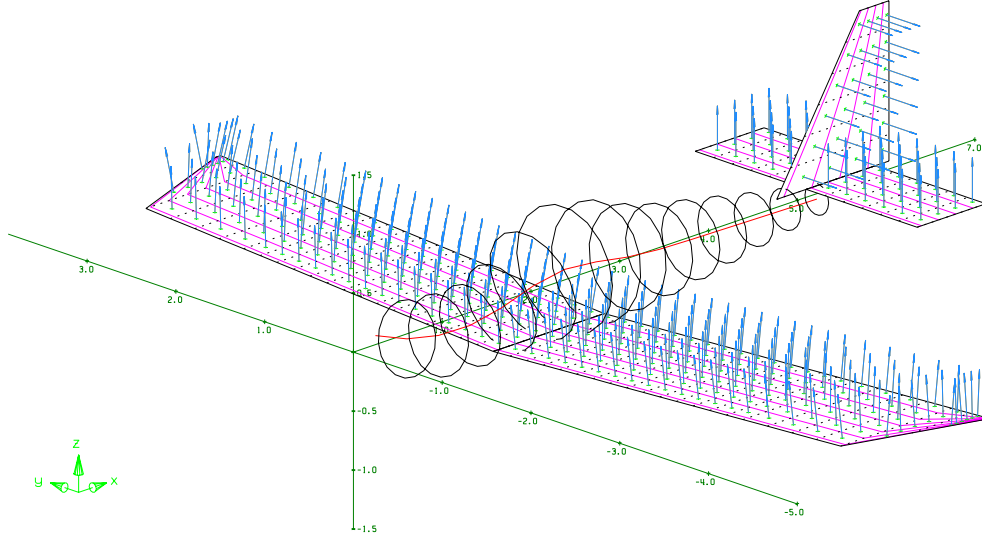


Figure 5.13: Airplane model in AVL software.

The model of the whole airplane has been split into panels of similar ratios. In the figure, the green stars show the position of the control points and the blue lines indicate the normals to each panel surface. The model coordinates are in the Design Reference Frame  $F_d$ .

The model same as in previous case, consists of the wing, fuselage, vertical and horizontal tail units. The wing has also been divided into 126 panels. The horizontal and vertical tail units feature 24 panels each. The shape of the fuselage is modeled using circles with the cross-section characteristics of the actual fuselage, hence AVL does not support fuselage fully. The fuselage has been divided into 15 parts by planes as shown in the Figure 5.13. The figure also show the red line indicating the center of the fuselage planes.

### 5.4.3 Datcom software estimates

A model of the experimental airplane was developed as a part of the “Smart Autopilot” project. It was based on the outputs of the USAF Datcom introduced in Section 4.4.3.

The model data from Datcom estimates are thoroughly described in [16].

## 5.5 Parameter estimation

The flight parameters were estimated using methods described in Section 4.5. The author’s contribution is beyond other also in the software implementation of all three algorithms in Matlab [65]. Both nonlinear and linear Equations of Motion were considered. Using both modeling approaches allows for a straight forward comparison of both approaches.

All flight parameters introduced in Section 3.4.2 were divided into two main types: force parameters and moment parameters. For the purposes of this thesis, only the longitudinal parameters are presented.

### 5.5.1 Force parameters

The force parameters are independent of the center of mass position. The force longitudinal parameters can be divided to respective drag parameters  $C_{Dx}$  and lift parameters  $C_{Lx}$ .

The drag curve slope  $C_{D\alpha}$  and lift curve slope  $C_{L\alpha}$  define the basic performance of an airplane. Both of these flight parameters depend on the shape, size and aerodynamic characteristics of the airplane. The  $C_{L\alpha}$  must be positive and its theoretical maximum is equal to  $2\pi$ .

The flight parameter  $C_{L0}$  is equal to lift coefficient  $C_L$  in the case when the angle-of-attack  $\alpha$  is equal to zero, elevator deflection  $\delta_e$  is equal to zero and pitch rate  $q$  is equal zero.. Similarly, the flight parameter  $C_{D0}$  is equal to drag coefficient  $C_D$  in case the angle-of-attack  $\alpha$  is equal zero and pitch rate  $q$  is equal zero.

Another lift parameter is the  $C_{Lq}$  (lift due to pitch rate) and  $C_{L\delta_e}$  (elevator effect on lift). The  $C_{Lq}$  could be neglected, as the effect of this flight parameter on the lift coefficient  $C_L$  is very small. The flight parameter  $C_{L\delta_e}$  depends on shape, size and characteristics of the elevator. The  $C_{L\delta_e}$  must be positive for classical airframe configurations.

The drag parameters  $C_{Dq}$  (drag due to pitch rate) and  $C_{D\delta_e}$  (elevator effect on drag) are neglected, as the effect of those flight parameters on drag coefficient  $C_D$  is very small.

The estimation results of the force parameters are shown in Figure 5.14. The lift parameters are compared to the a-priori values from the Tornado software, AVL software and Datcom. More details about the a-priori values are presented in Section 5.4.

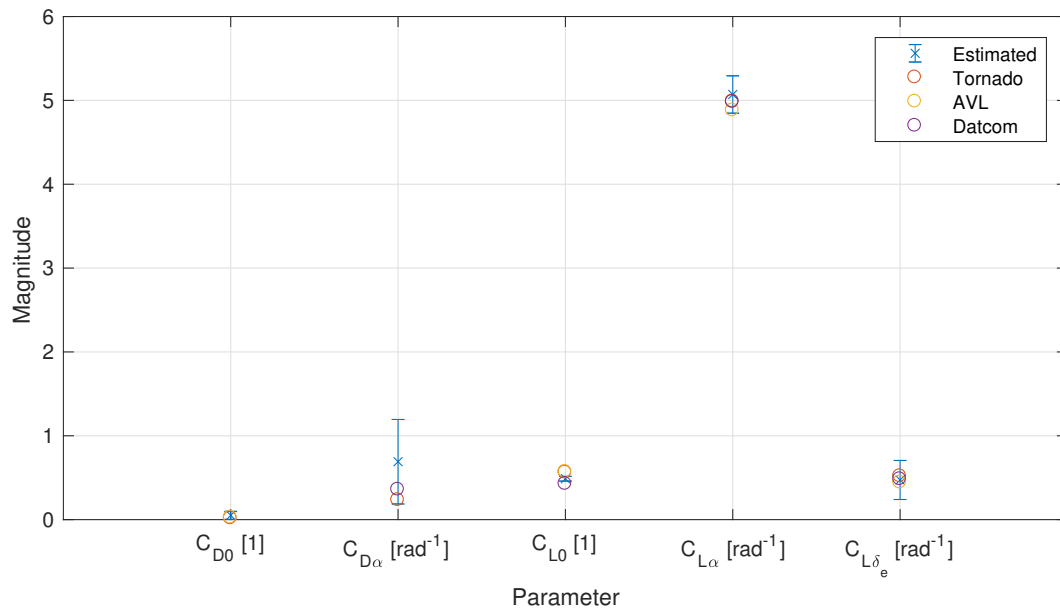


Figure 5.14: Graph of force parameters.

Figure 5.15 shows the dependence of the drag coefficient  $C_D$  whose Taylor's series expansion consist of the above discussed flight parameters ( $C_{Dx}$ ) as a function of the angle-of-attack  $\alpha$ . The blue stars show the data points from the identification maneuvers executed at altitude 915 m (3000 ft) and the red stars show the data points from the maneuvers performed at altitude 2438 m (8000 ft). The orange line presents a linear interpolation of the dependence of drag coefficient  $C_D$  on the angle-of-attack  $\alpha$ .

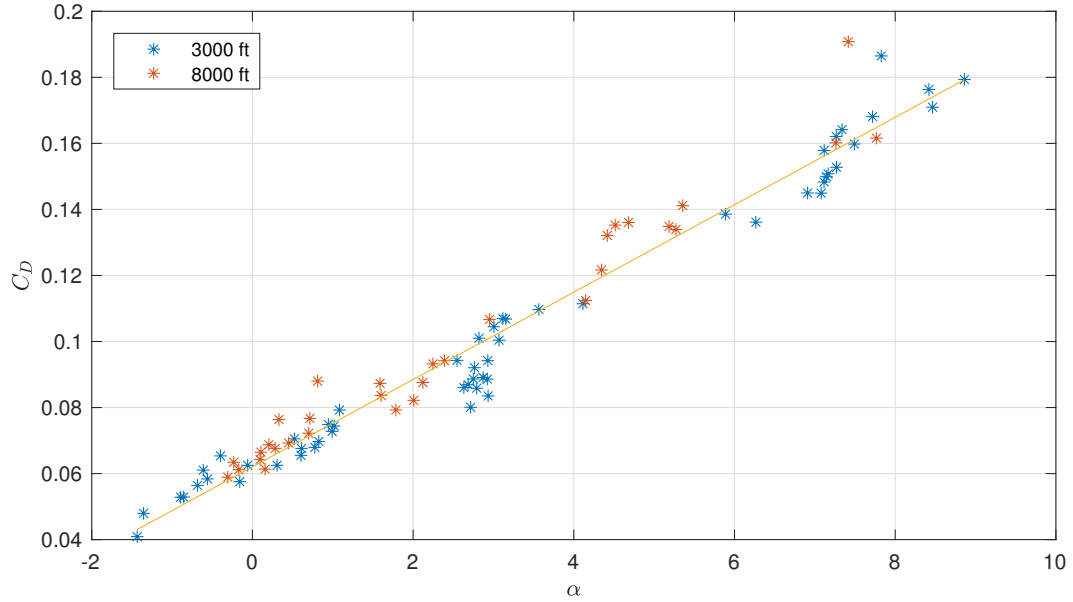


Figure 5.15: Graph of drag curve.

Figure 5.16 shows the dependence of the lift coefficient  $C_L$  whose Taylor's series expansion consist of the above discussed flight parameters ( $C_{Lx}$ ) as a function of the angle-of-attack  $\alpha$ .

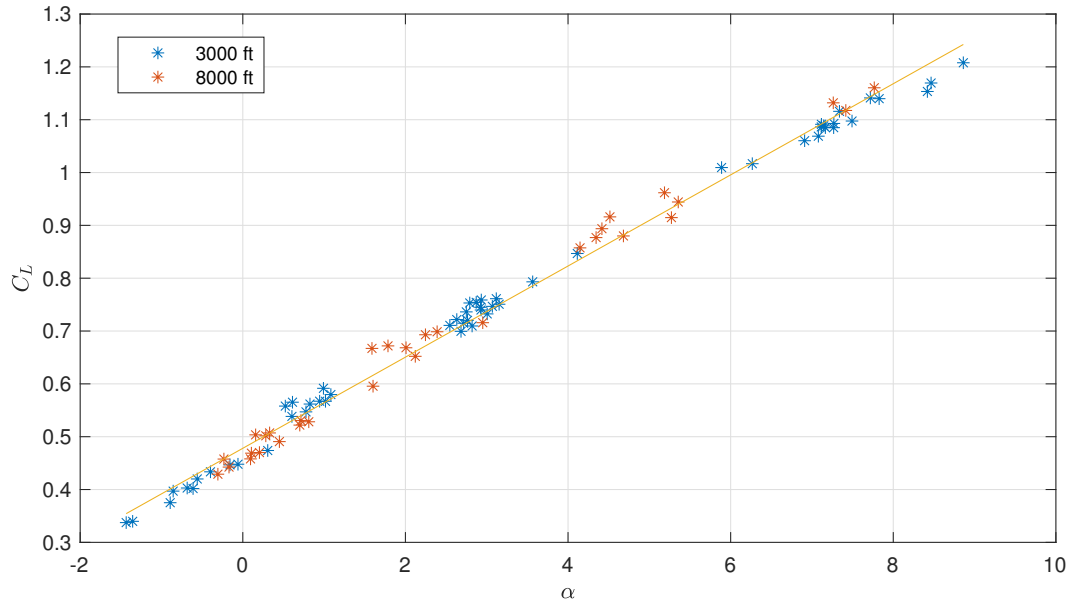


Figure 5.16: Graph of lift curve.

The blue stars show the data points from the maneuvers executed at altitude  $915\text{ m}$  ( $3000\text{ ft}$ ) and the red stars show the data points from the identification maneuvers executed at altitude  $2438\text{ m}$  ( $8000\text{ ft}$ ). The orange line presents a linear interpolation of the dependence of the lift coefficient  $C_L$  on the angle-of-attack  $\alpha$ .

### 5.5.2 Moment parameters

The moment parameters depend on the center of mass position. The moment longitudinal parameters are the pitch moment parameters  $C_{mx}$ .

The pitching moment slope  $C_{m\alpha}$  strongly depend on the center of mass position. The  $C_{m\alpha}$  should be negative as it defines the level of static stability [31].

The flight parameter  $C_{m0}$  is equal to the pitch moment coefficient  $C_m$  in the case that the angle-of-attack  $\alpha$  is equal to zero, pitch rate  $q$  is equal to zero and elevator deflection  $\delta_e$  is equal to zero.

The pitch damping parameter  $C_{mq}$  specifies the dynamic longitudinal behavior of the airplane. The parameter  $C_{mq}$  must be negative, otherwise the airplane will be dynamically unstable.

The elevator effect on pitching moment  $C_{m\delta_e}$  is the main control parameter in longitudinal motion. The flight parameter  $C_{m\delta_e}$  depends on shape, size and characteristics of the elevator. The  $C_{m\delta_e}$  should be negative for the classical tail configuration.

Results of the estimation of the moment parameters are presented in Figures 5.17 to 5.20. The position of the center of mass is expressed in a fraction of the Mean Aerodynamic Chord of main wing in percents.

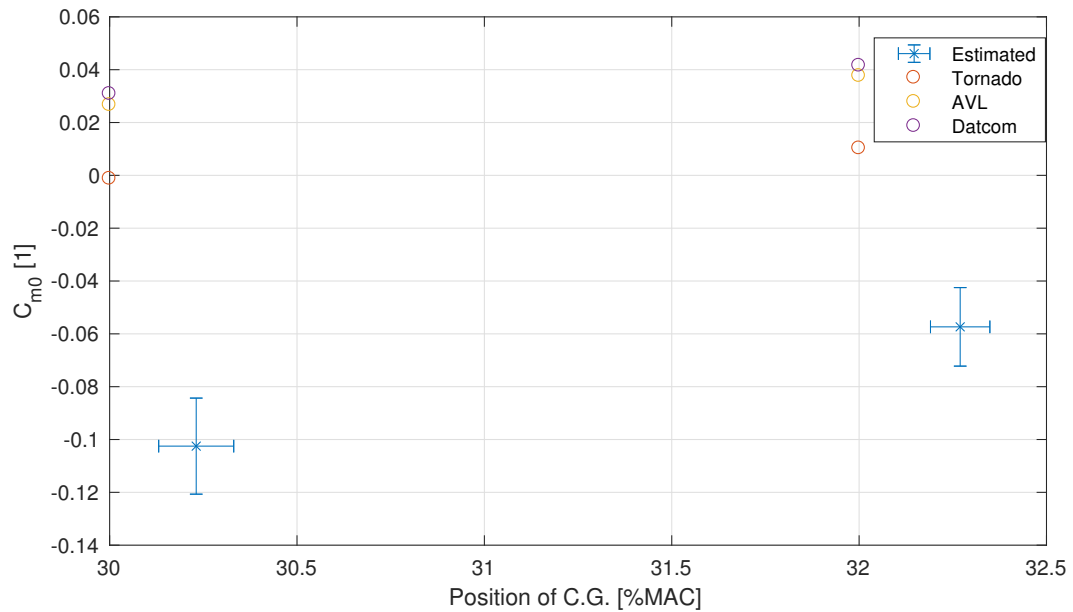


Figure 5.17: Graph of parameter  $C_{m0}$ .

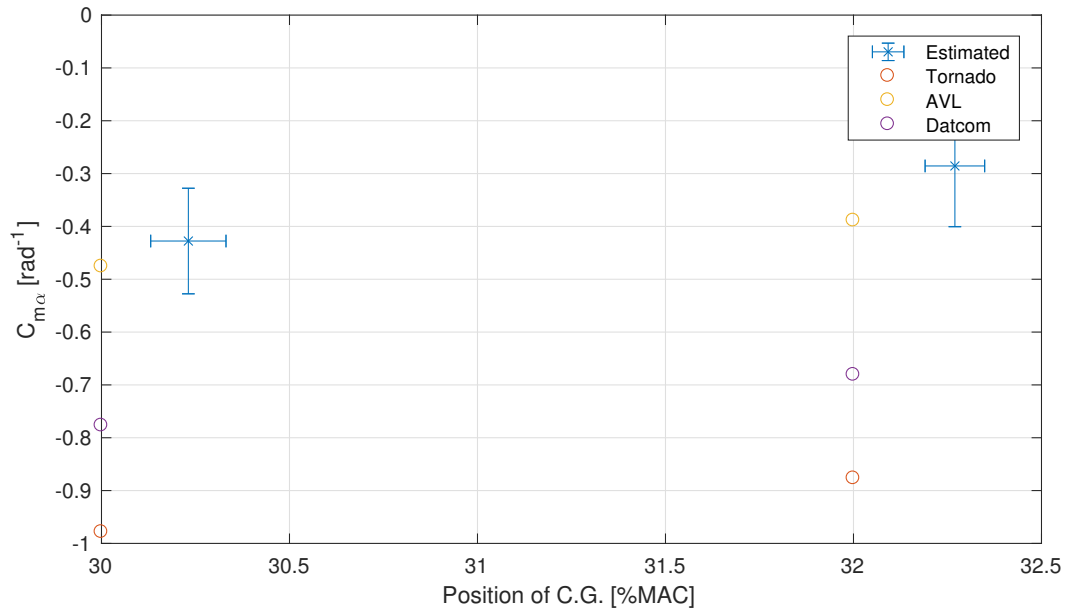


Figure 5.18: Graph of parameter  $C_{m\alpha}$ .

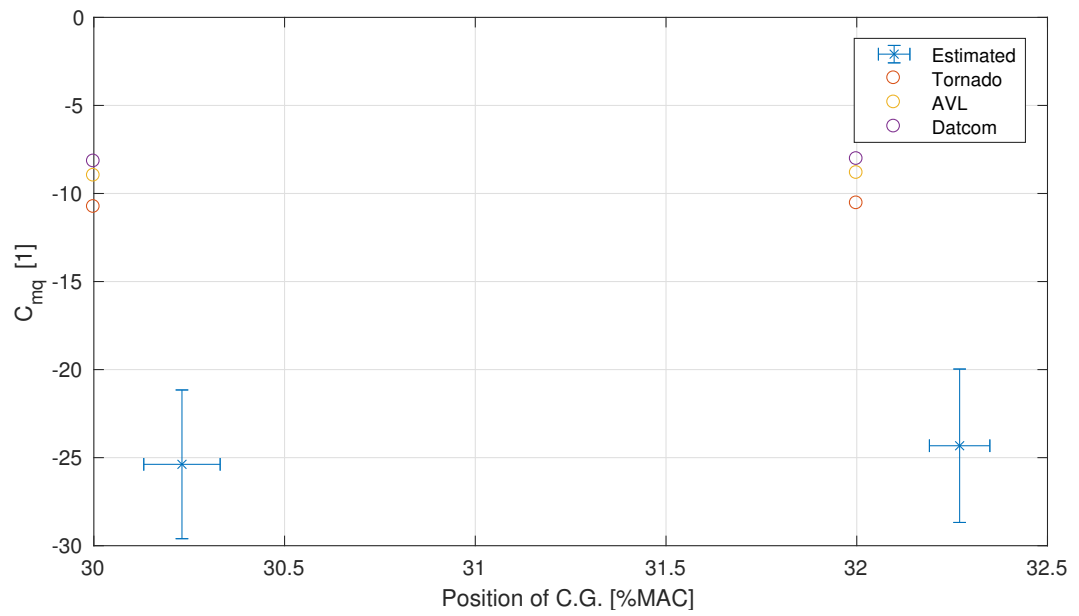


Figure 5.19: Graph of parameter  $C_{mq}$ .

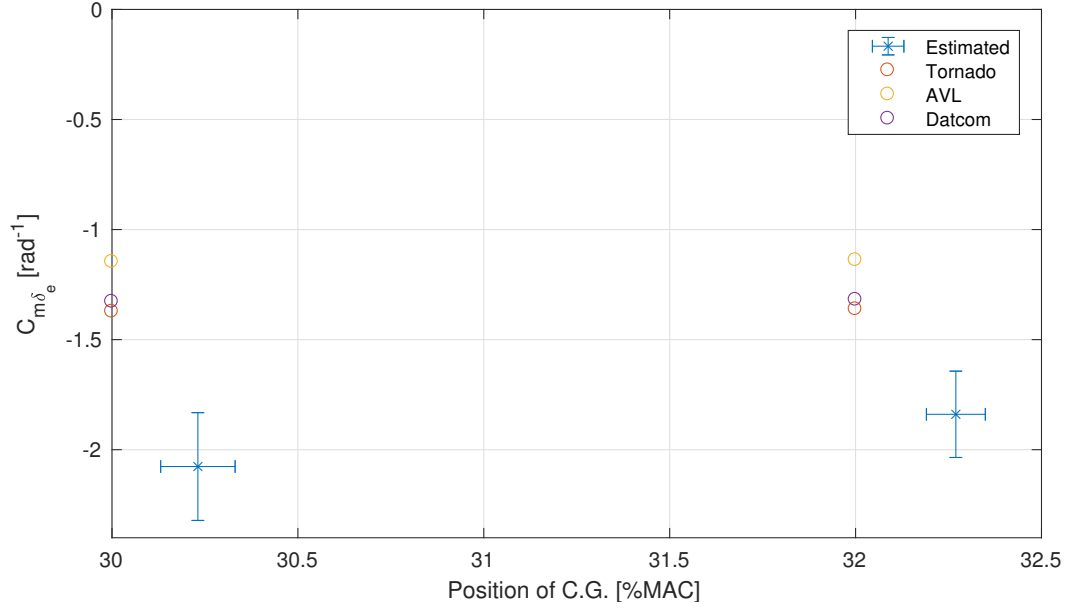


Figure 5.20: Graph of parameter  $C_{m\delta_e}$ .

### 5.5.3 Model validation

The dataset gathered during the flight campaign mentioned above was split into a training dataset and a validation dataset. The validation dataset contains the maneuvers used only for the validation of the estimated flight parameters. The estimated flight parameters were used for obtaining the simulated flight data. The simulation uses the input signal and initial conditions from the validation dataset. The outputs of the simulation were compared with measured flight data (see Figure 5.21).

The blue lines represents the measured flight data after the FPR process and the red lines represents the simulated flight data based on the estimated flight parameters. It can be seen in figure, that the airspeed  $V$ , angle-of-attack  $\alpha$ , pitch angle  $\theta$  and pitch rate  $q$  have a good fit. The translational accelerations  $a_x$  and  $a_z$  suffer from the vibrations caused by the 4 stroke combustion engine. As previously mentioned, an elevator doublet maneuver was used for the excitation. The elevator input is shown on last graph and does not contain a red line as the elevator is the input and thus it is not simulated.

After the comparison of the simulated and measured flight data it can be said that the simulated flight data based on the estimated flight parameters correspond sufficiently to the measured flight data. Therefore, it can be said, that the estimated flight parameters sufficiently describe the airplane aerodynamics and created model is sufficiently accurate.

Additional results of model validation are presented in Appendix G.

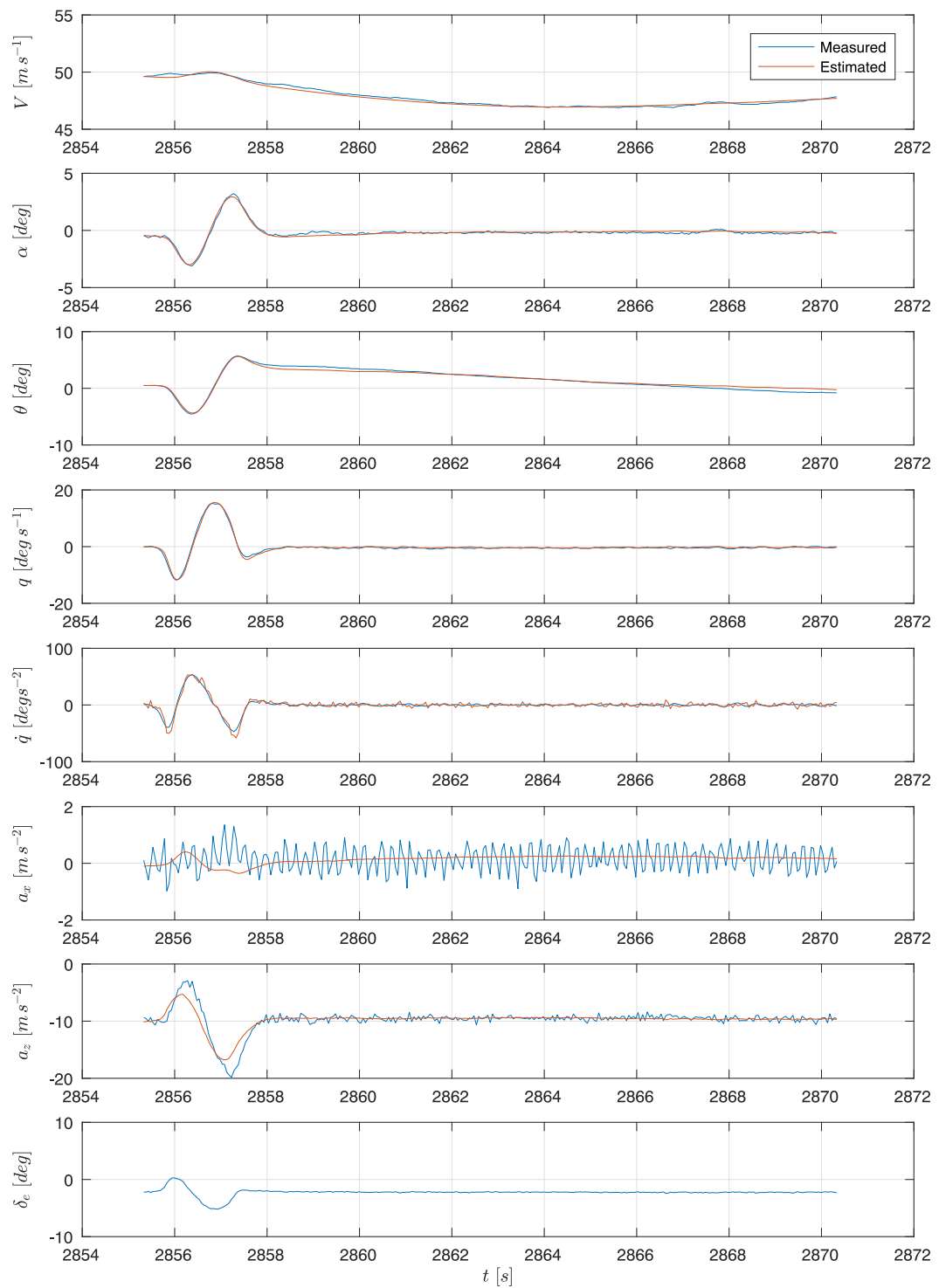


Figure 5.21: Recorded data for maneuver N° 124.

## 5.6 Summary

All flight parameters of the experimental airplane, which were estimated from the measured flight test data fall within the limits presented in Sections 5.5.1 and 5.5.2.

### 5.6.1 Linear dependency of parameters

The linear characteristics of the force coefficients were presented in Section 5.5.1. The Figures 5.15 and 5.16 shows the selected part of the flight envelope and a linear interpolation of force coefficients.

### 5.6.2 Simulation and model validation

In Section 5.5.3, it was shown, that the simulated flight data based on the estimated flight parameters sufficiently correspond to the measured flight data. Therefore, it can be said, that the estimated flight parameters sufficiently describe the airplane aerodynamics and the created model is sufficiently accurate.

### 5.6.3 Correction of a-priori values

All sources of the a-priori aerodynamic coefficient values, exhibit difficulties with the drag flight parameters. The relative values of drag based flight parameters range within [29%, 52%] of estimated flight parameters. The lift based flight parameters have a good a-priori prediction ranging within [87%, 117%] of estimated flight parameters.

Table 5.6: Comparison of a-priori force parameters and force parameters obtained by estimation methods based on experimental flight data.

Param.	Absolute values				Relative values			
	Est.	Tornado	AVL	Datcom	Est.	Tornado	AVL	Datcom
$C_{D0}$	0.0510	0.0148	0.0244	—	1.00	0.29	0.48	—
$C_{D\alpha}$	0.6908	0.2326	—	0.3574	1.00	0.34	—	0.52
$C_{L0}$	0.4879	0.5619	0.5692	0.4256	1.00	1.15	1.17	0.87
$C_{L\alpha}$	5.0702	4.9873	4.8796	4.9805	1.00	0.98	0.96	0.98
$C_{L\delta_e}$	0.4730	0.5175	0.4419	0.4820	1.00	1.09	0.93	1.02

Table 5.7: Comparison of a-priori moment parameters and moment parameters obtained by estimation methods based on experimental flight data at center of mass position 30%MAC.

Param.	Absolute values				Relative values			
	Est.	Tornado	AVL	Datcom	Est.	Tornado	AVL	Datcom
$C_{m0}$	-0.1025	-0.0013	0.0266	0.0308	1.00	0.01	-0.26	-0.30
$C_{m\alpha}$	-0.428	-0.979	-0.476	-0.777	1.00	2.29	1.11	1.81
$C_{mq}$	-25.379	-10.768	-8.992	-8.182	1.00	0.42	0.35	0.32
$C_{m\delta_e}$	-2.077	-1.373	-1.147	-1.328	1.00	0.66	0.55	0.64

Table 5.8: Comparison of a-priori moment parameters and moment parameters obtained by estimation methods based experimental flight data at center of mass position 32%MAC.

Param.	Absolute values				Relative values			
	Est.	Tornado	AVL	Datcom	Est.	Tornado	AVL	Datcom
$C_{m0}$	-0.0574	0.0102	0.0376	0.0415	1.00	-0.18	-0.66	-0.72
$C_{m\alpha}$	-0.286	-0.877	-0.389	-0.681	1.00	3.07	1.36	2.38
$C_{mq}$	-24.324	-10.562	-8.840	-8.047	1.00	0.43	0.36	0.33
$C_{m\delta_e}$	-1.839	-1.362	-1.139	-1.319	1.00	0.74	0.62	0.72

#### 5.6.4 Comparison with other airplane category

The ratios of the a-priori values relative to the values obtained by the estimation methods based experimental flight data on SportStar RTC are compared the correction factor of the a-priori values and wind-tunnel data values for a F-18 Hornet model published by J. Kay et al. [56]. The VLM (Vortex Lattice Method), used by J. Kay et al., is the underlying theory in Tornado and AVL software packages.

The relative values of the investigated longitudinal motion flight parameters are given in Table 5.9. The table, published for the F-18 Hornet model, can be found in Appendix H.

The differences between the correction factors of the Eveztor SportStar RTC and F-18 Hornet models are minor for the lift flight parameters, but higher for the pitch moment parameters.

Table 5.9: Comparison of relative values of low subsonic flight parameters between SportStar RTC and F-18 Hornet.

Parameter	SportStar RTC				F-18 Hornet		
	Est.	Tornado	AVL	Datcom	Data	VLM	Datcom
$C_{D0}$	1.00	0.29	0.48	—	—	—	—
$C_{D\alpha}$	1.00	0.34	—	0.52	—	—	—
$C_{L0}$	1.00	1.15	1.17	0.87	—	—	—
$C_{L\alpha}$	1.00	0.98	0.96	0.98	1.00	0.93	0.86
$C_{L\delta_e}$	1.00	1.09	0.93	1.02	1.00	0.89	0.84
$C_{m0}$	1.00	-0.18	-0.66	-0.72	—	—	—
$C_{m\alpha}$	1.00	3.07	1.36	2.38	1.00	0.90	0.95
$C_{mq}$	1.00	0.43	0.36	0.33	1.00	1.25	0.90
$C_{m\delta_e}$	1.00	0.74	0.62	0.72	1.00	0.97	0.89

## 6. Conclusion and future work

The objectives of this thesis were to study the theory of the flight data acquisition and flight parameter estimation; to select and implement algorithms suitable for flight parameters estimation of a light airplane. These objectives were met and the author identified the flight parameters of the investigated experimental light airplane.

All flight parameters of the experimental airplane which were estimated based on the measured flight test data fall within the presented limits. For the purposes of the flight parameter estimation, the author used the Equation Error Method, Output Error Method and Recursive Least-Squares methods. The force coefficients containing the longitudinal motion exhibit linear character in the investigated region of the flight envelope. The flight envelope was limited to conditions, in terms of altitudes, airspeed and position of center of mass, as consulted with the airplane manufacturer. Using the model validation process, the author have proved, that the simulated flight data based on the estimated flight parameters sufficiently corresponds to the measured flight data. Therefore, the estimated flight parameters sufficiently describe the airplane aerodynamics and the created model is sufficiently accurate. The flight parameters, the author estimated in this thesis can be used to build a high fidelity flight simulator, which will be able to match the behavior of the real airplane more precisely and therefore improve the airplane pilot training.

The lift based flight parameters have a good a-priori prediction ranging within [87%, 117%] of the estimated flight parameters. The relative values of the drag based flight parameters range within [29%, 52%] of the estimated flight parameters, which points to a weak spot of the a-priori data sources. The differences between the correction factors of the Evektor SportStar RTC and F-18 Hornet models are minor for the lift flight parameters, but higher for the pitch moment parameters. The presented correction factors are useful during the development phase of a new airplane to conservatively predict its aerodynamic characteristics. The resultant correction factors for the presented computational tools can be applied in the design of a similar category of airplanes, which can lower the expenses of the development cycle. The possible direction of further research is the estimation of the flight parameters for the lateral-directional motion.

The presented contributions were published in international conferences (mostly AIAA and DASC conferences), and these papers were cited several times (see attached List of authors publications and research activities).

# Bibliography

1. ACHARYA, Rajat. *Understanding Satellite Navigation*. Academic Press, 2014. ISBN 978-0-12-799949-4.
2. AIR NAVIGATION SERVICES OF THE CZECH REPUBLIC. *Aerodrome chart - ICAO Kunovice* [online] [visited on 2016-07-04]. Available from: [http://lis.rlp.cz/ais\\_data/aip/data/valid/a2-ku-adc.pdf](http://lis.rlp.cz/ais_data/aip/data/valid/a2-ku-adc.pdf).
3. ALLERTON, David. *Principles of Flight Simulation (AIAA Education Series)*. American Institute of Aeronautics and Astronautics, 2009. ISBN 978-1-60086-703-3.
4. AMS. *How to build a potentiometer with familiar outputs – and unfamiliar qualities* [online]. Graz, Austria: ams AG, 2015. ATA1415 [visited on 2016-02-10]. Available from: [http://ams.com/eng/content/download/795210/1979696/file/ams\\_TA\\_Contactless\\_Potentiometers.pdf](http://ams.com/eng/content/download/795210/1979696/file/ams_TA_Contactless_Potentiometers.pdf). Technical report.
5. ANSI/AIAA. *Recommended Practice for Atmospheric and Space Flight Vehicle Coordinate Systems*. Washington, DC: American Institute of Aeronautics and Astronautics, 1992. R-004-1992. ISBN 0930403827. Recommendation Practice.
6. ANTSAKLIS, Panos J; MICHEL, Anthony N. *A Linear Systems Primer*. Birkhäuser, 2010. ISBN 0817644601.
7. ARINC. *Mark 5 Subsonic Air Data System*. Annapolis, MD: Aeronautical Radio, Inc., 1988. 706-4. ARINC Characteristic.
8. BD SENSORS S.R.O. *BD SENSORS – Snímače Tlaku* [online] [visited on 2016-08-06]. Available from: <http://www.bdsensors.cz>.
9. BLOMBERG, H.; YLINEN, R. *Algebraic theory for multivariable linear systems, Volume 166 (Mathematics in Science and Engineering)*. Academic Press, 1983. ISBN 0121071502.
10. BRADY, Chris. *The Boeing 737 Technical Guide*. Tech Pilot Services Ltd., 2015. ISBN 978-1-4475-3273-6.
11. BRP-POWERTRAIN. *Operator's Manual For Rotax® Engine Type 912 Series*. Gunskirchen, Austria: BRP-Powertrain GmbH & Co KG., 2010. OM-912. Manual.
12. BRP-POWERTRAIN. *Rotax* [online] [visited on 2016-01-25]. Available from: <https://www.rotax.com/en/>.
13. CHATFIELD, A. *Fundamentals of High Accuracy Inertial Navigation (Progress in Astronautics and Aeronautics)*. American Institute of Aeronautics and Astronautics, 1997. ISBN 1-56347-243-0.
14. CHEN, Ben M.; LIN, Zongli; SHAMASH, Yacov. *Linear Systems Theory: A Structural Decomposition Approach (Control Engineering)*. Birkhäuser, 2004. ISBN 0817637796.
15. CHUDÝ, Peter; DITTRICH, Petr. *Primární letový displej: Technická dokumentace pro primární letový displej*. Brno, Czech Republic: Vysoké učení technické v Brně, 2013. AWPFD 1.2013. Technical report.
16. CHUDÝ, Peter; DITTRICH, Petr; VLK, Jan. *Dynamický model letounu: Dynamický model letounu kategorie ULL/LSA*. Brno, Czech Republic: Vysoké učení technické v Brně, 2011. AWDM 2.2011. Technical report.

17. COUNCIL OF EUROPEAN UNION. *Council regulation (EU) no 216/2008*. 2008. Available also from: <http://eur-lex.europa.eu/legal-content/EN/TXT/?uri=CELEX:02008R0216-20130129>.
18. DIRECT INDUSTRY. *Hybrid precision potentiometers SRS280* [online] [visited on 2016-08-04]. Available from: <http://www.directindustry.com/prod/penny-giles-controls/product-4591-59168.html>.
19. DRELA, Mark; YOUNGREN, Harold. *AVL* [online] [visited on 2016-08-06]. Available from: <http://web.mit.edu/drela/Public/web/avl/>.
20. EASA. *Certification Specifications and Acceptable Means of Compliance for Free Gas Balloons*. Brussels, Belgium: European Aviation Safety Agency, 2011. CS-31GB. Certification Specifications.
21. EASA. *Certification Specifications and Acceptable Means of Compliance for Tethered Gas Balloons*. Brussels, Belgium: European Aviation Safety Agency, 2013. CS-31TGB. Certification Specifications.
22. EASA. *Certification Specifications for Hot Air Balloons*. Brussels, Belgium: European Aviation Safety Agency, 2009. CS-31HB. Certification Specifications.
23. EASA. *Certification Specifications for Large Aeroplanes*. Brussels, Belgium: European Aviation Safety Agency, 2003. CS-25. Certification Specifications.
24. EASA. *Certification Specifications for Large Rotorcraft*. Brussels, Belgium: European Aviation Safety Agency, 2003. CS-29. Certification Specifications.
25. EASA. *Certification Specifications for Light Sport Aeroplanes*. Brussels, Belgium: European Aviation Safety Agency, 2011. CS-LSA. Certification Specifications.
26. EASA. *Certification Specifications for Normal, Utility, Aerobatic, and Commuter Category Aeroplanes*. Brussels, Belgium: European Aviation Safety Agency, 2003. CS-23. Certification Specifications.
27. EASA. *Certification Specifications for Sailplanes and Powered Sailplanes*. Brussels, Belgium: European Aviation Safety Agency, 2003. CS-22. Certification Specifications.
28. EASA. *Certification Specifications for Small Rotorcraft*. Brussels, Belgium: European Aviation Safety Agency, 2003. CS-27. Certification Specifications.
29. EASA. *Certification Specifications for Very Light Aeroplanes*. Brussels, Belgium: European Aviation Safety Agency, 2003. CS-VLA. Certification Specifications.
30. EASA. *Certification Specifications for Very Light Rotorcraft*. Brussels, Belgium: European Aviation Safety Agency, 2003. CS-VLR. Certification Specifications.
31. ETKIN, Bernard; REID, Lloyd Duff. *Dynamics of Flight: Stability and Control*. Wiley, 1995. ISBN 0-471-03418-5.
32. EVEKTOR. *SportStar RTC – Evekter* [online] [visited on 2016-07-04]. Available from: <http://www.evektor.cz/cz/sportstar-rtc>.
33. EVEKTOR–AEROTECHNIK. *Letová Příručka EV-97*. Kunovice, Czech Republic: Evekter–Aerotechnik, 2000. EV2000RLPCZ. Manual.
34. FALKENA, Wouter. *Investigation of Practical Flight Control Systems for Small Aircraft*. Delft, Netherlands, 2012. ISBN 978-94-6203-258-3. PhD thesis. Delft University of Technology, Faculty Aerospace Engineering.

35. FLOSCAN INSTRUMENT CO., INC. *FloScan Aircraft Flow Transducers* [online] [visited on 2016-08-06]. Available from: <http://www.floscan.com/html/blue/aviation.php>.
36. FRADEN, Jacob. *Handbook of Modern Sensors: Physics, Designs, and Applications*. Springer, 2010. ISBN 978-1-4419-6465-6.
37. FRANKLIN, Gene F.; POWELL, J. David; WORKMAN, Michael L. *Digital Control of Dynamic Systems*. Addison-Wesley, 1998. ISBN 0-201-33153-0.
38. GARMIN. *Garmin* [online] [visited on 2016-02-10]. Available from: <https://buy.garmin.com/en-US/US/oem/sensors-and-boards/glo-/prod109827.html>.
39. GOYER, Robert. *LSA Safety Picture Emerging* [online]. Winter Park, FL: Bonnier Corporation, 2009 [visited on 2016-08-23]. Available from: <http://www.flyingmag.com/pilot-reports/lsa/sport/lsa-safety-picture-emerging>.
40. GRANGER, Robert A. *Fluid Mechanics (Dover Books on Physics)*. Dover Publications, 1995. ISBN 0486683567.
41. GUDMUNDSSON, Snorri. *General Aviation Aircraft Design: Applied Methods and Procedures*. Butterworth-Heinemann, 2013. ISBN 978-0-12-397308-5.
42. HANAVAN, Ernest P. *A Mathematical Model Of The Human Body*. Wright-Patterson Air Force Base, OH: Aerospace Medical Research Laboratories, 1964. TR-64-102. AMRL.
43. HAZEWINKEL, Michiel. *Encyclopaedia of Mathematics (set)*. Netherlands: Springer, 1994. ISBN 978-1-55608-010-4.
44. HILTON, J. L.; HOHENKERK, C. Y. Rotation matrix from the mean dynamical equator and equinox at J2000.0 to the ICRS. *Astronomy and Astrophysics*. 2004, vol. 413, no. 2, pp. 765–770. Available from DOI: [10.1051/0004-6361:20031552](https://doi.org/10.1051/0004-6361:20031552).
45. HITCHENS, Frank. *Propeller Aerodynamics*. AUK Academic, 2015. ISBN 9781785381249.
46. HOAG, David. *Apollo Guidance and Navigation Considerations of Apollo IMU Gimbal Lock* [online]. Cambridge, MA: MIT Instrumentation Laboratory, 1963. E-1344 [visited on 2016-06-15]. Available from: <http://www.hq.nasa.gov/alsj/e-1344.htm>. Technical report.
47. HOTTINGER BALDWIN MESSTECHNIK GMBH. *HBM Test and Measurement* [online] [visited on 2016-08-06]. Available from: <https://www.hbm.com>.
48. ICAO. *Manual of the ICAO Standard Atmosphere*. Quebec, Canada: International Civil Aviation Organization, 1993. Doc 7488/3. ICAO.
49. IEEE. *IEEE Standard for Inertial Systems Terminology*. New York, NY: The Institute of Electrical and Electronics Engineers, Inc., 2009. 1559-2009. Standard.
50. ISO. *Flight dynamics – Concepts, quantities and Symbols—Part 1: Aircraft motion relative to the air*. Geneva, Switzerland: International Organization for Standardization, 1988. 1151-1:1988. Standard.
51. ISO. *Quantities and Units—Part 1: General*. Geneva, Switzerland: International Organization for Standardization, 2009. 80000-1:2009. Standard.
52. ISO. *Quantities and Units—Part 2: Mathematical signs and symbols to be used in the natural sciences and technology*. Geneva, Switzerland: International Organization for Standardization, 2009. 80000-2:2009. Standard.
53. ISO. *Standard Atmosphere*. Geneva, Switzerland: International Organization for Standardization, 1975. 2533:1975. Standard.

54. JATEGAONKAR, Ravindra V. *Flight Vehicle System Identification (Progress in Astronautics and Aeronautics)*. American Institute of Aeronautics and Astronautics, 2006. ISBN 1-56347-836-6.
55. JOSEFÍK, Miroslav. *Program a Metodiky: Zkoušek projektu „Chytrý autopilot“*. Kunovice, Czech Republic: Evektor spol.s r.o., 2012. RTC.206P.JOS/12. Technical report.
56. KAY, J.; MASON, W. H.; DURHAM, W.; LUTZE, F. Control Authority Assessment in Aircraft Conceptual Design. In: *AIAA Aircraft Design, Systems, and Operations Meeting*. Monterey, CA: American Institute of Aeronautics and Astronautics, 1993, p. 19. No. 3968. Available from DOI: [10.2514/6.1993-3968](https://doi.org/10.2514/6.1993-3968).
57. KENWRIGHT, Ben. A Beginners Guide to Dual-Quaternions. In: *WSCG'2012 Conference Proceedings*. Plzeň, Czech Republic: Vaclav Skala – Union Agency, 2012. ISBN 978-80-86943-79-4.
58. KLEIN, Vladislav; MORELLI, Eugene A. *Aircraft System Identification: Theory And Practice*. American Institute of Aeronautics and Astronautics, 2006. ISBN 1-56347-832-3.
59. KUNDU, Ajoy Kumar. *Aircraft Design (Cambridge Aerospace Series)*. Cambridge University Press, 2010. ISBN 978-0-521-88516-4.
60. LEWIS, Frank L.; XIE, Lihua; POPA, Dan. *Optimal and Robust Estimation: With an Introduction to Stochastic Control Theory, Second Edition (Automation and Control Engineering)*. CRC Press, 2007. ISBN 978-1-4200-0829-6.
61. LIVINGSTON, Sadie P.; GRACEY, William. *Tables of Airspeed, Altitude, and Mach Number Based on Latest International Values for Atmospheric Properties and Physical Constants*. Langley Field, VA: National Aeronautics and Space Administration, 1961. D-822. Technical Note.
62. LOMBAERTS, Thomas. *Fault Tolerant Flight Control – A Physical Model Approach*. Delft, Netherlands, 2010. ISBN 978-90-815443-1-3. PhD thesis. Delft University of Technology, Faculty Aerospace Engineering.
63. MAINE, R. E.; ILIFF, K. W. *Identification Of Dynamic Systems – Applications To Aircraft – Part 1: The Output Error Approach*. Neuilly sur Seine, France: Advisory Group for Aerospace Research and Development, 1986. 300 Vol.3. ISBN 92-835-1540-4. AGARDo-graph.
64. MARGHITU, Dan B. *Mechanical Engineer's Handbook (Engineering)*. Academic Press, 2001. ISBN 978-0-12471-370-3.
65. MATHWORKS. *MATLAB & Simulink* [online] [visited on 2016-08-06]. Available from: <https://www.mathworks.com/products/matlab.html>.
66. MELIN, Tomas. *A Vortex Lattice MATLAB Implementation for Linear Aerodynamic Wing Applications*. Stockholm, Sweden, 2000.
67. MERHAV, Shmuel. *Aerospace Sensor Systems and Applications*. Springer, 1998. ISBN 0-387-94605-5.
68. MINISTERSTVO OBRANY. *Ministerstvo obrany a Armáda České republiky* [online] [visited on 2016-01-27]. Available from: <http://www.army.cz>.
69. MORAVAN. *Letová Příručka Z-142*. Otrokovice, Czech Republic: Moravan, národní podnik Otrokovice, 1982. Technical report.

70. MORRIS, Alan S.; LANGARI, Reza. *Measurement and Instrumentation: Theory and Application*. Elsevier, 2012. ISBN 978-0-12-800884-3.
71. NATIONAL COORDINATION OFFICE FOR SPACE-BASED POSITIONING, NAVIGATION, AND TIMING. *GPS Overview* [online] [visited on 2016-02-04]. Available from: <http://www.gps.gov/systems/gps/>.
72. NATIONAL INSTRUMENTS CORPORATION. *LabVIEW System Design Software* [online] [visited on 2016-08-06]. Available from: <http://www.ni.com/labview/>.
73. NATIONAL INSTRUMENTS CORPORATION. *The CompactRIO Platform* [online] [visited on 2016-08-06]. Available from: <http://www.ni.com/compactrio/>.
74. NEBYLOV, Alexander. *Aerospace Sensors (Sensors Technology)*. Momentum Press, 2012. ISBN 1-60650-059-0.
75. NIMA. *World Geodetic System 1984—Its Definition and Relationships with Local Geodetic Systems*. St. Louis, MO: National Imagery and Mapping Agency, 2000. TR8350.2. NIMA.
76. PAMADI, Bandu N. *Performance, Stability, Dynamics, and Control of Airplanes, Second Edition (AIAA Education)*. American Institute of Aeronautics & Astronautics, 2004. ISBN 1-56347-583-9.
77. PATRANABIS, D. *Sensors and Transducers*. Prentice-Hall of India Pvt.Ltd, 2004. ISBN 8120321987.
78. PENNY&GILES. *SRS280 – Sealed Rotary Sensor* [online] [visited on 2016-08-06]. Available from: <http://www.cw-industrialgroup.com/Products/Sensors/Rotary-Hall-Effect-Position-Sensors/Sealed-Rotary-Sensor-SRS280.aspx>.
79. PIPISTREL. *Pilot's Operating Handbook and Training Supplement—Sinus FLEX LSA*. Gorizia, Italy: Pipistrel LSA s.r.l., 2010. Manual.
80. RAOL, Jitendra R.; SINGH, Jatinder. *Flight Mechanics Modeling and Analysis*. CRC Press, 2008. ISBN 978-1-4200-6753-8.
81. RED LION CONTROLS, INC. *Red Lion. Connect. Monitor. Control.* [online] [visited on 2016-08-06]. Available from: <http://www.redlion.net>.
82. REKTORYS, Karel. *Přehled užité matematiky*. Nakladatelství Prometheus, 1995. ISBN 80-8584-972-0.
83. ROGERS, Robert M. *Applied Mathematics in Integrated Navigation Systems, Third Edition (AIAA Education)*. American Institute of Aeronautics and Astronautics, 2007. ISBN 1-56347-927-3.
84. ИНФОРМАЦИОННО-АНАЛИТИЧЕСКИЙ ЦЕНТР. *ГЛОНАСС* [online] [visited on 2016-02-04]. Available from: <https://www.glonass-iac.ru>.
85. SPACEAGE CONTROL. *Data Sheet - 100400 Mini Air Data Boom* [online] [visited on 2016-08-04]. Available from: <http://spaceagecontrol.com/Main/S002c>.
86. STENGEL, Robert F. *Stochastic Optimal Control: Theory and Application*. Wiley-Interscience, 1986. ISBN 0-471-86462-5.
87. STEVENS, Brian L.; LEWIS, Frank L. *Aircraft Control and Simulation*. Wiley-Interscience, 2003. ISBN 0-471-37145-9.

88. STOCK FLIGHT SYSTEMS. *CANaerospace – Interface specification for airborne CAN applications V1.7* [online]. Berg/Farchach, Germany, 2006 [visited on 2016-07-05]. Available from: [http://www.stockflightsystems.com/tl\\_files/downloads/canaerospace/canas\\_17.pdf](http://www.stockflightsystems.com/tl_files/downloads/canaerospace/canas_17.pdf). Interface Specifications.
89. STOCK FLIGHT SYSTEMS. *IFNS* [online] [visited on 2016-08-06]. Available from: <http://www.stockflightsystems.com/ifns.html>.
90. TANEJA, H.C. *Advanced Engineering Mathematics: Volume I and II*. IK International Publishing House, 2009. ISBN 978-8189866570.
91. TEWARI, Ashish. *Atmospheric and Space Flight Dynamics: Modeling and Simulation with MATLAB® and Simulink® (Modeling and Simulation in Science, Engineering and Technology)*. Birkhäuser, 2007. ISBN 0-8176-4373-7.
92. UNITED STATES DEPARTMENT OF DEFENSE. *United States Department of Defense* [online] [visited on 2016-01-27]. Available from: <http://www.defense.gov>.
93. ÚŘAD PRO CIVILNÍ LETECTVÍ. *Přehled vydaných Oprávnění k provádění zkoušek letecké techniky podle Postupů CAA-TI-012-4/99* [online] [visited on 2016-08-06]. Available from: <http://www.caa.cz/letadla/prehled-vydanych-opravneni-k-provadeni-zkousek?highlightWords=1-3-060>.
94. ÚŘAD PRO CIVILNÍ LETECTVÍ. *Úřad pro civilní letectví* [online] [visited on 2016-01-27]. Available from: <http://www.caa.cz>.
95. USAF TEST PILOT SCHOOL. *Flying Qualities Textbook, Volume 2*. Edwards AFB, CA: USAF, 1986. USAF-TPS-CUR-86-02.
96. VISHAY PRECISION GROUP. *General Purpose Strain Gages 250UN* [online] [visited on 2016-08-06]. Available from: <http://www.vishaypg.com/micro-measurements/list/product-11298/>.
97. VISSER, Cornelis Coenraad de. *Global Nonlinear Model Identification with Multivariate Splines – Application to Aerodynamic Model Identification of the Cessna Citation II*. Delft, Netherlands, 2011. ISBN 978-90-8570-770-7. PhD thesis. Delft University of Technology, Faculty Aerospace Engineering.
98. WAGUESPACK, Curtis. *Mastering Autodesk Inventor 2015 and Autodesk Inventor LT 2015: Autodesk Official Press*. Sybex, 2014. ISBN 978-1-118-86213-1.
99. WILLIAMS, John E.; VUKELICH, Steven R. *The USAF Stability And Control Digital Datcom*. Wright–Patterson Air Force Base, OH, 1979. TR-679-3032. AFFDL.
100. WILSON, Jon S. *Sensor Technology Handbook*. Newnes, 2004. ISBN 0-7506-7729-5.
101. WYATT, David; TOOLEY, Mike. *Aircraft Electrical and Electronic Systems*. Routledge, 2008. ISBN 978-0-7506-8695-2.
102. XSENS. *MTi-G GPS-aided AHRS* [online] [visited on 2016-08-04]. Available from: <https://www.xsens.com/products/mti-g/>.
103. YECHOUT, Thomas R.; MORRIS, Steven L.; BOSSERT, David E.; HALLGREN, Wayne F. *Introduction to Aircraft Flight Mechanics: Performance, Static Stability, Dynamic Stability, and Classical Feedback Control (AIAA Education Series)*. American Institute of Aeronautics & Astronautics, 2003. ISBN 978-1-56347-577-1.

# A. Coordinate systems

There are four coordinate systems that are most commonly used in aerospace: Cartesian coordinate system, Cylindrical coordinate system, Spherical coordinate system and Geodetic coordinate system.

**Cartesian coordinate system** [82, 90] is multi-dimensional orthonormal space. For the purposes of this thesis we consider three-dimensional space only. Position  $\vec{r}_{Xf}$  of arbitrary point  $X$  relative to origin of the general reference frame  $F_f$  in Cartesian coordinate system is described as [82, 90]:

$$\vec{r}_{Xf} = \begin{bmatrix} x \\ y \\ z \end{bmatrix}_{Xf} \quad (\text{A.1})$$

where  $x_{Xf}$ ,  $y_{Xf}$  and  $z_{Xf}$  are positions along particular axes.

**Cylindrical coordinate system** [82, 90] is three-dimensional orthogonal space with cylindrical coordinate surfaces. This coordinate system is denoted by superscript  $C$ . Position  $\vec{r}_{Xf}^C$  of arbitrary point  $X$  relative to origin of the general reference frame  $F_f$  in Cylindrical coordinate system is [82]:

$$\vec{r}_{Xf}^C = \begin{bmatrix} r \\ \psi \\ z \end{bmatrix}_{Xf}^C \quad (\text{A.2})$$

where  $r_{Xf}^C$  is the radius (Euclidian distance from the  $z$ -axis) and  $\psi_{Xf}^C$  is the azimuth angle measured counterclockwise as seen from any point with positive  $z_{Xf}^C$  component. Component  $z_{Xf}^C$  in Cylindrical coordinate system is equal to component  $z_{Xf}$  in Cartesian coordinate system.

Conversion from Cylindrical coordinate system to Cartesian coordinate system can be computed using [82, 90]:

$$x_{Xf} = r_{Xf}^C \cos \psi_{Xf}^C \quad (\text{A.3a})$$

$$y_{Xf} = r_{Xf}^C \sin \psi_{Xf}^C \quad (\text{A.3b})$$

$$z_{Xf} = z_{Xf}^C \quad (\text{A.3c})$$

On the contrary, conversion from Cartesian coordinate system to Cylindrical coordinate system is given by:

$$r_{Xf}^C = \sqrt{x_{Xf}^2 + y_{Xf}^2} \quad (\text{A.4a})$$

$$\psi_{Xf}^C = \arctan \left( \frac{y_{Xf}}{x_{Xf}} \right) \quad (\text{A.4b})$$

$$z_{Xf}^C = z_{Xf} \quad (\text{A.4c})$$

**Spherical coordinate system** [82, 90] is three-dimensional orthogonal space with spherical coordinate surfaces. This coordinate system is denoted by superscript  $S$ . Position  $\vec{r}_{Xf}^S$  of arbitrary point  $X$  relative to origin of the general reference frame  $F_f$  in Spherical coordinate system is [82]:

$$\vec{r}_{Xf}^S = \begin{bmatrix} r \\ \psi \\ \theta \end{bmatrix}_{Xf}^S \quad (\text{A.5})$$

where  $r_{Xf}^S$  is the radial distance from origin of general reference frame  $F_f$ ,  $\theta_{Xf}^S$  is the elevation angle, and  $\psi_{Xf}^C$  is the azimuth angle measured counterclockwise as seen from any point with positive  $z_{Xf}$  component.

Azimuth angle  $\psi_{Xf}^S$  in Spherical coordinate system is equal to azimuth angle  $\psi_{Xf}^C$  in Cylindrical coordinate system.

Conversion from Spherical coordinate system to Cartesian coordinate system is described as follows [80, 82]:

$$x_{Xf} = r_{Xf}^S \cos \theta_{Xf}^S \cos \psi_{Xf}^S \quad (\text{A.6a})$$

$$y_{Xf} = r_{Xf}^S \sin \theta_{Xf}^S \quad (\text{A.6b})$$

$$z_{Xf} = r_{Xf}^S \cos \theta_{Xf}^S \sin \psi_{Xf}^S \quad (\text{A.6c})$$

On the contrary, conversion from Cartesian coordinate system to Spherical coordinate system is:

$$r_{Xf}^S = \sqrt{x_{Xf}^2 + y_{Xf}^2 + z_{Xf}^2} \quad (\text{A.7a})$$

$$\psi_{Xf}^S = \arctan \left( \frac{y_{Xf}}{x_{Xf}} \right) \quad (\text{A.7b})$$

$$\theta_{Xf}^S = \arcsin \left( \frac{z_{Xf}}{r_{Xf}^S} \right) \quad (\text{A.7c})$$

**Geodetic coordinate system**, sometimes called Geographic coordinate system, is a pseudo-spherical coordinate system, which is defined in the WGS84 [75]. This coordinate system is denoted by superscript  $G$ . Position  $\vec{r}_X^G$  of arbitrary point  $X$  in Geodetic coordinate system is [75, 83]:

$$\vec{r}_X^G = \begin{bmatrix} \ell \\ \varphi \\ h \end{bmatrix}_X^G \quad (\text{A.8})$$

where  $\ell$  is the geodetic longitude,  $\varphi$  is the geodetic latitude, and  $h$  is the height above the ellipsoid.

Geodetic longitude  $\ell_X$  of an arbitrary point  $X$  is the angle measured in equatorial plane between the prime meridian plane (xz-plane of ECEF reference frame) and the meridian plane of the point  $X$ . Geodetic longitude takes values in the range  $-\pi \leq \ell_X < \pi$  [75, 83].

Geodetic latitude  $\varphi_X$  of an arbitrary point  $X$  is the angle measured in meridian plane of the point  $X$  between equatorial plane (xy-plane of ECEF reference frame) and the surface normal of the point  $X$ . Geodetic latitude takes values in the range  $-\frac{\pi}{2} \leq \varphi_X \leq \frac{\pi}{2}$  [75, 83].

Geodetic height  $h_X$  of an arbitrary point  $X$  is the height above the surface of the WGS84 ellipsoid measured along the surface normal [75, 83].

Geodetic coordinate system is more human readable than Cartesian coordinate system. For example location of the fountain in the courtyard of the Faculty of Information Technology at Brno University of Technology in Geodetic coordinate system:

$$\vec{r}^G = \begin{bmatrix} \ell \\ \varphi \\ h \end{bmatrix}^G = \begin{bmatrix} 16.596713 \text{ deg} \\ 49.226523 \text{ deg} \\ 223.0 \text{ m} \end{bmatrix}^G \quad (\text{A.9})$$

is more human readable than location of the same place in Cartesian coordinate system in ECEF reference frame  $F_e$ :

$$\vec{r}_e = \begin{bmatrix} x \\ y \\ z \end{bmatrix}_e = \begin{bmatrix} 4001939.0 \\ 1192779.9 \\ 4809954.9 \end{bmatrix}_e \text{ m} \quad (\text{A.10})$$

## B. WGS84 model

There are several models of the Earth; however, the most widely used model is World Geodetic System 1984 (WGS84) [75], which is used in this thesis. The shape of the Earth is described as the WGS84 ellipsoid. The shape of the WGS84 ellipsoid is defined by semi-major axis  $a$  and flattening  $f$ . List of major parameters of the WGS84 model is given in Table B.1.

Table B.1: WGS84 Defining Parameters [75].

Parameter	Notation	Value
Semi-major axis	$a$	6378137.0 $m$
Reciprocal of flattening	$1/f$	298.257223563
Angular velocity	$\omega_{ei}$	$7.292115 \times 10^{-5} \text{ rad } s^{-1}$
Gravitational constant (mass of the Earth's atmosphere included)	$GM$	$3.986004418 \times 10^{14} \text{ m}^3 s^{-2}$

## C. ICAO Standard atmosphere

ICAO Standard Atmosphere [48] divides the Earth's atmosphere into several layers with specific characteristics. For the purposes of this thesis only the first layer (from 5 kilometers below mean sea level to 11 kilometers above mean sea level) is taken into account. Selected parameters of ICAO Standard Atmosphere are given in Table C.1.

Table C.1: Selected parameters of ICAO Standard Atmosphere [48].

Parameter	Notation	Value
Standard air pressure at sea level	$p_0$	101325 Pa
Standard thermodynamic temperature of air at sea level	$T_0$	288.15 K
Standard air mass density of dry air	$\rho_0$	1.2250 kg m <sup>-3</sup>
Ratio of specific heat at constant pressure to specific heat at constant volume	$\kappa$	1.4
Temperature gradient in the first layer of atmosphere	$L_1$	$-6.5 \times 10^{-3}$ K m <sup>-1</sup>

Specific gas constant for dry air  $R$  can be computed using ideal gas law [58]:

$$R = \frac{p_0}{\rho_0 T_0} \quad (C.1)$$

Based on parameters in Table C.1, the specific gas constant for dry air  $R$  is equal to 287.05287 J kg<sup>-1</sup>K<sup>-1</sup> [48]. Actual mass density of the air  $\rho$  can be computed similarly [58, 80]:

$$\rho = \frac{p_s}{RT} \quad (C.2)$$

where  $p_s$  is the instant static pressure of free stream and  $T$  is the instant thermodynamic temperature of the air.

The equation for computing static pressure from Geopotential pressure altitude  $H$  between  $-5000$  m and  $11000$  m is equal to [53]:

$$p_s = p_0 \left( 1 + \frac{L_1}{T_0} H \right)^{-\frac{G_0}{L_1 R}} \quad (C.3)$$

And vice versa, equation computing Geopotential pressure altitude from pressure 177 687 Pa to pressure 22 632 Pa is following:

$$H = \frac{T_0}{L_1} \left[ \left( \frac{p_s}{p_0} \right)^{-\frac{L_1 R}{G_0}} - 1 \right] \quad (C.4)$$

## D. Aircraft regulatory authorities

Aircrafts according to their size and/or purpose are regulated by several authorities. For the purposes of this thesis, the most important regulatory authority is EASA (European Aviation Safety Agency).

**European Aviation Safety Agency** is supervisory body in the field of civil aviation in European Union [17]. EASA regulation do not apply to aircraft belonging to one or more categories:

- Small unmanned aircrafts and Models of aircraft;
- Ultralight Aircrafts;
- Research, Experimental and Scientific aircrafts; and
- Military aircrafts.

Although EASA do not regulate these categories of aircrafts, it is recommended to act as there are regulated and comply with EASA requirements [17].

**Civil Aviation Authority** (CAA) act as a local supervisory body for EASA in Czech Republic [94]. CAA regulates on local level Small unmanned aircrafts, Models of aircraft, Research, Experimental and Scientific aircrafts.

**Light Aircraft Association of the Czech Republic** (LAA) act as complement of CAA and regulates on local level Ultralight Aircrafts, i.e., Ultralight Airplanes (ULA), Ultralight Helicopters (ULH), Ultralight Gliders (ULG), with Maximum Take-off Weight (MTOW) up to 450 kg.

**Military authorities** regulates military aircrafts in individual countries, e.g., Ministry of Defence and Armed Forces of Czech Republic [68] or United States Department of Defense [92].

## E. EASA classification of aircraft

Aircrafts under EASA regulations can be divided into two main categories according to their weight: **Aerodynes** (aircrafts heavier than air) and **Aerostats** (aircrafts lighter than air, e.g., balloons or airships) [20, 21, 22].

The detailed description of Aerostats and its division into particular categories is out of the scope of this thesis. For more information about aerostats please see [20, 21, 22].

This thesis is focused on Aerodynes, particularly on Light airplanes. Aerodynes, in general, can be divided into following three categories according to type of wings:

**Rotorcrafts** are aerodynes with rotating wing, sometimes called helicopters. Rotorcrafts can be divided into three categories according to Maximum Take-off Weight:

**Very light rotorcraft** (VLR) have to meet condition  $MTOW < 600\text{kg}$ . Regulations according to this category of aircraft are given in standard EASA CS-VLR [30].

**Small rotorcraft** have to meet condition  $MTOW < 3175\text{kg}$ . Regulations according to small rotorcrafts are given in standard EASA CS-27 [28]. Small rotorcraft category contains for example Bell 407, Robinson R44 and Eurocopter AS350.

**Large rotorcraft** have to meet condition  $MTOW > 3175\text{kg}$ . Regulations according to this category of aircraft are given in standard EASA CS-29 [24]. Large rotorcraft category contains for example PZL<sup>1</sup> W-3A, Kamov Ka-32 and Sikorsky S-92A.

**Ornithopters** are aircraft with moving wings. Because ornithopters are very unusual type of aircrafts, EASA does not have standard to certify it.

**Fixed-wing** aircrafts are divided into two categories according to engine presence:

**Without engine** are called sailplanes or gliders. Regulations according to this category of aircraft are given in standard EASA CS-22 [27]. Sailplanes and gliders category contains for example Blanik Limited L23 Super, VSO 10 and Alexander Schleicher ASW 27.

**Engine powered** are called airplanes. Airplanes are divided into four categories according to MTOW:

**Light Sport Airplane** (LSA) have to meet condition  $MTOW < 600\text{kg}$ . Regulations according to this category of aircraft are given in standard EASA CS-LSA [25]. Light Sport Airplane category contains for example Eveztor Sport-Star RTC and Czech Sport Aircraft P-28 Cruiser.

**Very Light Airplane** (VLA) have to meet condition  $MTOW < 750\text{kg}$ . Regulations according to this category of aircraft are given in standard EASA CS-VLA [29]. Very Light Airplane category contains for example Eveztor EV-97 VLA and Tecnam P2008.

---

<sup>1</sup>PZL – Polskie Zakłady Lotnicze

**Normal, utility, aerobatic and commuter airplanes** have to meet condition  $MTOW < 5670\text{kg}$ . Regulations according this category of aircraft are given in standard EASA CS-23 [26]. Normal, utility, aerobatic and commuter airplanes category contains for example Evektor VUT-100 Cobra, ZLIN Aircraft Z-142 and Cessna 172.

**Large airplane** have to meet condition  $MTOW > 5670\text{kg}$ . Regulations according this category of aircraft are given in standard EASA CS-25 [23]. Large airplane category contains for example Boeing 737, Airbus A330 and Antonov An-26.

Given that this thesis is focused on light airplanes, only LSA and VLA categories are considered.

## F. Airplane structure description

Airplane (based on definition in Appendix E) consists of a fuselage, fixed-wing, empennage and single non-turbine engine with propeller, see Figure F.1.

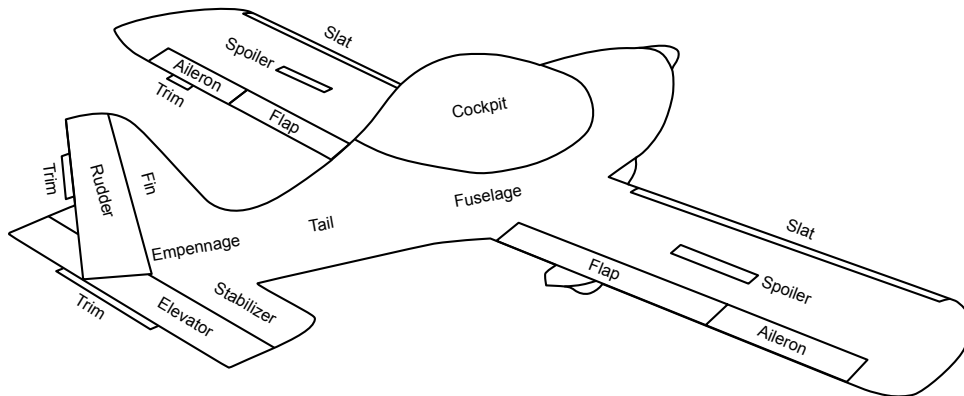


Figure F.1: Airplane control surfaces.

**Fuselage** is main part of the airplane dedicated for pilot, passenger and cargo load. VLA [29] and LSA [25] have maximum of two persons onboard including the pilot. Most of the airplanes in the VLA and LSA category have a single fuselage, so the center of mass of the whole airplane  $G$  is inside the fuselage and also the inertial sensors (i.e., accelerometer and gyroscope) are placed there. Tail part of the fuselage is usually free of magnetic parts; therefore, the magnetometer is usually placed in this section. The Global Positioning System (GPS) antenna is usually placed behind cockpit on upper side for maximum sky visibility. Landing gear is usually attached to the fuselage or wing. Fuselage can contain parachute recovery system.

**Wing** contains main control surfaces called ailerons placed on the outer wing section. The ailerons control roll motion of the airplane (rotation about  $x_b$  axis) and they are set by the side movement of stick or rotation of yoke [41]. The left and right aileron usually move together anti-symmetrically and the downward deflection is smaller than the upward deflection [41]. Deflection of the trailing edge of an aileron downward is considered a positive deflection. Differential ailerons deflection is implemented to prevent the adverse yaw motion caused by an increasing drag on one half of the wing. The aileron can feature a trimming tab (called aileron trim). The aileron trim balances the control force necessary to maintain the correct attitude of the airplane [10].

The wing usually contains some secondary control surfaces: flaps, slats, spoilers or airbrakes. Flaps and slats serve for increasing the lift during take-off and landing [41]. Flaps cannot be set to arbitrary position, every type of airplane has several predefined positions for cruise, take-off or landing (Z-142 has closed/cruise, take-off and landing positions [69]; EV-97 has closed/cruise, take-off and two landing positions [33]). Spoilers or airbrakes are used for decreasing lift, increasing drag and reducing the kinetic energy [10]. Airbrakes are very

rarely used in LSA and VLA, spoilers are more common (e.g., Pipistrel Sinus [79]).

Pressure and temperature sensors are located usually on the bottom side of wing. Some airplanes have landing lights embedded into the wing (e.g., EV-97 [33]).

**Empennage** contains the main control surfaces called elevator (or pitch motivator) and rudder (or yaw motivator). The elevator controls the pitch motion of an airplane (rotation about  $y_b$  axis) and it is set by push–pull movement of the stick or yoke [76]. The deflection of the trailing edge of the elevator downward is considered as a positive deflection. The rudder controls the yaw motion of airplane (rotation about  $z_b$  axis) and it is operated by pedals [76]. The deflection of the trailing edge of the rudder to left is considered a positive deflection. The elevator has an attached trimming tab (called elevator trim). The elevator trim balances the control force necessary to maintain the correct attitude of the airplane [10, 76]. Similarly, some airplanes have a trimming tab attached to the rudder [10].

**Propulsion system** in LSA and VLA category is often placed in the front part of the fuselage and it consists of an engine and a propeller. Some types of engines have a reduction gearbox (e.g., Bombardier Rotax 912 family [11]).

Some airplanes have differently called control surfaces as they join more than one function to a set of control surfaces (e.g., elevons – elevator/aileron [41], spoileron – spoiler/aileron [45], flaperon – flaps/aileron [41]).

## G. Additional results of model validation

Additional results of model validation presented in Section 5.5.3 are given in Figures G.1 to G.6.

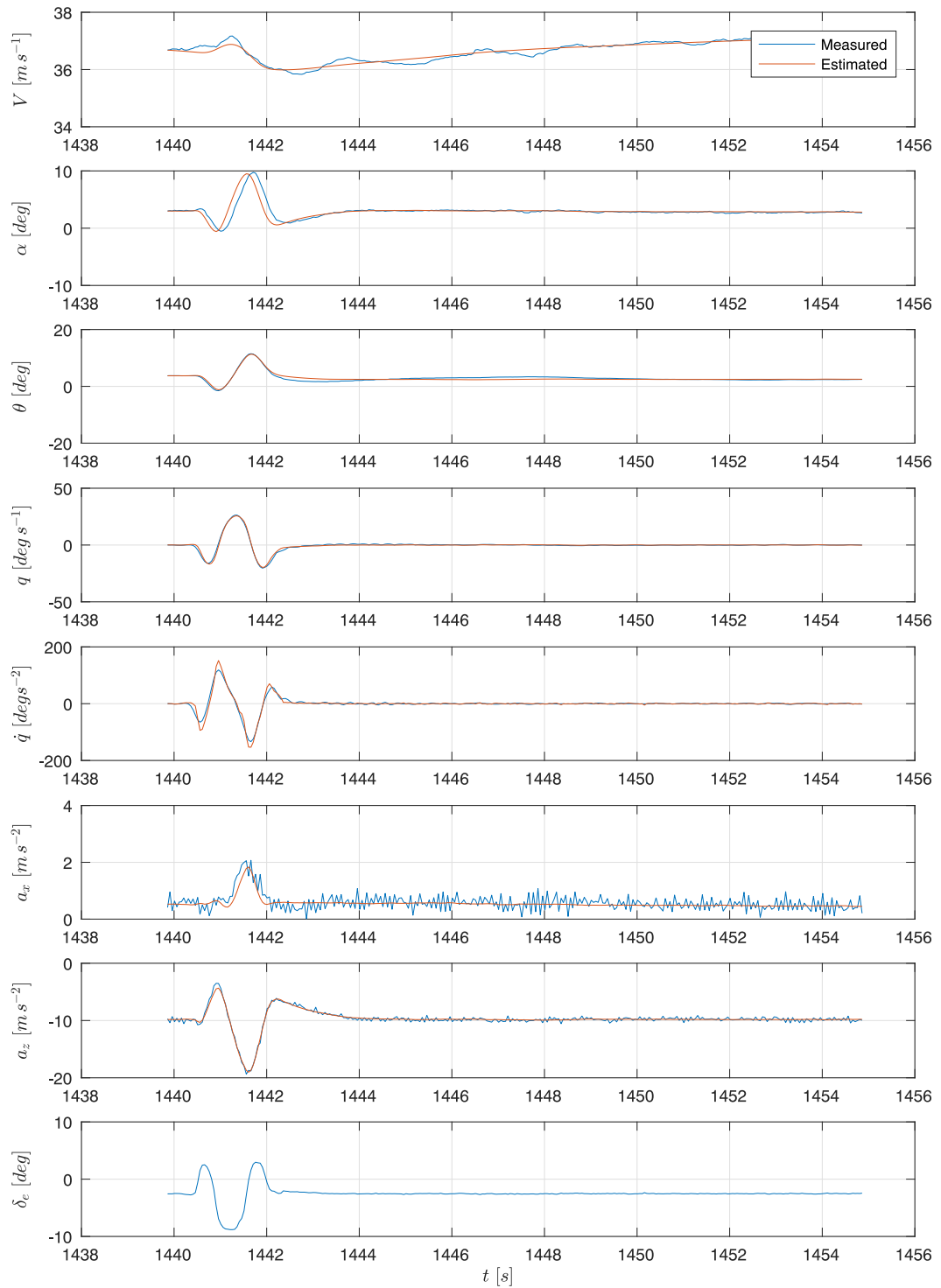


Figure G.1: Recorded data for maneuver N° 24

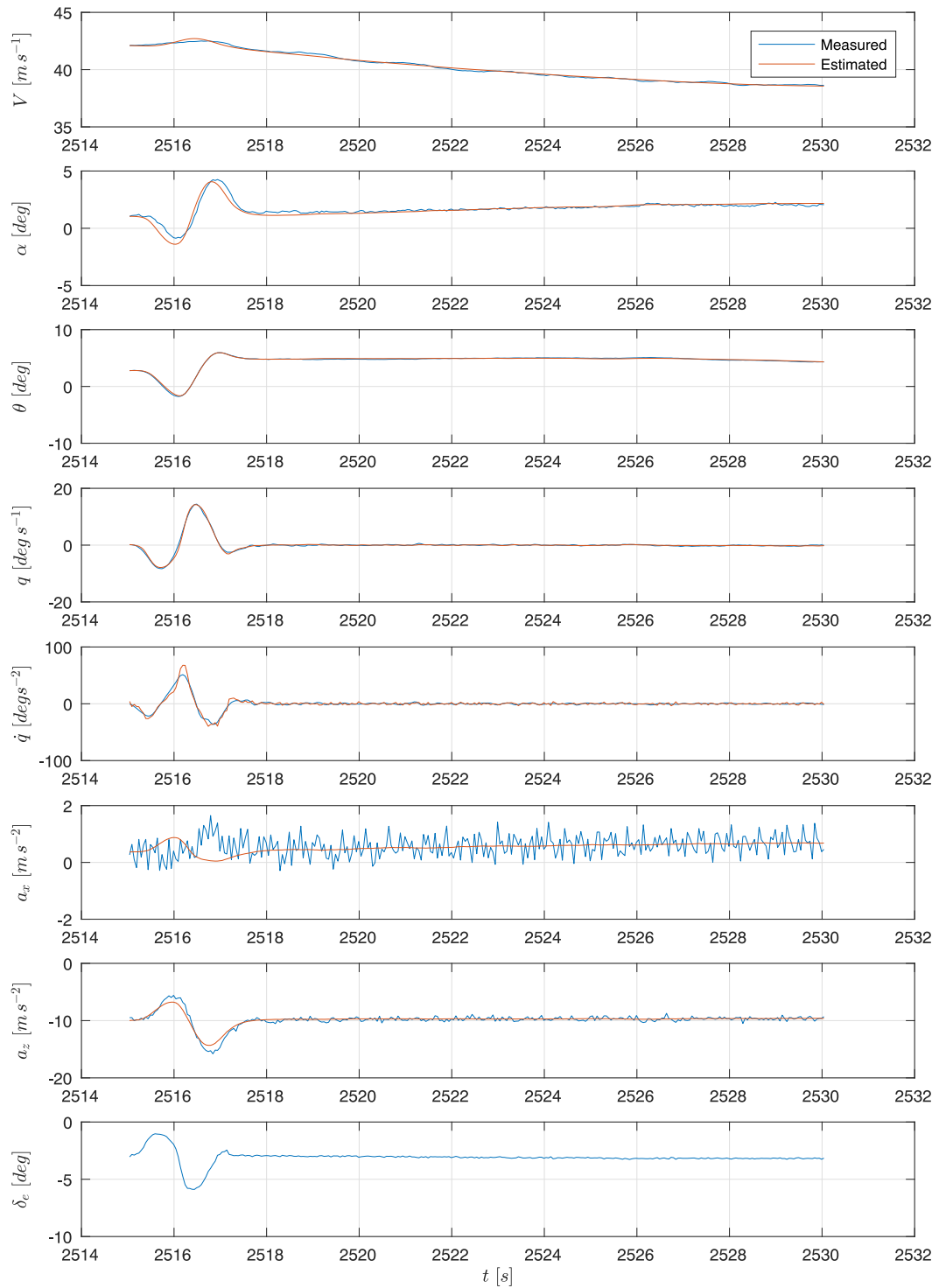


Figure G.2: Recorded data for maneuver N° 127

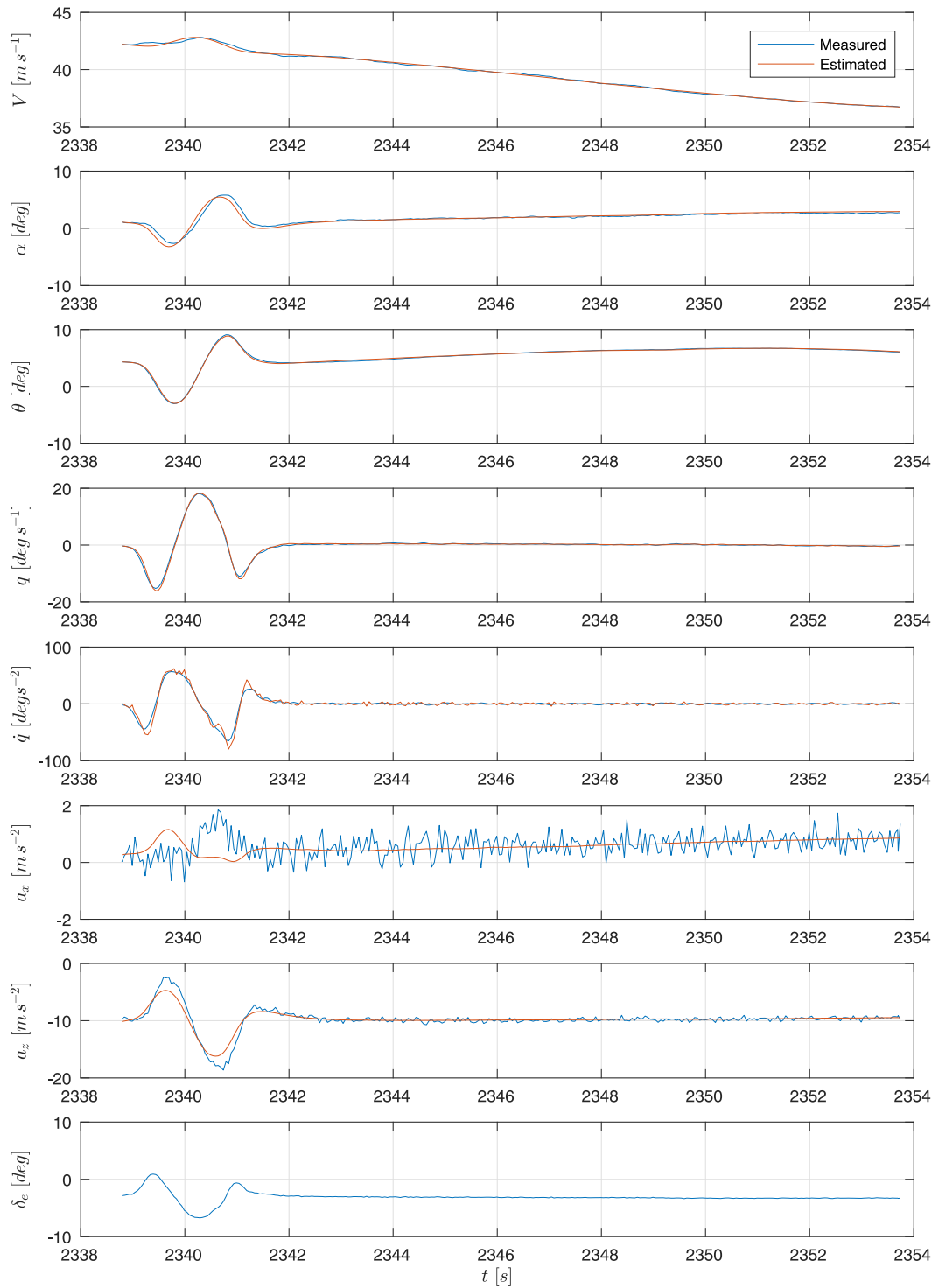


Figure G.3: Recorded data for maneuver N° 129

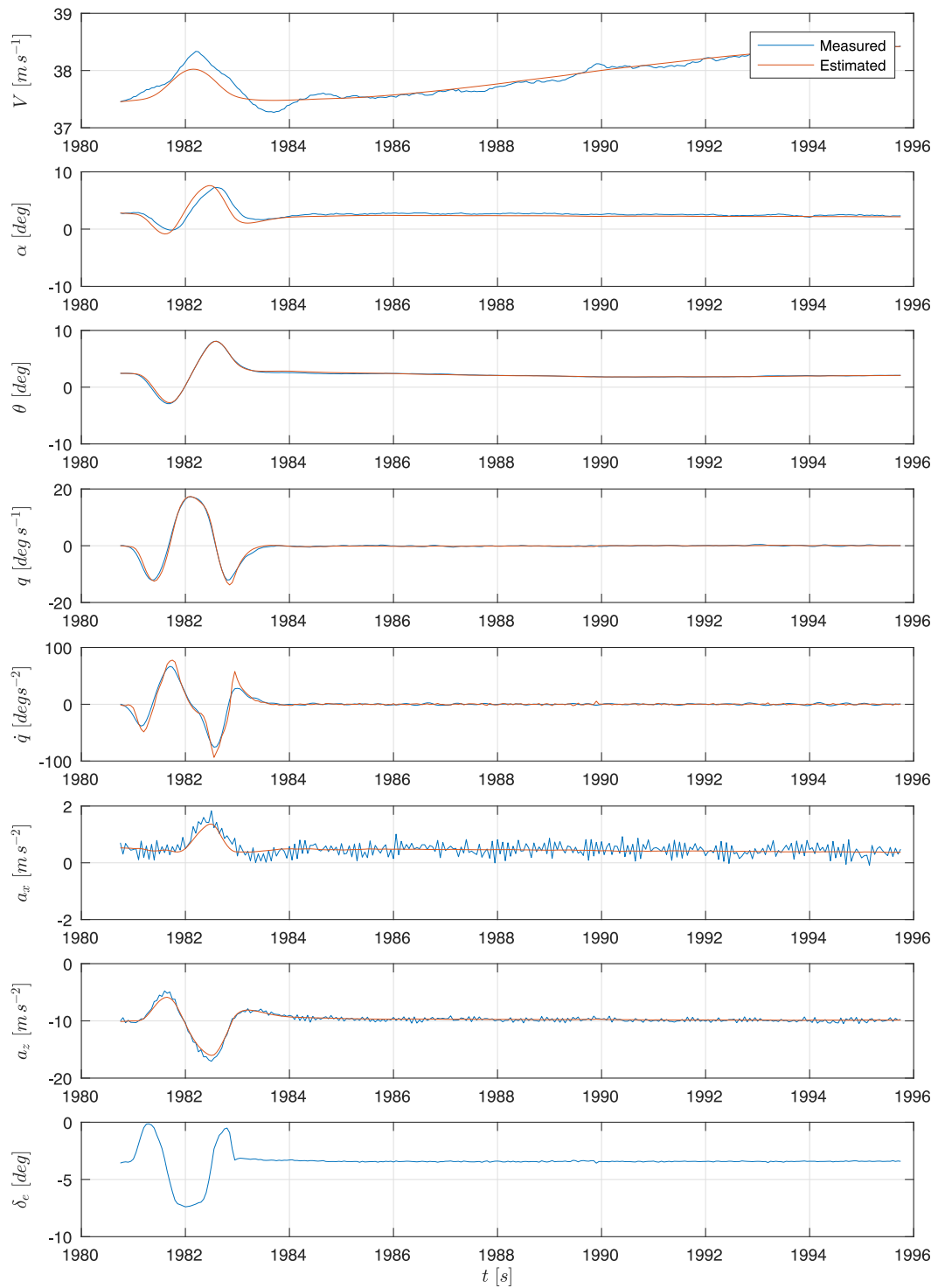


Figure G.4: Recorded data for maneuver N° 132

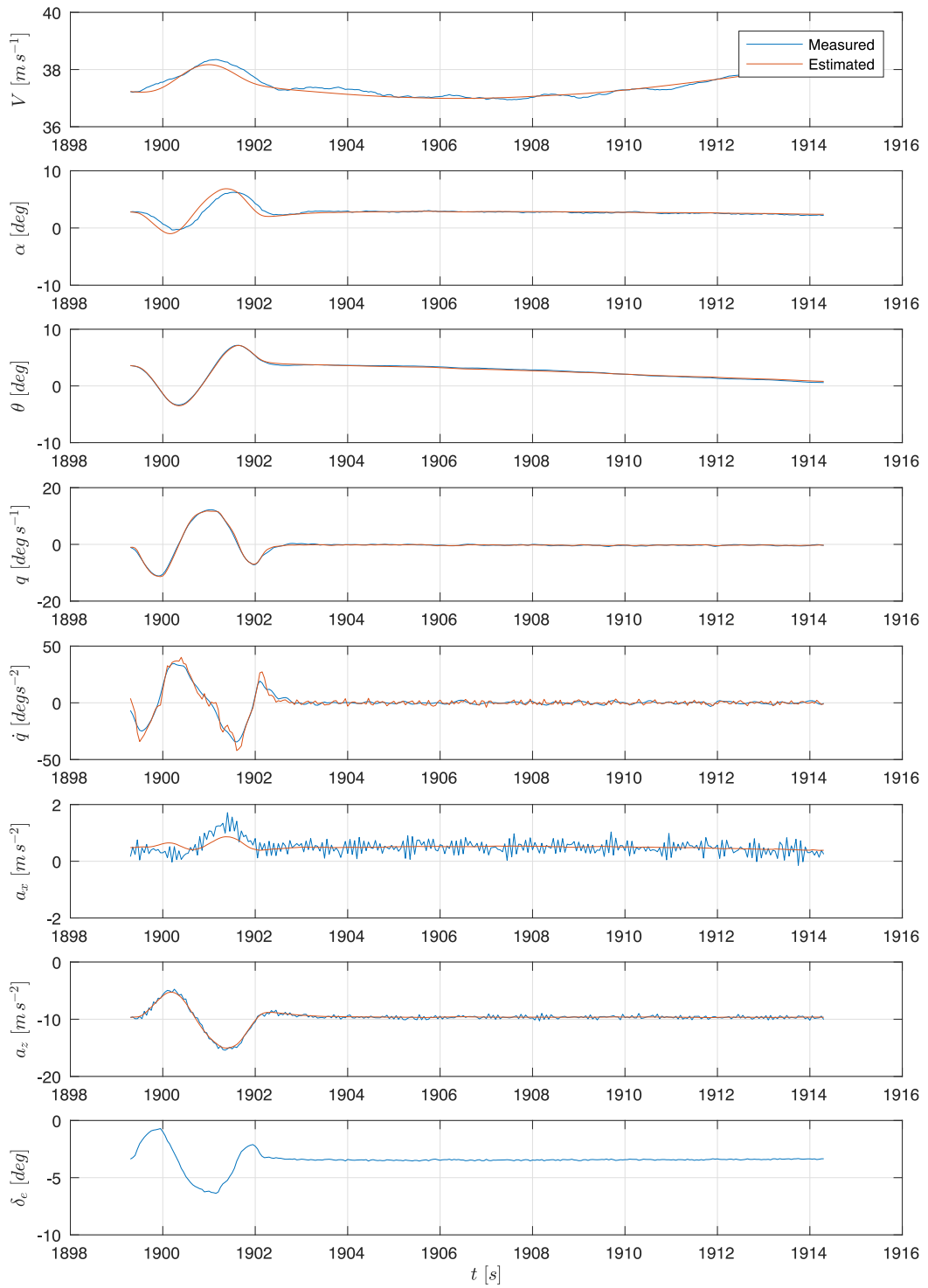


Figure G.5: Recorded data for maneuver N° 133

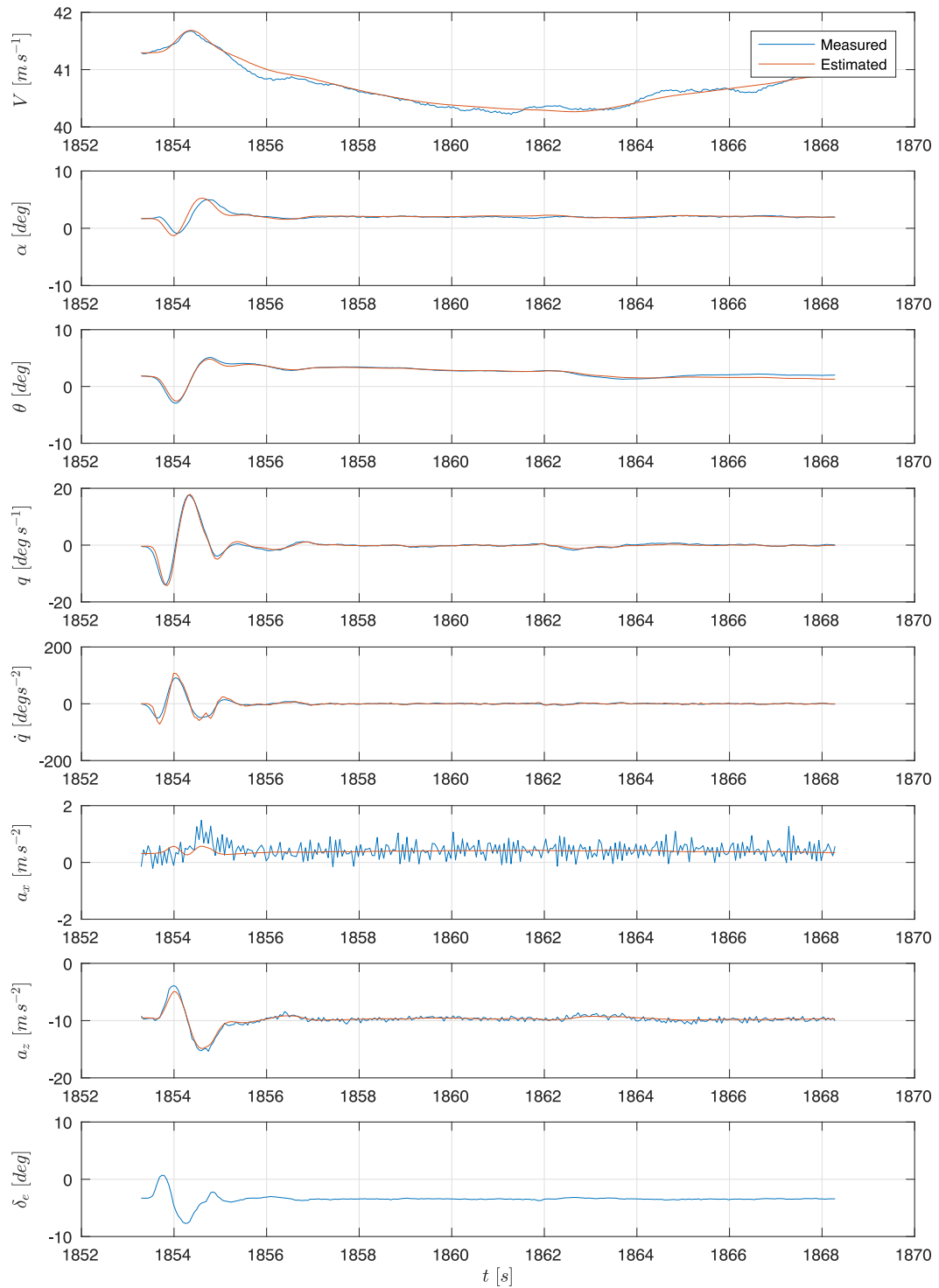


Figure G.6: Recorded data for maneuver N° 182

## H. Model of an F-18 Hornet

The article [56], published J. Kay et al., presents the corrections of flight parameter estimations for F-18 Hornet at Mach 0.2. The corrections are the ratios of the a-priori values and wind-tunnel data values. The values are extracted into Table H.1.

Table H.1: Corrections of flight parameter estimations for a F-18 Hornet model at Mach 0.2 [56].

Parameter	Absolute values			Relative values		
	Data	VLM	Datcom	Data	VLM	Datcom
$C_{L\alpha}$	4.300	4.00	3.70	1.00	0.93	0.86
$C_{Lq}$	4.375	8.15	4.50	1.00	1.86	1.03
$C_{L\delta_e}$	0.950	0.85	0.80	1.00	0.89	0.84
$C_{L\delta_f}$	0.830	0.92	1.35	1.00	1.11	1.63
static margin	5.625	5.25	6.65	1.00	0.93	1.18
$C_{m\alpha}$	-0.250	-0.225	-0.24	1.00	0.90	0.95
$C_{mq}$	-4.800	-6.00	-4.30	1.00	1.25	0.90
$C_{m\delta_e}$	-1.160	-1.13	-1.03	1.00	0.97	0.89
$C_{m\delta_f}$	0.165	0.15	—	1.00	0.91	—
$C_{Y\beta}$	-0.900	-0.55	-0.57	1.00	0.61	0.63
$C_{Yr}$	0.200	0.49	0.22	1.00	2.45	1.10
$C_{Y\delta_r}$	0.135	0.11	0.103	1.00	0.79	0.76
$C_{l\beta}$	-0.050	-0.08	-0.055	1.00	1.60	1.10
$C_{lr}$	0.078	0.07	0.03	1.00	0.89	0.40
$C_{l\delta_e}$	0.103	0.11	—	1.00	1.07	—
$C_{l\delta_f}$	0.125	0.165	—	1.00	1.32	—
$C_{l\delta_a}$	0.150	0.17	0.14	1.00	1.10	0.90
$C_{l\delta_r}$	0.120	0.17	0.15	1.00	1.42	1.25
$C_{lp}$	-0.410	-0.43	-0.30	1.00	1.05	0.73
$C_{n\beta}$	0.095	0.085	0.065	1.00	0.89	0.68
$C_{np}$	-0.085	-0.125	-0.03	1.00	1.47	0.35
$C_{nr}$	-0.174	-0.21	-0.06	1.00	1.21	0.34
$C_{n\delta_r}$	-0.046	-0.05	-0.03	1.00	0.98	0.65